UNIVERSIDADE DO VALE DO RIO DOS SINOS - UNISINOS
UNIDADE ACADÊMICA DE PESQUISA E PÓS-GRADUAÇÃO
PROGRAMA DE PÓS-GRADUAÇÃO EM GEOLOGIA
NÍVEL MESTRADO

DISSERTAÇÃO DE MESTRADO

NANOFÓSSEIS CALCÁRIOS DO ALBIANO–CENOMANIANO NO DSDP *SITE* 364 (BACIA DE KWANZA - ANGOLA): BIOESTRATIGRAFIA E IMPLICAÇÕES PALEOCEANOGRÁFICAS PARA O ATLÂNTICO SUL

MAURO DANIEL RODRIGUES BRUNO

São Leopoldo
2018

Mauro Daniel Rodrigues Bruno

NANOFÓSSEIS CALCÁRIOS DO ALBIANO–CENOMANIANO NO DSDP *SITE* 364 (BACIA DE KWANZA - ANGOLA): BIOESTRATIGRAFIA E IMPLICAÇÕES PALEOCEANOGRÁFICAS PARA O ATLÂNTICO SUL

Área de Concentração: Geologia Sedimentar
Linha de Pesquisa: Paleontologia Aplicada
Tema de interesse: Micropaleontologia – Nanofósseis Calcários

Dissertação apresentada como requisito parcial para a obtenção do título de Mestre, pelo Programa de Pós-Graduação em Geologia da Universidade do Vale do Rio dos Sinos - UNISINOS

Orientador: Prof. Dr. Gerson Fauth
Coorientador: Prof. Dr. David K. Watkins (University of Nebraska/EUA)

B898n Bruno, Mauro Daniel Rodrigues.

Nanofósseis calcários do Albiano-Cenomaniano do DSDP *SITE* 364 (Bacia de Kwanza - Angola): bioestratigrafia e implicações paleoceanográficas para o Atlântico Sul / Mauro Daniel Rodrigues Bruno. – 2018.

67 f. : il. color. ; 30 cm.

Dissertação (mestrado) – Universidade do Vale do Rio dos Sinos, Programa de Pós-Graduação em Geologia, São Leopoldo, 2018.

“Orientador: Prof. Dr. Gerson Fauth ; Coorientador: Prof. Dr. David K. Watkins.”

1. Nanofósseis. 2. Sedimentos (Geologia). 3. Geologia estratigráfica. I. Título.

CDU 56

Dados Internacionais de Catalogação na Publicação (CIP)
(Bibliotecária: Bruna Sant’Anna – CRB 10/2360)

SUMÁRIO

RESUMO 4

APRESENTAÇÃO 5

ALBIAN–CENOMANIAN CALCAREOUS NANNOFOSSILS FROM DSDP SITE 364 (KWANZA BASIN - ANGOLA): BIOSTRATIGRAPHIC AND PALEOCEANOGRAPHIC IMPLICATIONS FOR THE SOUTH ATLANTIC 7

KEY POINTS: 7

ABSTRACT 7

1. INTRODUCTION 8

2. MATERIALS AND METHODS 9

2.1 SITE INFORMATION 9

2.2 SAMPLE PREPARATIONS AND ANALYSIS 10

2.3 PALEOECOLOGICAL ANALYSIS 11

3. RESULTS 12

4. DISCUSSION 15

4.1 BIOSTRATIGRAPHY 15

4.2 CALCAREOUS NANNOFOSSIL PRESERVATION, PALEOECOLOGY AND PALEOCEANOGRAPHIC INFERENCES 16

5. CONCLUSIONS 21

REFERENCES 22

CONSIDERAÇÕES FINAIS 43

FIGURE 1 31

FIGURE 2 32

FIGURE 3 33

FIGURE 4 34

FIGURE 5 35

FIGURE 6. 35

TABLE 1 36

TABLE 2 37

FIGURE S1 38

FIGURE S2 39

TABLE S1. 40

TABLE S2 41

TABLE S3 42

RESUMO

O intervalo Albiano–Cenomaniano foi um período de condições climáticas extremas relacionadas a condições de *Greenhouse*, neste intervalo de tempo também são registradas significativas mudanças na paleogeografia e paleoceanografia dos oceanos que causaram evoluções nos ecossistemas marinhos em escala global. Neste estudo foi analisada a assembleia de nanofósseis calcários das amostras recuperadas no *Site* 364 (Bacia do Kwanza, Angola), perfurado pelo *Deep Sea Drilling Project*. Foi recuperada uma assembleia com afinidade subtropical-tropical, que fornece um excelente registro bioestratigráfico do intervalo Albiano–Cenomaniano superior, e indica conexão de águas rasas entre as regiões sul e central do Oceano Atlântico, pelo menos até Angola. Os dados mostram que a sedimentação foi predominantemente calcária e pelágica durante o intervalo Albiano–Cenomaniano, exceto na seção basal do *Site* 364 onde os depósitos de folhelhos pretos ocorrem intercalados com calcário dolomítico e margas. A dissolução do carbonato de cálcio é um processo significativo registrado no Site 364 e foi observado na maioria das amostras, seus efeitos são seletivos na assembleia e não foi possível verificar a relação entre as camadas de deposição de folhelhos pretos e a alta fertilidade de nanofósseis calcários. Apesar da dissolução, a assembleia recuperada é relativamente bem diversificada e os táxons suscetíveis à dissolução são observados, mas não muito abundantes. Evidências paleontológicas e geoquímicas sugerem aumento da fertilidade/produtividade da água superficial nos intervalos onde diminui os efeitos da dissolução.

APRESENTAÇÃO

Durante o Cretáceo ocorreram os estágios finais da fragmentação do Gondwana e no desenvolvimento de oceanos, extensas plataformas carbonáticas e mares epicontinentais que influenciaram na evolução da biota marinha. O intervalo Albiano–Cenomaniano é descrito na literatura como a última expressão de fragmentação e separação das placas Sul-Americana e Africana, portanto é um intervalo de tempo relevante na evolução geológica do Oceano Atlântico. Para este intervalo de tempo, os dados litológicos, geoquímicos e bioestratigráficos têm sido discutidos com o objetivo de caracterizar as condições paleoceanográficas do Oceano Atlântico (e.g., Wagner & Pletsch, 1999; Moulin et al., 2010; Pérez-Díaz & Eagles, 2017).

Estudos indicam que durante o Albiano, a configuração do Oceano Atlântico seria de mar aberto com livre circulação das massas de água oceânica, adequadas à sobrevivência e distribuição de microrganismos marinhos. Entretanto, também tem sido discutida uma configuração distinta, na qual este oceano teria sido um mar epicontinental com relativa estabilidade tectônica entre as margens continentais da África e América do Sul. Diversos trabalhos atribuem distintos momentos para a livre circulação das massas de água, nos estudos modernos foi inferido que esta fase evolutiva do oceano teria ocorrido durante o intervalo Aptiano–Cenomaniano (e.g., Kellogg & Mohriak, 2001; Azevedo, 2004; Eagles, 2007; Moulin et al., 2010). Não existe um consenso sobre as idades/estágios de deposição e afinidade paleobiogeográfica dos microrganismos marinhos, e a evolução paleoceanográfica do Oceano Atlântico durante o Cretáceo ainda é um tema de amplo debate na comunidade cientifica.

As sequências carbonáticas intercaladas com camadas ricas em matéria orgânica, recuperadas no *Site* 364 perfurado pelo *Deep Sea Drilling Project* (DSDP) na Bacia de Kwanza em Angola, possuem registros das fases evolutivas do Oceano Atlântico. O estudo dos nanofósseis calcários, na seção relacionada ao Cretáceo Inferior do *Site* 364, infere datações relativas para os estratos e apresenta evidencias relacionadas a eventos paleoceanográficos. Os índices paleoecológicos deste grupo fóssil foram analisados conjuntamente aos dados geoquímicos de isótopos estáveis de carbono e oxigênio, susceptibilidade magnética, carbono orgânico e carbonato de cálcio com o intuito de reconhecer e entender os eventos paleoceanográficos registrados na seção sedimentar estudada.

A hipótese testada neste estudo é a seguinte:

(i) O estudo da assembleia de nanofósseis calcários no *Site* 364 pode refinar o posicionamento bioestratigráfico dos estratos, contribuir no entendimento da afinidade paleobiogeográfica deste grupo fóssil e fornecer indícios sobre os eventos paleoceanográficos ocorridos durante o Cretáceo Inferior no Oceano Atlântico.

O artigo elaborado foi submetido ao periódico *Paleoceanography and Paleoclimatology*, conceito A1 na plataforma Qualis da Capes, que incentiva a publicação de resultados em temas como a bioestratigrafia e a paleoceanografia.

Albian–Cenomanian calcareous nannofossils from DSDP Site 364 (Kwanza Basin - Angola): biostratigraphic and paleoceanographic implications for the South Atlantic

Mauro Daniel Rodrigues Bruno[1], David K. Watkins[2], Jairo Francisco Savian[3], Gerson Fauth[1]

[1]itt Fossil – Instituto Tecnológico de Micropaleontologia, Unisinos University, São Leopoldo, Brazil,

[2]Department of Earth and Atmospheric Sciences – University of Nebraska, Lincoln, Nebraska, USA,

[3]Departamento de Geologia – Instituto de Geociências, Universidade Federal do Rio Grande do Sul, Porto Alegre, Brazil.

Corresponding author: Mauro D. R. Bruno (danielr.bruno@hotmail.com)

Key Points:

- Paleontological evidence suggests a surface water connection between the Central and South Atlantic oceans during the Albian–Cenomanian
- Calcareous nannofossil abundance and geochemical signals indicate dissolution, although it did not heavily affect species richness

Abstract

The Albian–Cenomanian was an interval of extreme warmth due to greenhouse climatic conditions, and in which are registered significant changes in the paleogeography and paleoceanography of the oceans, which affected the evolution of marine ecosystems on a global scale. This study analyzed the calcareous nannofossil assemblages from samples recovered from Site 364 (Kwanza Basin, Angola), drilled by the Deep Sea Drilling Project (DSDP) Leg 40. The assemblages were observed to have a subtropical-tropical affinity, which could provide an excellent biostratigraphic record of the Albian–Cenomanian interval, and are indicative of a surface water connection between the Central Atlantic and the South Atlantic oceans at least up to offshore Angola. Sedimentation for the area was predominantly calcareous and pelagic during this interval, with the exception of the basal section, where Albian black shale layers interbedded with dolomitic and marly limestone can be seen.

Dissolution is a significant process in Site 364 that can be observed in the majority of the studied samples, though not to the point where species richness was severely impacted, as small amounts of dissolution-susceptible taxa were observed. Dissolution showed a marked decreased in intervals in which paleontological and geochemical data indicated an increase in surface water fertility/productivity. Still, it affected assemblage composition in a way that did not allow for a proper consideration of the relationship between the deposition of black shale layers and the high fertility of calcareous nannofossils.

1. Introduction

Fragmentation of the Gondwana paleocontinent resulted in significant changes of the global paleogeographic configuration, leading to the opening and development of the South Atlantic ocean. This process produced various submarine physiographic features, such as sedimentary basins and plateaus. The stratigraphic evolution of the sedimentary basins in the South Atlantic ocean follows a well-defined pattern, beginning with continental sequences that gradually evolve into marine ones (e.g., Kellogg & Mohriak, 2001; Milani et al., 2007; Beglinger et al., 2012). In the Early Cretaceous, the first marine incursions were recorded by the deposition of evaporites in many sedimentary basins of the Brazilian and African continental margins. Sediments deposited above evaporites mark the moment of transition from a restricted to an open marine environment phase, allowing for the connection between the Central Atlantic and the South Atlantic oceans (Azevedo, 2004; Eagles, 2007; Moulin et al., 2010). During the Albian–Cenomanian the South Atlantic ocean already had open marine conditions, evidenced mainly by the diversity of marine fossils and extensive limestone layers deposited in shallow marine carbonate shelfs (Melguen, 1978; Wagner & Pletsch, 1999; Mohriak et al., 2008; Beglinger et al., 2012).

The Albian–Cenomanian was a key period for the evolution of marine ecosystems. It was an interval of high atmospheric CO_2 content related to greenhouse climatic conditions, it marked an increase in the eustatic sea-level, and it registered numerous changes in the paleogeography and paleoceanography of the oceans (Poulsen et al., 1999, 2001; Leckie et al., 2002; Huber et al., 2002; Hay, 2008; Torsvik et al., 2009; Haq, 2014). In this global context, numerous episodes of anoxia and dysoxia were registered in the oceans, resulting in the deposition and preservation of organic carbon-rich sediments, black shales, associated with Ocean Anoxic Events (OAEs; Schlanger & Jenkyns, 1976; Arthur & Schlanger, 1979; Erbacher et al., 1996; Leckie et al., 2002; Watkins et al., 2005; Jenkyns, 2010; Wang et al., 2011). During these episodes changes in the physicochemical conditions in the water column were responsible for the enhanced fertility and dissolution of specific calcareous nannofossil species, selectively affecting the planktonic communities (e.g., Roth & Bowdler, 1981; Stradner et al., 1984; Fisher & Hay, 1999; Herrle et al., 2003; Watkins et al., 2005).

The geochemical composition of carbonate rocks records global marine signals, and their correlation with paleoecological data from calcareous nannofossils can provide a better understanding of the paleoceanographic changes that occurred in the South Atlantic ocean during the Albian–Cenomanian. One such calcareous nannofossil record was analyzed from the Kwanza Basin (Deep Sea Drilling Project - DSDP) Site 364 from Leg 40. The paleontological record from this site exhibits paleobiogeographic and biostratigraphic discrepancies between its Lower Cretaceous calcareous nannofossil, benthic and planktonic foraminifera assemblages (Bolli et al., 1978; Kochhann et al., 2013, 2014). The main objectives of this paper are to restudy the calcareous nannofossil assemblages recovered from the Albian–Cenomanian of DSDP Site 364 and their biostratigraphy, to complement the data reported during Leg 40 by Proto Decima et al. (1978). The present paleoenvironmental study of this interval also uses the analysis of micropaleontological data, total organic carbon (TOC), calcium carbonate content ($CaCO_3$), magnetic susceptibility (MS) and stable isotopes ($\delta^{18}O$ and $\delta^{13}C$) values.

2. Materials and Methods

2.1 Site Information

This study analyzed Site 364 (11º34.32’S, 11º58.30’E, 2448 m water depth), which was drilled during the DSDP Leg 40 in the Kwanza Basin, Angola Continental Margin (Figure 1). The studied section comprises the interval from cores 42 to 26 (between 1032.37–715.34 mbsf). During the deposition of this interval, Site 364 was located at a low latitude (24ºS to 28ºS), with an estimated paleodepth of 1000 m (Roth & Bowdler, 1981; Roth & Krumbach, 1986). Benthic foraminifera assemblages indicate that this interval was deposited at upper bathyal to shallow neritic depths (Holbourn et al., 2001; Kochhann et al., 2014), which is in agreement with recent paleobathymetric models that estimate a depth between neritic to bathyal for the Angola Continental Margin (Pérez-Díaz & Eagles, 2017).

Two sedimentary units are described for the studied section: units 7 and 6, from bottom to top (Bolli et al., 1978). Unit 7 is characterized by the occurrence of black shale, and is divided into two subunits (7b and 7a): subunit 7b consists of dolomitic limestone and black shale (1032.37-1009.79 mbsf interval samples); subunit 7a is composed of marly limestone interbedded with black shales (1008.41-968.45 mbsf interval samples). Unit 6 is characterized by the increased occurrence of limestones, and is divided into three subunits (6c, 6b and 6a): subunit 6c is composed of limestone and marly limestone (955.75-825.73 mbsf interval samples); subunit 6b consists of limestone (810.94-768.19 mbsf interval samples); and the subunit 6a contain marly nannofossil chalk, observed between 753.64-717.32 mbsf interval samples (Figure 2).

2.2 Sample Preparations and Analysis

For the study of calcareous nannofossil, 72 smear slides from Site 364 were prepared, following the double slurry method detailed by Watkins and Bergen (2003) and Blair and Watkins (2009). They were analyzed to determinate qualitative preservation, quantitative species abundances, and biostratigraphic ranges. One sample per section was taken, with an average spacing of 1.5 m within the cores. They were examined using a Zeiss Axio Imager A2 microscope, at approximately 1000× magnification. The smear slides are stored in the collection of the Museum of Geological History of Rio Grande do Sul, Unisinos University, Brazil, under the curatorial numbers ULVG 12337 to ULVG 12409.

Preservation of calcareous nannofossils was evaluated using qualitative criteria to assess the degree of etching (E) and/or overgrowth (O), where E1 or O1 are relatively good – specimens exhibited little or no dissolution and/or overgrowth; E2 or O2 are moderate - specimens exhibited moderate dissolution and/or overgrowth, and were easily recognizable; and E3 or O3 are poor - specimens exhibited extreme dissolution and/or overgrowth (Roth & Thierstein, 1972; Roth, 1983). For the quantitative analysis, each slide was randomly scanned until 456 specimens had been counted; this number assures accurate abundance estimates at the 95% confidence interval (Chang, 1967; Watkins & Bergen, 2003). These results are shown in the distribution chart (see supporting information Table S1). The biostratigraphic analysis was based on the First appearance datum (FAD) and Last appearance datum (LAD) of markers species, following CC zones of Sissingh (1977) and Perch-Nielsen (1979, 1985). Comparison of these zones to the BC zonation of Bown et al., (1998) and the UC of Burnett et al., (1998), which are shown plotted next to the CC zones.

Analyzes of TOC, $CaCO_3$, MS, $\delta^{18}O$ and $\delta^{13}C$ were conducted on a number of samples from DSDP Site 364 (supporting information Table S2). TOC and $CaCO_3$

measurements were performed from 51 samples using 0.26 g. For TOC, these sediments were manually fragmented and acidified using HCl 6N (1:1) for 24 hours. These were determined through the method described by Huerta-Diaz et al. (2011), using the Leco Elemental Analyzer model SC-144DR of the Technological Institute of Micropaleontology itt Fossil (Unisinos University). MS measurements of 49 samples were analyzed and normalized by mass. These values were obtained in low (χlf = 976 Hz) and high (χhf = 15 616 Hz) frequencies, with a MFK1-FA Multifunction Kappabridge magnetic susceptibility analyzer, at Paleomagnetism Laboratory (USPMag), University of São Paulo. This method resulted in the evaluation of the concentration of ultrafine (<0.03 μm) superparamagnetic (SP) ferromagnetic minerals in transition to stable single domain (Bloemendal et al., 1985; Dearing et al., 1996; Hrouda & Pokorný, 2012). We also calculated the percentage frequency-dependent magnetic susceptibility χfd % with the Equation:

$$\chi fd\ \% = (\chi lf - \chi hf)/\chi lf \times 100.$$

Thirty-one samples were measurement for the $\delta^{18}O$ and $\delta^{13}C$ on bulk sediments; these analyses were published by Kochhann et al. (2013), with the isotopic values having been reported in standard delta notation (δ) relative to the Vienna Pee Dee Belemnite (VPDB).

2.3 Paleoecological Analysis

Species and genera of calcareous nannofossils relevant for paleoenviromental interpretations were selected based on several studies that highlighted their quantitative and qualitative relevance in the analysis of Cretaceous paleoceanographic events (Table 1). In several of these studies, it was interpreted that shifts in the faunal composition of the assemblages are related to relative changes in surface water fertility, being controlled mainly by the input of nutrients in the paleoenvironment. These studies also provide information regarding the diagenesis of the analyzed strata, noting that some species appear to be particularly resistant to dissolution.

For the paleoecological analysis, different statistical data-processing techniques were used, including Pearson correlation coefficient (r), species richness (S), equitability (E) and Shannon Diversity Index (H). The software package PAST – Paleontological Statistics (Hammer et al., 2001) was utilized. Pearson correlation is used to quantify the extent to which two variables are linearly related, with the result being a coefficient (r) between -1 and 1 (Fisher & Hay, 1999). Species richness (S) is simply the number of different species in an assemblage, which is a rough measure of the relative stability of the ecological conditions when more species occur (Watkins, 1989). Equitability (E) is a measure of the proportional distribution of species, used to reflect the distribution of the energy flux through the ecosystem, larger values indicate relatively more stable conditions (Watkins, 1989). The Shannon Diversity Index (H) is an unbiased measure of diversity based on both species richness and equitability (Pielou, 1969). For the study of surface water fertility/productivity, were analyzed the Nutrients Index (NI), based on the studies of Herrle et al., (2003) and Watkins et al., (2005). This index was established through the relative abundance of two high-fertility taxa, and *W. barnesiae* abundant under low-fertility conditions. The Nutrients Index (NI) per sample was established by the relative abundances of two high-fertility taxa (*Discorhabdus ignotus* and *Biscutum* spp.) and *W. barnesiae* (abundant under low-fertility conditions), with the formula:

$$NI = [\ (Di + Bi) / (Di + Bi + Wb)\ ]100$$

where Di = *D. ignotus*, Bi = *Biscutum* spp., and Wb = *W. barnesiae*. The specie *Zeugrhabdotus erectus*, commonly used in NI calculations (Herrle et al., 2003; Watkins et al., 2005), dues to being indicative of high-fertility (Table 1), has a low occurrence in the Site 364 (abundance of 1 %, with an average abundance value of 0.05 %) and was not used in constructing the NI.

3. Results

A total of 103 taxa were identified in the 72 studied samples (core 42–26). Calcareous nannofossil biostratigraphy indicates that the section spans the Albian–Cenomanian (Figure 2). In the basal section of Site 364, between 1032.37–772.34 mbsf (Cores 42–29), the Albian can be inferred by the *Prediscosphaera columnata* Zone (CC 8), defined at the base by the occurrence of *P. columnata*, and by the FAD of *Eiffellithus turriseiffelii* at the top. Perch-Nielsen (1979) used the FAD *Tranolithus orionatus* to subdivide this biozone, with the stratigraphic interval 1032.37–1008.41 mbsf being defined at the base by the occurrence of *P. columnata* and at the top by the FAD *T. orionatus* (CC 8a subzone, equivalent to the BC 23 zone of Bown et al., 1998), and the stratigraphic interval (1008.41–772.34 mbsf) being assigned to the CC 8b subzone, between the FAD *T. orionatus* and the FAD *E. turriseiffelii*. Bown et al., (1998) and many later authors having used the FADs of *Axopodorhabdus biramiculatus* and *Eiffellithus monechiae* to subdivide CC 8b; the stratigraphic interval 1008.41–951.47 mbsf is defined at the base by the FAD *T. orionatus* and at the top by FAD *A. biramiculatus* (Zone BC 24); the interval 951.47–875.96 mbsf was assigned to Zone BC 25 defined at the top by the FAD *E. monechiae*; and the interval 875.96–772.34 mbsf is defined by the FAD *E. turriseiffelii* (Zone BC 26). The late Albian to early Cenomanian interval can be inferred by the *Eiffellithus turriseiffelii* Zone (CC 9), identified in the 772.34–726.66 mbsf interval. This zone is defined in this study by the interval from the FAD of *E. turriseiffelii* at the base and by the LAD of *Watznaueria britannica*. The specie *Microrhabdus decoratus* that normally marks the top of this zone was not found. Perch-Nielsen (1979) used the LADs of *Braarudosphaera africana* and *W. britannica* to subdivide this biozone, with the LAD of *B. africana* having been identified at 752.37 mbsf and the LAD of *W. britannica* at 726.66 mbsf. The top section of Site 364, ranging from 725.24 to 717.23 mbsf can be inferred as being of late Cenomanian age, based on the consistent occurring of *Cretarhabdus striatus, Eiffellithus perch-nielseniae, Rhagodiscus asper* and *A. biramiculatus*, which are characteristic of the subzone CC 10a or zone UC1b/UC 4a. No evidence of reworking was observed in the species that are considered zonal markers.

Only one (912.02 mbsf, core 36) of the 72 studies samples displayed low nannofossil abundance (297 specimens), being which led to it being excluded from the paleoecological analyses. Assemblages are dominated by *Watznaueria barnesiae*, with an abundance range of 27–94 %, and an average abundance value of 64 %. The remaining 102 taxa recognized have averages less than 10 %. The preservation of calcareous nannofossil is variable throughout Site 364, with indications of dissolution and recrystallization can be analyzed by means of lithological, micropaleontological and geochemical data.

The basal strata of Site 364, ranging between 1032.37 and 968.45 mbsf (cores 42–39, with 21 samples), is referred to as sedimentary unit 7 (Bolli et al., 1978), and is marked by the deposition of dolomitic limestone with black shale intervals (7b subunit) and marly limestone interbedded with black shale layers (7a subunit). In general, the preservation of calcareous nannofossil in sedimentary unit 7 is moderate, with minor overgrowth (O1) and minor to moderate etching (E1-E2), with only three samples (988.42, 987.42 and 975.49 mbsf) showing slightly increased overgrowth (O2) (supporting information Table S1). For sedimentary unit 7, the average species richness is 31 taxa, with a minimum of 15 and a maximum of 44. Shannon Diversity Index values vary from 0.37–2.2, with an average value of 1.42. For Equitability, the average value is 0.41, with values between 0.14–0.60 (Figure 3). The TOC values show the highest values in this interval, ranging from 0.40–8.91 %, with an average value of 3 %. The $CaCO_3$ varies from 11.08–75.26 %, with an average value of 45.40 % (Figure 4). *W. barnesiae* shows high-abundance in this sedimentary unit, comprising between 53–94 % of the assemblage, with an average value of 71 %. On the other hand, the NI shows the lowest values in this interval ranging from 1–13 and with an average value of 5 (Figure 3). Regarding isotopic measurements, the $\delta^{18}O$ values vary from -5.47 to -3.05 ‰, with a mean value of about -4.52 ‰; and the $\delta^{13}C$ values vary between -2.59 to 1.36 ‰, averaging at -0.27 ‰ (Figure 4). The analyzed data shows a positive correlation ($r = 0.32$, $p = 0.53$) between $\delta^{18}O$ and $\delta^{13}C$ stable isotopes to basal strata of Site 364. Results obtained for MS show consistently low values for sedimentary unit 7, ranging between 1.15–4.01×10-8 m^3/kg in low frequency and between 1.02–3.75×10-8 m^3/kg in high frequency; which χfd varying from -3.22 to 14.56 % (supporting information Table S3).

The interval 955.75–717.23 mbsf (cores 38–26, with 51 samples) is referred to as sedimentary unit 6, and is characterized by a high occurrence of limestones. In this unit, the calcareous nannofossil assemblage shows preservation variation between minor to moderate overgrowth (O1-O2) and etching (E1-E2) (supporting information Table S1). This assemblage is dominated by *W. barnesiae*, which comprises between 27–90 %, with an average value of 61 %, occurring in low percentages (<40 %) in only five samples (Table 2). In these five samples, the highest values of NI from studied interval were observed, varying from 1–67 and with an average value of 17 (Figure 3). This may be related to the relative abundance of *D. ignotus* (which reaches values of 20 %), and of species of the genus *Biscutum*, grouped in *Biscutum* spp., reaching 58 % (Table 2). Several studies related the high abundance of these two taxa as indicators of high carbonate productivity and surface water fertility, with a preference for nearshore environments (Table 1).

For sedimentary unit 6, the average species richness (S) is 33 taxa, varying between 20 and 43. Shannon Diversity Index values vary from 0.62–2.77, with an average value of 1.71. For Equitability, the average value is 0.49, varying between 0.19–0.77 (Figure 3). TOC values show a considerable decrease in sedimentary unit 6, varying between 0.55 to 2.89 % and with an average value of 0.3 % (Figure 4). Sample 894.99 mbsf (core 35) is an exception, with a value of 2.89 % (Figure 4). On the other hand, $CaCO_3$ content shows high-values in this sedimentary unit, ranging between 17.45 and 90.64 % with an average value of 64.22 %. MS data shows a significant increase when compared to sedimentary unit 7, with values between 1.14 x10-8 and 7.12x10-7 m^3/kg in low frequency; and between 1.04×10-8–6.91×10-7 m^3/kg in high frequency (Figure 4). The highest values of MS were observed in the interval between 845.92–844.57 mbsf (Core 33), which χfd varying from 1.35 to 13.27 %. The $\delta^{18}O$ isotope values vary between -4.49 and -2.68 ‰, with an average of -3.55 ‰; and the $\delta^{13}C$ isotope values vary between 1.06–2.94 ‰, with an average value of 2.03 ‰ (supporting information Table S3).

4. Discussion

4.1 Biostratigraphy

The study of the calcareous nannofossil recovered from Site 364 (core 42–26), allowed for the classification of 103 taxa, as well as the identification of three intervals: Albian, late Albian–early Cenomanian and middle–late Cenomanian. Assemblage containing *Prediscosphaera columnata, Hayesites albiensis, Tranolithus orionatus, Axopodorhabdus biramiculatus* and *Eiffellithus monechiae* was observed, indicating the presence of zones CC 8 or BC 23 to BC 26, of Albian age. The stratigraphic interval between the FAD of *Eiffellithus turriseiffelii* and LAD of *Watznaueria britannica* was attributed to Zones CC 9 or UC 0/UC 1a, of late Albian–early Cenomanian. The middle–late Cenomanian can be inferred due to the consistent occurrences of *Cretarhabdus striatus, Eiffellithus perch-nielseniae, Rhagodiscus asper* and *A. biramiculatus*, which are indicative of zones CC 10a or UC 1b/UC 4a (Figure 2). No evidence of reworking for species that are considered zonal markers was observed, and all zonal marker-species are cosmopolitan. The most conspicuous difference between the biostratigraphic zonation reported by Proto Decima (1978), for DSDP Site 364, and the present study is the identification of the middle–late Cenomanian.

The calcareous nannofossil biostratigraphy analysis registered a continuous sequence of Albian bioevents in the interval between cores 42-29, with the biozones CC 8 or BC 23, BC 24, BC 25 and BC 26 having been identified (Figure 2). The Albian can also be inferred by ammonites (Wiedmann & Neugebauer, 1978) and palynomorphs (Morgan, 1978). On the other hand, the biostratigraphic study of Caron (1978) with planktonic foraminifera indicates a late Aptian between the cores 41–35, early-middle Albian between 35–31 cores, and middle-late Albian to 31–29 cores interval. Kochhann et al., (2013) studied this fossil group and inferred the late Aptian for cores 37 to 33, also suggesting a biostratigraphic unconformity within core 31 that separates the early Albian (between cores 33–31) and late Albian (between cores 31–29). Scheibnerová (1978) identified benthic foraminifera that assigned a late Aptian age for cores 41–38, early-middle Albian for cores 35–31, and late Albian to cores 31–29.

For the intervals inferred by calcareous nannofossils as being late Albian–early Cenomanian (cores between 29-27) and middle–late Cenomanian (cores between 27-26), Caron (1978) registered, with planktonic foraminifera, the middle–late Albian between cores 34-31. However, studies with ammonites (Wiedmann & Neugebauer, 1978), palynomorphs (Morgan, 1978), benthonic foraminifera (Scheibnerová, 1978) and planktonic foraminifera (Kochhann et al., 2013) indicate a late Albian age for this stratigraphic interval. According to Morgan (1978), radiolarians are rare, with poor preservation, and tentatively indicate an Aptian–Albian age.

4.2 Calcareous Nannofossil Preservation, Paleoecology and Paleoceanographic Inferences

New data regarding the strata deposited during the Albian–Cenomanian of Site 364 was acquired in this study. From the total of 72 analyzed samples, only sample 912.02 mbsf showed low species abundance (297 specimens), possibly due to marly lithological composition, which led to being excluded from the paleoecological inferences to avoid data interpretation errors. The assemblages are mostly dominated by *Watznaueria barnesiae*; several studies noted that a high abundance of *W. barnesiae* is indicative of dissolution, assemblages that contain an abundance of this taxon exceeding 40% are considered strongly altered to the extent that the fossil assemblage no longer reflect the biocoenosis (Thierstein, 1981; Roth & Bowdler, 1981; Roth, 1981, 1986; Roth & Krumbach, 1986). The effects of dissolution may be selective, leading to an increase in the percentage of *W. barnesiae* and, at the same time, reducing the overall abundance and richness of the assemblage. Dissolution can also be inferred by low species diversity (Erba, 1992a; Luciani et al., 2001), and the increase in the relative abundance of high-fertility species may result in a lower abundance of *W. barnesiae* (Roth & Krumbach, 1986; Roth, 1989). Moreover, the high abundance of this specie may be related to deep basin deposits and low-fertility conditions (Table 1). The analyzed data shows a high negative correlation ($r = -0.87$) between the Shannon Diversity Index and a high percentage of *W. barnesiae*, suggesting that the assemblage suffered from dissolution (Figure 5). In the 72 studied samples, *W. barnesiae* distribution shows an abundance of more than 40 % in 67 samples, suggesting that dissolution affected the calcareous nannofossil assemblage of Site 364. The magnetic susceptibility values can also be used as indicative of an increase in dissolution, as it would contribute to a higher concentration of magnetic particles. The χ variation in marine deposits can be due to the changes in the concentration of magnetic minerals, which include diamagnetic (for example calcite), paramagnetic (for example clay) and ferromagnetic (for example magnetite). These variations reflect the balance between terrigenous influxes (high MS, Figure 4) and/or carbonate dissolution (low MS, Figure 4). The χ also can represent changes in magnetic mineralogy, which might be related to redox conditions on the seafloor – magnetite vs. hematite – or it might be related to the nature of the weathering in the continental source area (Liu et al., 2012). The susceptibility was calculated on a carbonate-free based (CFB) in order to account for dilution by carbonate (Figure 4, red lines), which is visible the difference between black and red lines. Large values of χfd% (Figure 4) are indicative of a significant proportion of grains near the single domain (SD)/superparamagnetic (SP) boundary (Bloemendal et al., 1985; Thompson & Oldfield, 1986). Chemical reactions that occur during dissolution can be an important determinant of the MS signal in marine sediments (Liu et al., 2012). The results show an inverse relationship between MS and $CaCO_3$ in the dissolution intervals, which suggest an indicative of climatic controlled dilution of the magnetic signal (e.g., Thompson & Oldfield, 1986; Robinson, 1986; Bloemendal et al., 1988, 1992; Meynadier et al., 1995; Lean & McCave, 1998; Haag, 2000, Lopes et al., 2017).

In spite of the abundance of *W. barnesiae* the assemblages are relatively well diversified and show only moderate signs of dissolution and recrystallization. Moreover, dissolution-susceptible taxa were observed, although they were not very abundant. Therefore, some general trends can be identified and are discussed. The rarefaction curve suggests that the majority of the calcareous nannofossil species have been found in this study, demonstrating that the dissolution did not affect species richness, only the abundance of taxa (supporting information Figure S2).

In the five samples that the relative abundance of *W. barnesiae* is less than 40 %, it could be observed that the relative abundance of *D. ignotus* and *Biscutum* spp. (indicative of the NI) show the highest values registered in the study (Table 2). Therefore, in samples with low dissolution the recovered assemblage shows high carbonate productivity and surface water fertility. In addition, several studies report that *D. ignotus*, *Biscutum* spp., *Nannoconus* spp. and *Braarudosphaera* spp. have a preference to nearshore paleoenvironments, and the high abundance of *W. barnesiae* is related to deep basin deposits (Table 1).

The low-abundance of *Nannoconus* spp. and *Braarudosphaera* spp. (Figure 3) in the studied samples do not support the hypothesis of nearshore deposition except in one sample (749.19 mbsf, core 28), in which the benthic foraminifera assemblages is indicative of a shallow to deep neritic paleoenvironment (Kochhann et al., 2014). In this sample, the low value of CaCO3 (30.90 %), high values of magnetic susceptibility (between 2.44×10-7–2.30×10-7 m3/kg for low and high frequency, respectively), high NI value (67), and an Equitability value of 0.40 (related to the high-abundance of the genus *Biscutum* spp., at 58 %) suggests that these sediments contained a high amount of nutrients, and that they were deposited in a shallow to deep neritic paleoenvironment (Table 2).

The relative abundance of *D. ignotus, Z. erectus* and *Biscutum* spp. are normally used to determinate the NI. However, *Z. erectus* is relatively rare in Site 364. Several studies have considered *Z. erectus* more susceptible to dissolution than *Biscutum* spp. and *Discorhabdus ignotus* (Roth & Krumbach, 1986). According to Fisher and Hay (1999), *Z. erectus* and *Biscutum* spp. are indicative of different levels of increased fertility, with *Z. erectus* being more abundant in high fertility conditions, and *Biscutum* spp. sensitive to very high fertility conditions. On the other hand, Erba (1992a) described *Z. erectus* as being more abundant in eutrophic environments, whereas *Biscutum* spp. has a preference for mesotrophic environments. In general, *D. ignotus*, *Z. erectus* and *Biscutum* spp. are widely used in paleoecological studies for indicating high fertility/productivity (Table 1). In this study, assemblage analysis appears to indicate that *Biscutum* spp. is less susceptible to dissolution than *Z. erectus*, and that *Biscutum* spp. is more abundant in very high fertility conditions, in accordance to Fisher and Hay (1999). Between the five samples in which the relative abundance of *W. barnesiae* is less than 40%, four had a relative abundance of *D. ignotus* (Table 2). In these samples, it could also be observed high values of $CaCO_3$ (between 78.16–90.03 %), Shannon Diversity Index (between 2.20–2.77 %), the occurrence of planktonic foraminifera and absence of benthonic forms (Kochhann et al., 2013), and low values of magnetic susceptibility (2.60×10-8 for low frequency and 2.54×10-8 m^3/kg for high frequency) (Table 2). This suggests that, for these samples, deposition occurred with high carbonate productivity.

During the Cretaceous, many sedimentary basins of the Brazilian and African continental margins show evidence of marine incursions deposited above evaporites, as evidenced by numerous marine fossils and extensive biogenic limestone layers. Several studies that analyze these deposits mark them as the moment of transition from restrict to open marine environment conditions, when the waters of the Central Atlantic and the South Atlantic oceans became connected (e.g., Azevedo, 2004; Eagles, 2007; Moulin et al., 2010). During the Albian–Cenomanian interval, the South Atlantic Ocean already had open sea conditions, with extensive, shallow marine carbonate shelfs (Melguen, 1978; Mohriak et al., 2008; Beglinger et al., 2012; Wagner & Pletsch, 1999). The calcareous nannofossils recovered in this study shows an assemblage with subtropical-tropical affinity, evidencing an influence of the Central Atlantic for this area during the Albian–early Cenomanian. It also gives support to the idea that there was a surface water connection between the Central Atlantic and the South Atlantic oceans, at least up to the Kwanza Basin (north of the Walvis Ridge-Rio Grande Rise). In addition, the absence of high latitude indicator species (Panera, 2011) show that there was no influence of cold surface waters in the area. According to Kochhann et al., (2013), this subtropical-tropical affinity can also observed in the planktonic foraminifera observed in the same interval, in contrast to the benthic foraminiferal assemblage, which shows an Austral/Transitional province affinity (Scheibnerová, 1978; Kochhann et al., 2014). This paleobiogeographic contrast between the assemblages of planktonic and benthonic microfossils suggests a water column with a well-developed thermal gradient, as reported by Kochhann et al., (2014). These variations in seawater could have been caused by fluctuations in the inflow of surface and deep-water masses, by the influence of wind in surface waters, by subtropical arid circulation, by the progressive subsidence of the basin, and/or by relative oscillations in the sea level (Figure 6) (e.g., Poulsen et al., 2001; Hay, 2008; Hasegawa et al., 2012; Haq, 2014; Pérez-Díaz & Eagles, 2017).

The Cretaceous ocean anoxic events are interesting not only due to the fact that they created particularly favorable conditions for the accumulation and preservation of organic-rich sediments, but also because they provide valuable micropaleontological and geochemical data for paleoceanographic studies. The black shale horizons from the basal strata of Site 364 (between 1032.37–968.45 mbsf; cores 42–39, with 21 samples), referred alongside the dolomitic and marly limestones that surround them as sedimentary unit 7 (Bolli et al., 1978), were deposited during the Albian, as indicated by the presence of zone CC 8 or subzones BC 23 to BC 24, and represent an important record of the paleoceanographic changes that occurred during that time in the South Atlantic ocean. These black shale horizons are characterized by calcareous and pelagic sedimentation with a high percentage of marine organic matter (type II kerogen; Bolli et al., 1978; Tissot et al., 1980; Magniez-Jannin & Muller, 1987; Herbin et al., 1987), being of probable algal origin with low organic diagenesis (Raynaud & Robert, 1978), containing extensive dissolution that is reflected in the low abundance of benthonic foraminifera (Scheibnerová, 1978; Kochhann et al., 2014), and by low primary productivity (Melguen, 1978). The biogenic carbonate fraction of the studied sediments is mainly composed of planktonic and benthonic foraminifera (Melguen, 1978) and calcareous nannofossil. In smear slides, most of the inorganic carbonates consist mainly of calcite, dolomite, and unspecified carbonate particles (Siesser & Bremner, 1978). These horizons present a good potential for the exploration of hydrocarbons, as they were formed in situ by the low temperature degradation of organic matter (Kendrick et al., 1978; Hunt, 1978; Tissot et al., 1980), and have been interpreted as a local response to OAEs events (e.g. Bralower et al., 1994; Kochhann et al., 2013; Naafs & Pancost, 2014). The TOC analysis for this unit shows the highest values for the studied interval, ranging from 0.40 to 8.91 %; on the other hand, the $CaCO_3$ values registered were the lowest, being in the 11.08–75.26 % range. Geochemical data shows a positive correlation (r = 0.32) between $\delta^{18}O$ and $\delta^{13}C$ stable isotopes in the basal strata of Site 364, suggesting low diagenetic action as reported by Kochhann et al., (2013). The data also shows a negative correlation (r = -0.75) between TOC and $CaCO_3$; therefore, different physicochemical conditions related to black shale preservation/deposition seem to have been responsible for the dissolution of $CaCO_3$ and the increased TOC content in this interval. According to Bolli et al., (1978) this interval is characterized by the low-deposition of terrigenous sediments, showing a more calcareous and pelagic sedimentation style, with the low values of $CaCO_3$ being caused by low primary productivity in euxinic conditions (anoxic and sulfidic). These oceanic conditions would have controlled the primary productivity and affected the preservation of carbonates in the Kwanza Basin.

In sedimentary unit 7, the calcareous nannofossil assemblage shows minor to moderate preservation and a richness of 44 species, averaging at 31 species. *W. barnesiae* shows high-abundance in this sedimentary unit; on the other hand, NI values are the lowest for the whole interval. The analyzed data shows a high negative correlation (r = -0.97) between the Shannon Diversity Index and percentage of *W. barnesiae,* strongly suggesting that dissolution affected the assemblage composition of sedimentary unit 7. In spite of the high-abundance of *W. barnesiae*, the black shale intervals of Site 364 show a moderately preserved, relatively rich assemblage of calcareous nannofossils, with dissolution-susceptible taxa being present, albeit in relatively low quantities. The combination of calcareous nannofossil and geochemistry data alongside the occurrence of dolomite might suggest that, during deposition, the area did not display euxinic conditions. In addition, the dissolution effect on the assemblage composition makes it impossible to discuss the relationship between the black shale layers and the NI. The dissolution observed also prevented the correlation between the Albian black shales from Kwanza Basin and the OAEs described for this time interval. The black shales layers show low magnetic susceptibility and is predominantly controlled by the paramagnetic minerals (Chadima et al., 2006).

For the interval between 955.75 and 717.23 mbsf (cores 33–26), no black shale layers were observed (Bolli et al., 1978), and the TOC content is low, with only sample 894.99 mbsf (Core 35) showing a high TOC value (2.89 %). For sample 894.99 mbsf, the high TOC value may be related to carbon-rich organic sediments, although fertility (NI = 13) and MS (5.76×10-8 and 5.54×10-8 m^3/kg, low and high frequency respectively) are not high. In the interval between 850.15–845.90 mbsf (core 33) is observed the highest values of MS being observed, this might be associated with the high clay content recorded for this interval (Bolli et al., 1978).

5. Conclusions

The calcareous nannofossil assemblages of Site 364 (cores 42–26) display a subtropical-tropical affinity, providing an excellent biostratigraphic record of the Albian–late Cenomanian interval of the South Atlantic Ocean. The paleobiogeographic affinity of the nannofossil assemblage, comparable to that of planktonic foraminifera found in the same site, indicate that there was a surface water connection between the Central Atlantic and the South Atlantic oceans at least up to offshore Angola, north of the Walvis Ridge-Rio Grande Rise.

These assemblages, alongside geochemical data, show that sedimentation was predominantly calcareous and pelagic during the Albian–late Cenomanian interval of the Kwanza Basin, with the exception of its basal section, where black shale layers interbedded with dolomitic and marly limestone of Albian age can be observed. In this section, the black shale layers are dominated by Type II kerogen (Tissot et al., 1980; Magniez-Jannin and Muller, 1987; Herbin et al., 1987). This, alongside geochemical data and the low values of magnetic susceptibility, suggest that these organic carbon-rich sediments with high TOC values were deposited due to the high fertility of the marine waters at the time. The calcareous nannofossils recovered show moderate signs of dissolution and recrystallization; as a result, they likely do not reflect the original abundance of dissolution-susceptible species and the Nutrients Index values of the black shale layers. In spite of the dissolution, assemblages are relatively well diversified, with dissolution-susceptible taxa having been observed in low abundance. This suggests that the effects of dissolution may have been selective, limiting the abundance but not significantly affecting species richness, and also indicating that, during deposition, the environment did not display euxinic conditions. Also due to the effects of dissolution, the relationship between the deposition of black shale layers and high fertility of calcareous nannofossils could not be properly verified.

Nannofloral distribution patterns observed could, however, give a measure of the fertility and productivity of the strata above the black shale layers. They show that there was a decline in the effects of dissolution in the composition of the fossil assemblages and in the geochemical signals for these deposits. Geochemical data and the high relative abundance of *Discorhabdus ignotus* suggest that, during deposition, there was high carbonate productivity, though not necessarily high fertility. The large abundance of the genus *Biscutum* spp. could indicate that this genus is less susceptible to dissolution than *Zeugrhabdotus erectus*, and previous studies show that *Biscutum* spp. is more abundant in very high fertility conditions and in shallow to deep neritic paleoenvironments.

Acknowledgments

We would like to thank the International Ocean Discovery Program (IODP) for providing the samples for this study. We thank the staff of the Technological Institute of Micropaleontology (itt Fossil) of the Unisinos University for the TOC/$CaCO_3$ analyses and for all support. We are grateful to the Paleomagnetism Laboratory (USPMag) of University of São Paulo for the magnetic susceptibility analyzes. The results of this paper are part of the projects: IODP/CAPES 8888.091703/2014-01; IGCP 609; and CAPES-PVE 88881.062157/2014-01. JFS acknowledges the Fundação de Amparo à Pesquisa do Estado do Rio Grande do Sul (FAPERGS) (16/2551-0000213-4) for financial support.

References

Arthur, M. A., & Schlanger, S. O. (1979). Cretaceous “Oceanic Anoxic Events” as causal factors in development of reef-reservoired giant oil fields. The American Association of Petroleum Geologists Bulletin, 63(6), 870-885.

Azevedo, R. D. (2004). Paleoceanografia e a evolução do Atlântico Sul no Albiano. Boletim de Geociências da PETROBRAS, 12(2), 231-249.

Beglinger, S. E., Doust, H., & Cloetingh, S. (2012). Relating petroleum system and play development to basin evolution: Brazilian South Atlantic margin. Petroleum Geoscience, 18(3), 315-336, doi: 10.1144/1354-079311-022

Blair, S. A., & Watkins, D. K. (2009). High-resolution calcareous nannofossil biostratigraphy for the Coniacian/Santonian Stage boundary, Western Interior Basin. Cretaceous Research, 30(2), 367-384, doi: 10.1016/j.cretres.2016.08.015

Bloemendal, J., Barton C. E., & Radhakrishnamurthy, C. (1985). Correlation between Rayleigh loops and frequency-dependent and quadrature susceptibility: Application to magnetic granulometry of rocks. Journal of Geophysical Research, 90, 8789-8792, doi: 10.1029/JB090iB10p08789

Bloemendal, J., Lamb, N., & King, J. (1988). Paleoenvironmental implications of rock magnetic properties of late quaternary sediment cores from the Eastern Equatorial Atlantic. Paleoceanography, 3, 61-87, doi: 10.1029/PA003i001p00061

Bloemendal, J., King, J. W., Hall, F. R., & Doh, S. J. (1992). Rock magnetism of Late Neogene and Pleistocene deep-sea sediments: relationship to sediment source, diagenetic processes and sediment lithology. Journal of Geophysics Research, 97, 4361-4375, doi: 10.1029/91JB03068

Bolli, H. M., Ryan, W. B. F., Foresman, J. B., Hottman, W. E., Kagami, H., Longoria, J. F., & Siesser, W. G. (1978). Angola continental margin-Sites 364 and 365. Initial Reports of the Deep Sea Drilling Project, 40, 357-390, doi:10.2973/dsdp.proc.40.104.1978

Bown, P. R., Rutledge, D. C., Crux, J. A., & Gallagher, L. T. (1998). Lower Cretaceous. In P. R. Bown (Ed.), Calcareous Nannofossil Biostratigraphy, (Vol. 1, pp. 86–131). Kluwer Academic Publishers, Dordrecht.

Bralower, T. J., Arthur, M. A., Leckie, R. M., Sliter, W. V., Allard, D. J., & Schlanger, S. O. (1994). Timing and paleoceanography of oceanic dysoxia/anoxia in the late Barremian to early Aptian (Early Cretaceous). Palaios, 9(4), 335-369, doi: 10.2307/3515055

Browning, E. L., & Watkins, D. K. (2008). Elevated primary productivity of calcareous nannoplankton associated with ocean anoxic event 1b during the Aptian/Albian transition (Early Cretaceous). Paleoceanography, 23(2), doi: 10.1029/2004PA001097

Burnett, J. A. (1998). Upper Cretaceous. In P. R. Bown (Ed.), Calcareous Nannofossil Biostratigraphy, (Vol. 1, pp. 132–199). Kluwer Academic Publishers, Dordrecht.

Busson, G., & Noel, D. (1991). Les nannoconidés, indicateurs environnementaux des océans et mers épicontinentales du Jurassique terminal et du Crétacé inférieur. Oceanologica Acta, 14(4), 333-356.

Caron, M. (1978). Cretaceous planktonic foraminifers from DSDP Leg 40, southeastern Atlantic Ocean. Initial Reports of the Deep Sea Drilling Project, 40, 651-678, doi: 10.2973/dsdp.proc.40.114.1978

Chadima, M., Pruner, P., Slechta, S., Grygar, T., & Hirt, A. M. (2006). Magnetic fabric variations in Mesozoic black shales, Northern Siberia, Russia: Possible paleomagnetic implications. Tectonophysics, 418, 145-162, doi: 10.1016/j.tecto.2005.12.018

Chang, Y. M. (1967). Accuracy of fossil percentage estimation. Journal of Paleontology, 500-502.

Dearing, J. A., Dann, R. J. L., Hay, K., Lees, J. A., Loveland, P. J., Maher, B. A., & O'Grady, K. (1996). Frequency-dependent susceptibility measurements of environmental materials.

Geophysical Journal International banner. 124, 228-240, doi: 10.1111/j.1365-246X.1996.tb06366.x

Doeven, P. H. (1983). Cretaceous stratigraphy and paleoecology of the Canadian Atlantic margin; Geological Survey of Canada Bulletin, 356, p.1-70.

Eagles, G. (2007). New angles on South Atlantic opening. Geophysical Journal International, 168(1), 353-361, doi: 10.1111/j.1365-246X.2006.03206.x

Erba, E. (1992a). Middle Cretaceous calcareous nannofossils from the western Pacific (Leg 129): evidence for paleoequatorial crossings. Proceedings of the Ocean Drilling Program, Scientific Results, 129, 189-201, doi: 10.2973/odp.proc.sr.129.119.1992

Erba, E. (1992b). Calcareous nannofossil distribution in pelagic rhythmic sediments (Aptian–Albian Piobbico core, central Italy). Rivista Italiana di Paleontologia e Stratigrafia (Research in Paleontology and Stratigraphy), 97(3-4), 455-484, doi: 10.13130/2039-4942/8959

Erba, E., Castradori, D., Guasti, G., & Ripepe, M. (1992). Calcareous nannofossils and Milankovitch cycles: the example of the Albian Gault Clay Formation (southern England). Palaeogeography, Palaeoclimatology, Palaeoecology, 93(1-2), 47-69, doi: 10.1016/0031-0182(92)90183-6

Erba, E. (1994). Nannofossils and superplumes: the early Aptian “nannoconid crisis”. Paleoceanography, 9(3), 483-501, doi: 10.1029/94PA00258

Erba, E., Watkins, D. K., & Mutterlose, J. (1995). Campanian dwarf calcareous nannofossils from Wodejebato Guyot. Proceedings of the Ocean Drilling Program, Scientific Results, 144, 141-156.

Erbacher, J., Thurow, J., & Littke, R. (1996). Evolution patterns of radiolaria and organic matter variations: a new approach to identify sea-level changes in mid-Cretaceous pelagic environments. Geology, 24(6), 499-502, doi: 10.1130/0091-7613(1996)024<0499:EPORAO>2.3.CO

Eshet, Y., & Almogi-Labin, A. (1996). Calcareous nannofossils as paleoproductivity indicators in Upper Cretaceous organic-rich sequences in Israel. Marine Micropaleontology, 29(1), 37-61, doi: 10.1016/0377-8398(96)00006-0

Fisher, C. G., & Hay, W. W. (1999). Calcareous nannofossils as indicators of mid-Cretaceous paleofertility along an ocean front, US Western Interior. Special Papers-Geological Society of America, 332, 161-180, doi: 10.1130/0-8137-2332-9.161

Friedrich, O., Herrle, J. O., & Hemleben, C. (2005). Climatic changes in the late Campanian–early Maastrichtian: Micropaleontological and stable isotopic evidence from an epicontinental sea. Journal of Foraminiferal Research, 35(3), 228-247, doi: 10.2113/35.3.228

Gardin, S., & Monechi, S. (1998). Palaeoecological change in middle to low latitude calcareous nannoplankton at the Cretaceous/Tertiary boundary. Bulletin de la Société géologique de France, 169(5), 709-723, doi: 10.1661/0026-2803(2003)049[0189:CINCOT]2.0.CO;2

Gardin, S. (2002). Late Maastrichtian to early Danian calcareous nannofossils at Elles (Northwest Tunisia). A tale of one million years across the K–T boundary. Palaeogeography, Palaeoclimatology, Palaeoecology, 178(3-4), 211-231, doi: 10.1016/S0031-0182(01)00397-2

Haag, M. (2000). Reliability of relative paleointensities of a sediment core with climatically triggered strong magnetization changes. Earth and Planetary Science Letters, 180, 49-59, doi: 10.1016/S0012-821X(00)00145-X

Hammer, O., Harper, D. A. T., & Ryan, P. D., (2001). PAST: paleontological statistics software package for education and data analysis. Palaeontologia Electronica, 4(1), 1-31.

Haq, B. U. (2014). Cretaceous eustasy revisited. Global and Planetary Change, 113, 44-58, doi: 10.1016/j.gloplacha.2013.12.007

Hardas, P., & Mutterlose, J. (2007). Calcareous nannofossil assemblages of Oceanic Anoxic Event 2 in the equatorial Atlantic: Evidence of an eutrophication event. Marine Micropaleontology, 66(1), 52-69, doi: 10.1016/j.marmicro.2007.07.007

Hasegawa, H., Tada, R., Jiang, X., Suganuma, Y., Imsamut, S., Charusiri, P., & Khand, Y. (2012). Drastic shrinking of the Hadley circulation during the mid-Cretaceous Supergreenhouse. Climate of the Past, 8(4), 1323-1337, doi: 10.5194/cp-8-1323-2012

Hay, W. W. (2008). Evolving ideas about the Cretaceous climate and ocean circulation. Cretaceous Research, 29(5-6), 725-753, doi: 10.1016/j.cretres.2008.05.025

Herbin, J. P., Müller, C., Graciansky, P. C., Jacquin, T., Magniez-Jannin, F., & Unternehr, P. (1987). Cretaceous Anoxic Events in the South Atlantic. Revista Brasileira de Geociências, 17 (2), 92-99.

Herrle, J. O., Pross, J., Friedrich, O., Kößler, P., & Hemleben, C. (2003). Forcing mechanisms for mid-Cretaceous black shale formation: evidence from the upper Aptian and lower Albian of the Vocontian Basin (SE France). Palaeogeography, Palaeoclimatology, Palaeoecology, 190, 399-426, doi: 10.1016/S0031-0182(02)00616-8

Holbourn, A., Kuhnt, W., & Soeding, E. (2001). Atlantic paleobathymetry, paleoproductivity and paleocirculation in the late Albian: the benthic foraminiferal record. Palaeogeography, Palaeoclimatology, Palaeoecology, 170(3-4), 171-196, doi: 10.1016/S0031-0182(01)00223-1

Hrouda, F., & Pokorný, J., (2012). Modelling accuracy limits for frequency-dependent anisotropy of magnetic susceptibility of rocks and soils. Studia Geophysica et Geodaetica, 56, 789-802, doi: 10.1007/s11200-011-9009-5

Huber, B. T., Norris, R. D., & MacLeod, K. G. (2002). Deep-sea paleotemperature record of extreme warmth during the Cretaceous. Geology, 30(2), 123-126, doi: 10.1130/0091-7613(2002)030<0123:DSPROE>2.0.CO;2

Huerta-Diaz, M. A., Delgadillo-Hinojosa, F., Otero, X. L., Segovia-Zavala, J. A., Hernandez-Ayon, J. M., Galindo-Bect, M. S., & Amaro-Franco, E. (2011). Iron and trace metals in microbial mats and underlying sediments: results from Guerrero Negro saltern, Baja California Sur, Mexico. Aquatic geochemistry, 17(4-5), 603-628, doi: 10.1007/s10498-011-9126-3

Hunt, J. M. (1978). Light hydrocarbons in Holes 361 and 364, Leg 40. Initial Reports of the Deep Sea Drilling Project, 40, 649-650, doi:10.2973/dsdp.proc.38394041s.303.1978

Jenkyns, H. C. (2010). Geochemistry of oceanic anoxic events. Geochemistry, Geophysics, Geosystems, 11(3), 1-30, doi: 10.1029/2009GC002788

Kellogg, J. N., & Mohriak, W. U. (2001). The tectonic and geological environment of coastal South America. In U. Seeliger and B. Kjerfve (Eds.), Coastal Marine Ecosystems of Latin America (Vol. 1, pp. 1-16). Springer, Berlin, Heidelberg.

Kendrick, J. M., Hood, A., & Castaño, J. R. (1978). Petroleum-Generating Potential of Sediments from Leg 40, Deep Sea Drilling Project. Initial Reports of the Deep Sea Drilling Project, 40, 671-676, doi:10.2973/dsdp.proc.38394041s.307.1978

Kochhann, K. G., Koutsoukos, E. A., Fauth, G., & Sial, A. N. (2013). Aptian–Albian Planktic Foraminifera from DSDP Site 364 (Offshore Angola): Biostratigraphy, Paleoecology, and Paleoceanographic Significance. Journal of Foraminiferal Research, 43(4), 443-463, doi: 10.2113/gsjfr.43.4.443

Kochhann, K. G., Koutsoukos, E. A., & Fauth, G. (2014). Aptian–Albian benthic foraminifera from DSDP Site 364 (offshore Angola): a paleoenvironmental and paleobiogeographic appraisal. Cretaceous Research, 48, 1-11, doi: 10.1016/j.cretres.2013.11.009

Kulhanek, D. K., & Wise, S. W. (2006). Albian calcareous nannofossils from ODP Site 1258, Demerara Rise. Revue de micropaleontologie, 49(3), 181-195, doi: 10.1016/j.revmic.2006.06.002

Lean, C. M. B., & McCave, I. N. (1998). Glacial to interglacial mineral magnetic and paleoceanographic changes at Chatham Rise, SW Pacific Ocean. Earth and Planetary Science Letters, 163, 247-260, doi: 10.1016/S0012e821X(98)00191-5

Leckie, R. M., Bralower, T. J., & Cashman, R. (2002). Oceanic anoxic events and plankton evolution: Biotic response to tectonic forcing during the mid-Cretaceous. Paleoceanography, 17(3), 1-29, doi: 10.1029/2001PA000623

Lees, J. A., Bown, P. R., & Mattioli, E. (2005). Problems with proxies? Cautionary tales of calcareous nannofossil paleoenvironmental indicators. Micropaleontology, 51(4), 333-343, doi: 10.2113/gsmicropal.51.4.333

Linnert, C., Mutterlose, J., & Herrle, J. O. (2011). Late Cretaceous (Cenomanian–Maastrichtian) calcareous nannofossils from Goban Spur (DSDP Sites 549, 551): implications for the palaeoceanography of the proto North Atlantic. Palaeogeography, Palaeoclimatology, Palaeoecology, 299(3), 507-528, doi: 10.1016/j.palaeo.2010.12.001

Liu. C., Deng, C., & Liu, Q. (2012). Mineral magnetic studies of the vermiculated red soils in southeast China and their paleoclimatic significance. Palaeogeography, Palaeoclimatology, Palaeoecology, 329-330, 173-183, doi: 10.1016/j.palaeo.2012.02.035

Lopes, F. M., Koutsoukos, E. A. M., Kochhann, K. G. D., Savian, J. F., & Fauth, G. (2017). Benthic foraminiferal paleoecology and depositional patterns during the Albian at DSDP Site

327 (Falkland Plateau). Journal of South American Earth Sciences, 78, 126-133, doi: 10.1016/j.jsames.2017.06.010

Luciani, V., Cobianchi, M., & Jenkyns, H. C. (2001). Biotic and geochemical response to anoxic events: the Aptian pelagic succession of the Gargano Promontory (southern Italy). Geological Magazine, 138(3), 277-298, doi: 10.1017/S0016756801005301

Magniez-Jannin, F. & Müller, C. (1987). Cretaceous stratigraphic and paleoenviromental data from the South Atlantic (foraminiferal and nannoplankton). Revista Brasileira de Geociências, 17(2), 100-105.

Melguen, M. (1978). Facies evolution, carbonate dissolution cycles in sediments from the eastern South Atlantic (DSDP Leg 40) since the Early Cretaceous. Initial Reports of the Deep Sea Drilling Project, 60, 543-586, doi:10.2973/dsdp.proc.40.129.1978

Meynadier, L., Valet, J-P., & Grousset, F. E. (1995). Magnetic properties and origin of upper Quaternary sediments in the Somali Basin, Indian Ocean. Paleoceanography, 10, 459-472, doi: 10.1029/94PA03151

Milani, E. J., Rangel, H. D., Bueno, G. V., Stica, J. M., Winter, W. R., Caixeta, J. M., & Neto, O. P. (2007). Bacias sedimentares brasileiras: cartas estratigráficas. Anexo ao Boletim de Geociências da Petrobrás, 15(1).

Mohriak, W., Nemčok, M., & Enciso, G. (2008). South Atlantic divergent margin evolution: rift-border uplift and salt tectonics in the basins of SE Brazil. In: R. J. Pankhurst, R. A. J. Trouw, B. B. Brito Neves & M. J. de Wit (Eds.), Geological Society, (vol. 294, pp. 365–398), London, Special Publications, doi: 10.1144/SP294.19

Morgan, R. (1978). Albian to Senonian Palynology of Site 364, Angola Basin. Initial Reports of the Deep Sea Drilling Project, 40, 915-951, doi: 10.2973/dsdp.proc.40.126.1978

Moulin, M., Aslanian, D., & Unternehr, P. (2010). A new starting point for the South and Equatorial Atlantic Ocean. Earth-Science Reviews, 98(1-2), 1-37, doi: 10.1016/j.earscirev.2009.08.001

Mutterlose, J., & Kessels, K. (2000). Early Cretaceous calcareous nannofossils from high latitudes: implications for palaeobiogeography and palaeoclimate. Palaeogeography, Palaeoclimatology, Palaeoecology, 160(3-4), 347-372, doi: 10.1080/00241160600763925

Naafs, B. D. A., & Pancost, R. D. (2014). Environmental conditions in the South Atlantic (Angola Basin) during the Early Cretaceous. Organic Geochemistry, 76, 184-193, doi: 10.1016/j.orggeochem.2014.08.005

Panera, J. P. P. (2011). The calcareous nannofossil Sollasites falklandensis (Coccolithophyceae) and its biostratigraphic and palaeoceanographic importance in the Albian of the Austral Basin, Argentina. Cretaceous Research, 32(6), 723-737, doi: 10.1016/j.cretres.2011.05.001

Perch-Nielsen, K. (1979). Calcareous nannofossils from the Cretaceous between the North Sea and the Mediterranean. Aspekte der Kreide Europas. IUGS Series A, 6, 223-272.

Perch-Nielsen, K. (1985). Mesozoic calcareous nannofossils. In H. M. Bolli, J. B. Saunders & K. Perch-Nielsen (Eds.), Plankton Stratigraphy (Vol. 1, pp. 329–426). Cambridge University Press, New York.

Pérez-Díaz, L., & Eagles, G. (2017). South Atlantic paleobathymetry since Early Cretaceous. Scientific Reports, 7(1), 11819, doi: 10.1038/s41598-017-11959-7

Pielou, E. C. (1969). An Introduction to Mathematical Ecology, 286 pp., John Wiley, New York.

Poulsen, C. J., Barron, E. J., Johnson, C. C., & Fawcett, P. (1999). Links between major climatic factors and regional oceanic circulation in the mid-Cretaceous. Special Papers-Geological Society of America, 332, 73-90, doi: 10.1130/0-8137-2332-9.73

Poulsen, C. J., Barron, E. J., Arthur, M. A., & Peterson, W. H. (2001). Response of the mid-Cretaceous global oceanic circulation to tectonic and CO2 forcings. Paleoceanography, 16(6), 576-592, doi: 10.1029/2000PA000579

Premoli Silva, I., Erba, E., & Tornaghi, M. E. (1989). Paleoenvironmental signals and changes in surface fertility in Mid Cretaceous Corg-Rich pelagic facies of the Fucoid Marls (Central Italy). Geobios, 22, 225-236, doi: 10.1016/S0016-6995(89)80059-2

Proto Decima, F., Medizza, F., & Todesco, L. (1978). Southeastern Atlantic Leg 40 calcareous nannofossils. Initial Reports of the Deep Sea Drilling Project, 40, 571-634, doi:10.2973/dsdp.proc.40.112.1978

Raynaud, J. F., & Robert, P. (1978). Microscopical survey of organic matter from DSDP Sites 361, 362, and 364. Initial Report of the Deep Sea Drilling Project, 40, 663-669, doi:10.2973/dsdp.proc.38394041s.306.1978

Robinson, S. G. (1986). The Late Pleistocene paleoclimatic record of the North Atlantic deep-sea sediments revealed by mineral-magnetic measurements. Physics of the Earth and Planetary Interior, 42, 22-47, doi: 10.1016/S0031-9201(86)80006-1.

Roth, P. H. (1981). Mid-Cretaceous calcareous nannoplankton from the Central Pacific: implications for paleoceanography. Initial Reports of the Deep Sea Drilling Project, 62, 471-489, doi: 10.2973/dsdp.proc.62.113.1981

Roth, P. H. (1983). Jurassic and Lower Cretaceous calcareous nannofossils in the western North-Atlantic (Site-534)-biostratigraphy, preservation, and some observations on biogeography and paleoceanography. Initial Reports of the Deep Sea Drilling Project, 76, 587-621, doi: 10.2973/dsdp.proc.76.125.1983

Roth, P. H. (1984). Preservation of calcareous nannofossils and fine-grained carbonate particles in mid-Cretaceous sediments from the southern Angola Basin. Initial Reports of the Deep Sea Drilling Project, 75, 651-655, doi: 10.2973/dsdp.proc.75.112.1984

Roth, P. H. (1986). Mesozoic palaeoceanography of the North Atlantic and Tethys oceans. Geological Society, London, Special Publications, 21(1), 299-320, doi: 10.1144/GSL.SP.1986.021.01.22

Roth, P. H. (1989). Ocean circulation and calcareous nannoplankton evolution during the Jurassic and Cretaceous. Palaeogeography, Palaeoclimatology, Palaeoecology, 74(1-2), 111-126, doi: 10.1016/0031-0182(89)90022-9

Roth, P. H. & Thierstein, H. (1972). Calcareous Nannoplankton: Leg 14 of the Deep Sea Drilling Project. Initial Reports of the Deep Sea Drilling Project, 14, 421-485, doi:10.2973/dsdp.proc.14.114.1972

Roth, P. H., & Bowdler, J. L. (1981). Middle Cretaceous calcareous nannoplankton biogeography and oceanography of the Atlantic Ocean. Society of Economic Paleontologists and Mineralogists, Special Publication, 32, 517-546, doi: 10.1016/0377-8398(86)90031-9

Roth, P. H., & Krumbach, K. R. (1986). Middle Cretaceous calcareous nannofossil biogeography and preservation in the Atlantic and Indian Oceans: implications for paleoceanography. Marine Micropaleontology, 10(1-3), 235-266, doi: 10.1016/0377-8398(86)90031-9

Scheibnerová, V. (1978). Aptian and Albian benthic foraminifers of Leg 40, Sites 363 and 364, southern Atlantic. Initial Reports of the Deep Sea Drilling Project, 40, 741-757, doi: 10.2973/dsdp.proc.40.117.1978

Schlanger, S. O., & Jenkyns, H. C. (1976). Cretaceous oceanic anoxic events: causes and consequences. Geologie en Mijnbouw, 55(3-4), 179-184.

Siesser, W. G., & Bremner, J. M. (1978). X-ray mineralogy of cores from Leg 40, Deep Sea Drilling Project. Initial Reports of the Deep Sea Drilling Project, 40, 541-548, doi:10.2973/dsdp.proc.40.109.1978

Sissingh, W. 1977. Biostratigraphy of Cretaceous calcareous nannoplankton. Geologie en Mijnbouw, 56, 37–65.

Stradner, H., Steinmetz, J., & Svabenicka, L. (1984). Cretaceous Calcareous Nannofossils from the Angola Basin, Deep-Sea Drilling Project Site 530. Initial Reports of the Deep Sea Drilling Project, 75, 565-647, doi:10.2973/dsdp.proc.75.111.1984

Street, C., & Bown, P. R. (2000). Palaeobiogeography of Early Cretaceous (Berriasian–Barremian) calcareous nannoplankton. Marine Micropaleontology, 39(1-4), 265-291, doi: 10.1016/S0377-8398(00)00024-4

Thibault, N., & Gardin, S. (2006). Maastrichtian calcareous nannofossil biostratigraphy and paleoecology in the Equatorial Atlantic (Demerara Rise, ODP Leg 207 Hole 1258A). Revue de micropaléontologie, 49(4), 199-214, doi: 10.1016/j.revmic.2006.08.002

Thibault, N., & Husson, D. (2016). Climatic fluctuations and sea-surface water circulation patterns at the end of the Cretaceous era: Calcareous nannofossil evidence. Palaeogeography, Palaeoclimatology, Palaeoecology, 441, 152-164, doi: 10.1016/j.palaeo.2015.07.049

Thierstein, H. R. (1976). Mesozoic calcareous nannoplankton biostratigraphy of marine sediments. Marine Micropaleontology, 1, 325-362, doi: 10.1016/0377-8398(76)90015-3

Thierstein, H. R. (1981). Late Cretaceous Nannoplankton and the change at the Cretaceous Tertiary Boundary. The Society of Economic Paleontologists and Mineralogists (SEPM) SEPM Special Publication, 32, 355-394, doi: 10.2110/pec.81.32.0355

Thompson, R., & Oldfield, F., (1986). Environmental Magnetism, 227 pp., George Allen & Unwin, London.

Tissot, B., Demaison, G., Masson, P., Delteil, J. R., & Combaz, A. (1980). Paleoenvironment and petroleum potential of middle Cretaceous black shales in Atlantic basins. AAPG Bulletin, 64(12), 2051-2063, doi: 10.1306/2F919738-16CE-11D7-8645000102C1865D

Torsvik, T. H., Rousse, S., Labails, C., & Smethurst, M. A. (2009). A new scheme for the opening of the South Atlantic Ocean and the dissection of an Aptian salt basin. Geophysical Journal International, 177(3), 1315-1333, doi: 10.1111/j.1365-246X.2009.04137.x

Wagner, T., & Pletsch, T. (1999). Tectono-sedimentary controls on Cretaceous black shale deposition along the opening Equatorial Atlantic Gateway (ODP Leg 159). Geological Society, London, Special Publications, 153(1), 241-265, doi: 10.1144/GSL.SP.1999.153.01.15

Wang, C., Hu, X., Huang, Y., Wagreich, M., Scott, R., & Hay, W. (2011). Cretaceous oceanic red beds as possible consequence of oceanic anoxic events. Sedimentary Geology, 235(1-2), 27-37, doi: 10.1016/j.sedgeo.2010.06.025

Watkins, D. K. (1989). Nannoplankton productivity fluctuations and rhythmically-bedded pelagic carbonates of the Greenhorn Limestone (Upper Cretaceous). Palaeogeography, Palaeoclimatology, Palaeoecology, 74(1-2), 75-86, doi: 10.1016/0031-0182(89)90020-5

Watkins, D. K., & Bergen, J. A. (2003). Late Albian adaptive radiation in the calcareous nannofossil genus Eiffellithus. Micropaleontology, 49(3), 231-251, doi: 10.1661/0026-2803(2003)049[0231:LAARIT]2.0.CO;2

Watkins, D. K., & Self-Trail, J. M. (2005). Calcareous nannofossil evidence for the existence of the Gulf Stream during the late Maastrichtian. Paleoceanography, 20(3), doi: 10.1029/2004PA001121

Watkins, D. K., Cooper, M. J., & Wilson, P. A. (2005). Calcareous nannoplankton response to late Albian oceanic anoxic event 1d in the western North Atlantic. Paleoceanography, 20(2), 1-14, doi: 10.1029/2004PA001097

Wiedmann, J. & Neugebauer, J. (1978). Lower Cretaceous Ammonites from the South Atlantic Leg 40 (DSDP), Their Statrigraphic Value and Sedimentological Properties. Initial Reports of the Deep Sea Drilling Project, 40, 709-734, doi: 10.2973/dsdp.proc.38394041s.312.1978

Williams, J. R., & Bralower, T. J. (1995). Nannofossil assemblages, fine fraction stable isotopes, and the paleoceanography of the Valanginian–Barremian (Early Cretaceous) North Sea Basin. Paleoceanography, 10(4), 815-839, doi: 10.1029/95PA00977

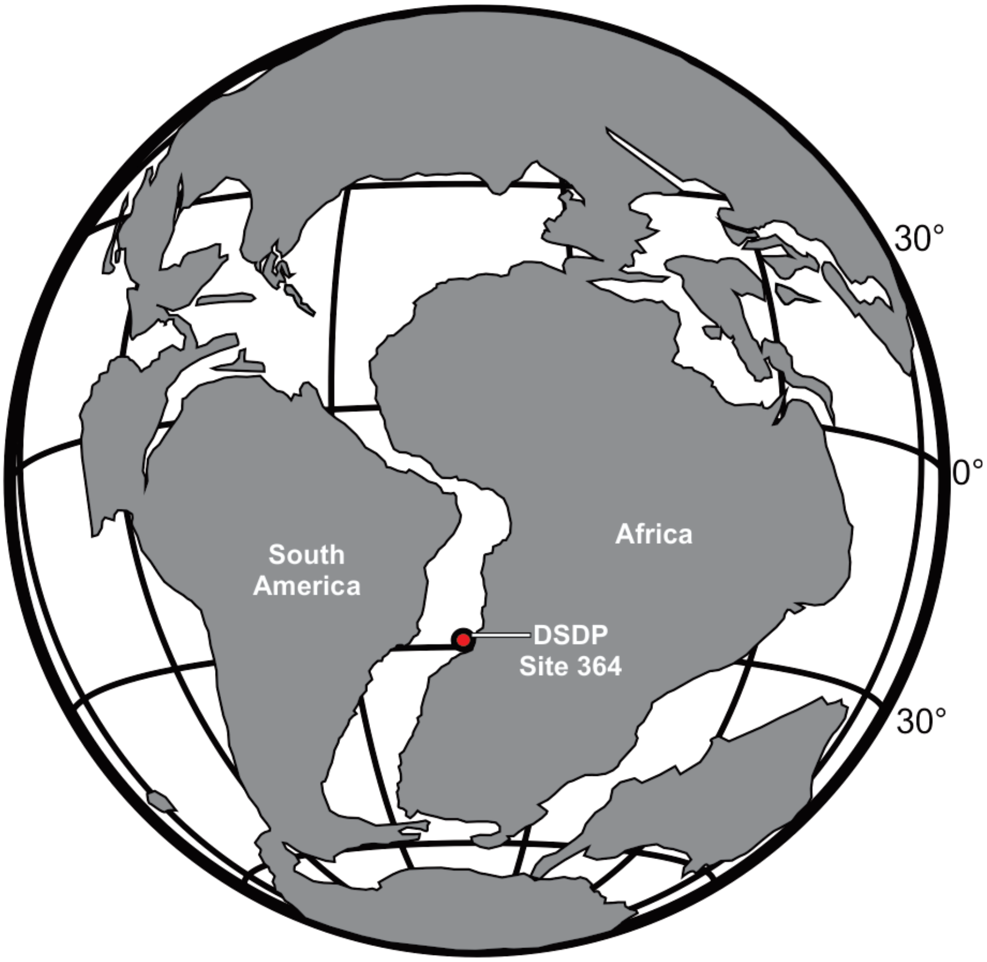

882 **Figure 1.** Paleogeographic reconstruction for 110 Ma. Modified from ODSN Plate Tectonic
883 Reconstruction Service, showing the inferred location of Site 364.

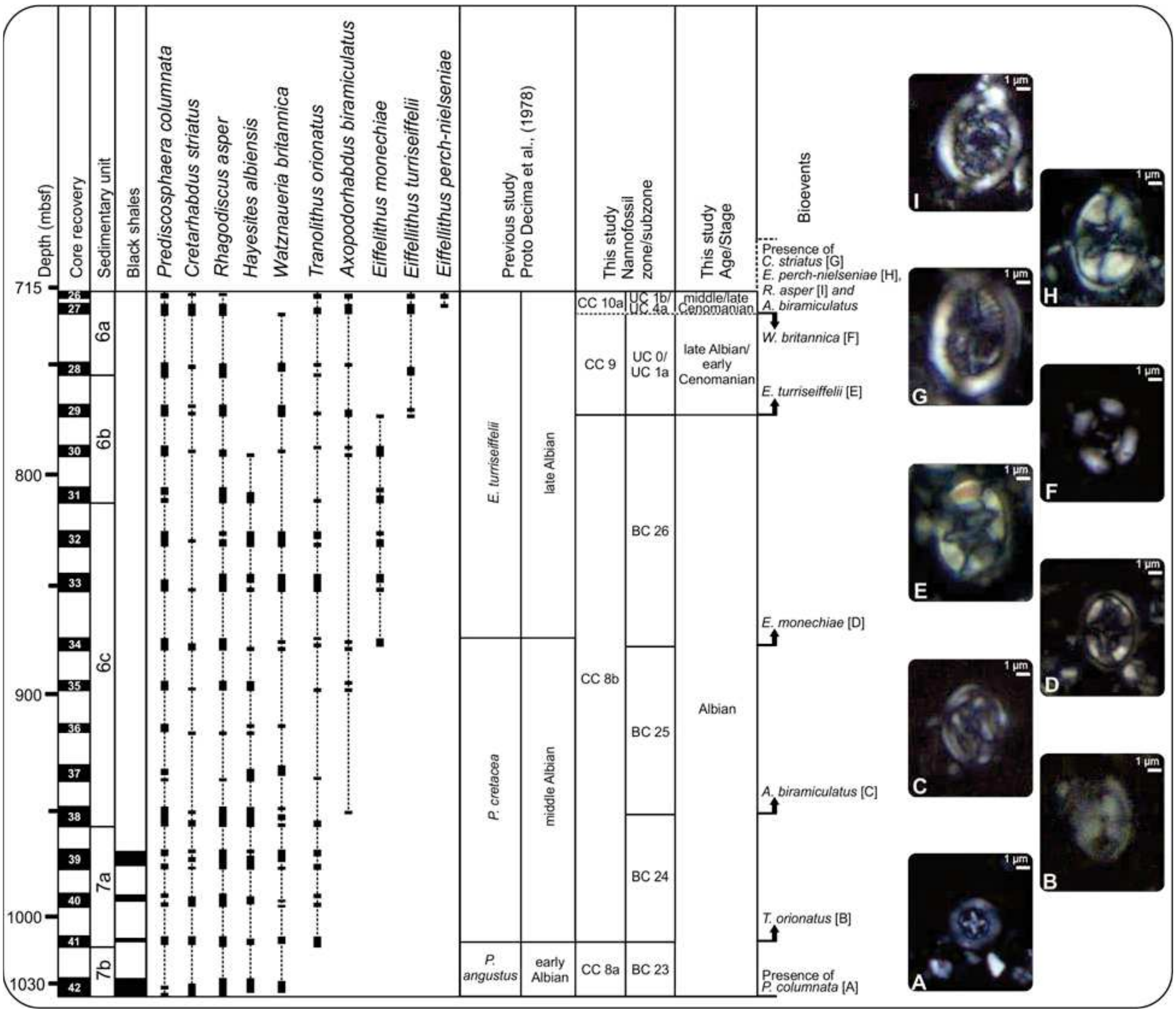

Figure 2. Biostratigraphic of selected taxa from Site 364. Calcareous nannofossil biostratigraphy is based on the zonation schemes: CC zones of Sissingh (1977) and Perch-Nielsen (1979, 1985), BC zonation of Bown et al., (1998) and the UC of Burnett et al., (1998). The distribution of black shale layers and sedimentary units is based on data from Bolli et al., (1978).

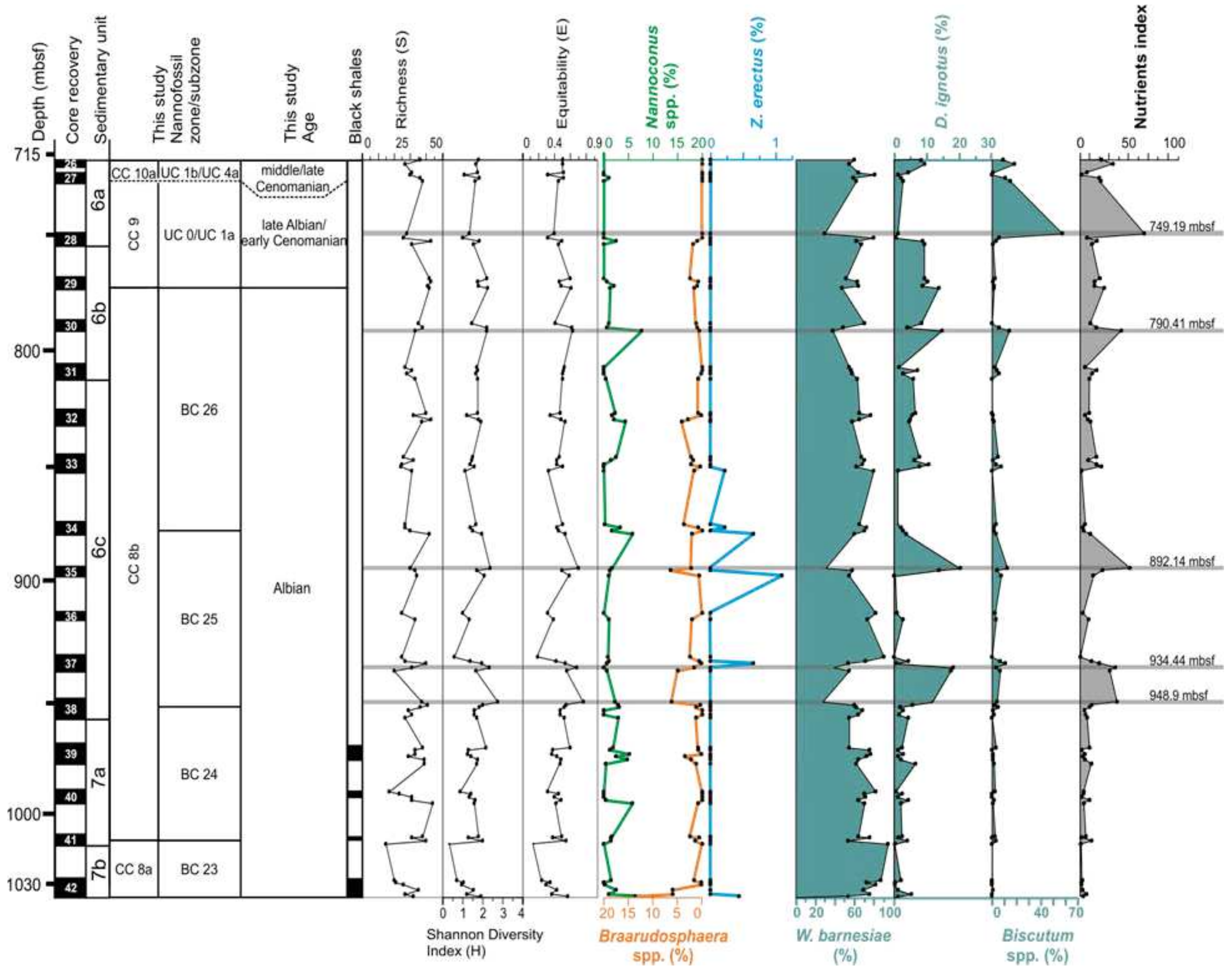

893 **Figure 3.** Values for Richness (S), Shannon Diversity Index (H), Equitability (E), abundances of major taxa and the Nutrients Index from Site 364. The samples with increased Nutrients Index and low-abundance of Watznaueria barnesiae are indicated by gray horizontal shading.

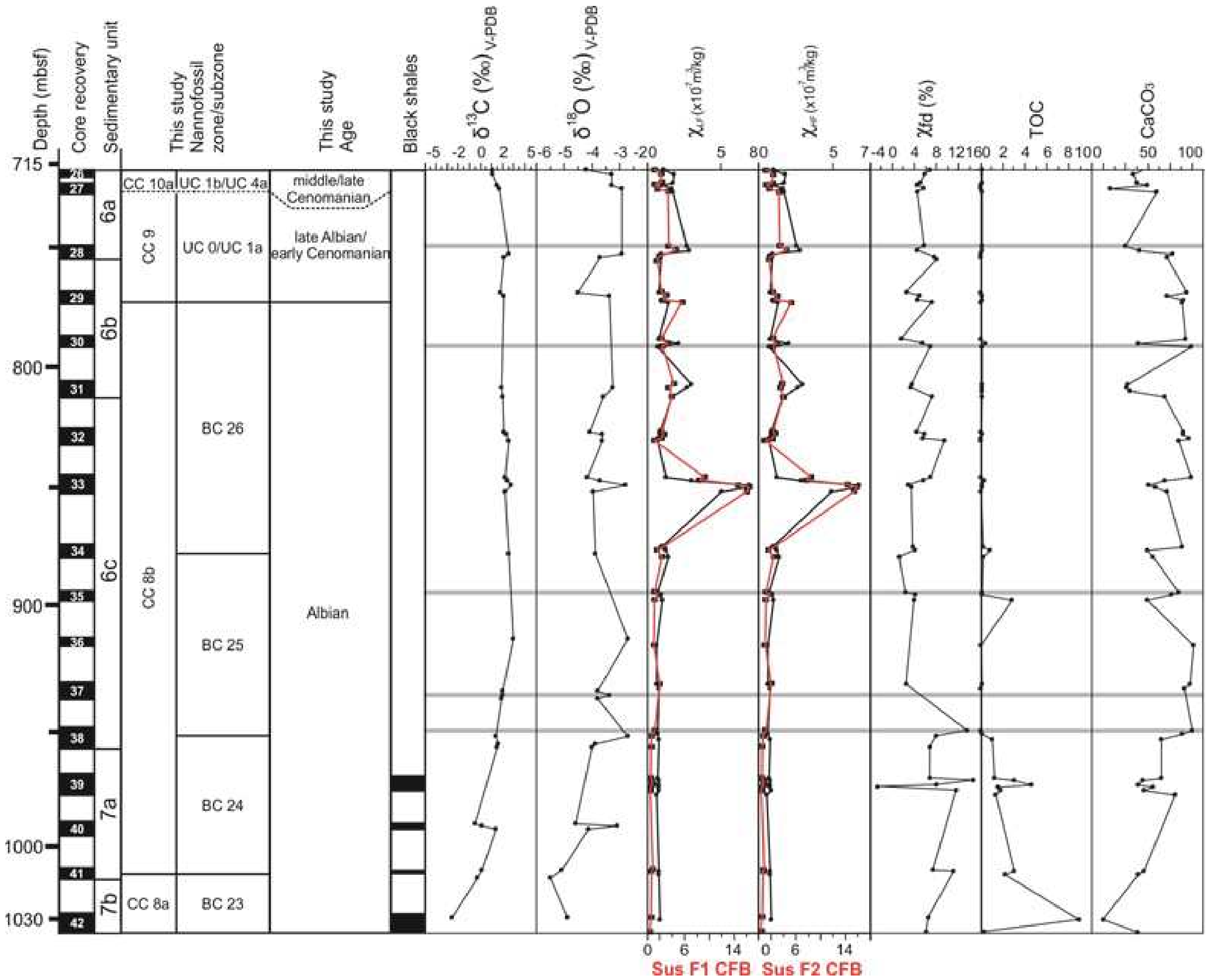

Figure 4. Distribution of carbon ($\delta^{13}C$) and oxygen ($\delta^{18}O$) isotope values, magnetic susceptibility (χ_{lf}, χ_{hf}, χ_{fd}%, and carbonate-free based), TOC and CaCO3 in the Site 364. The samples with increased Nutrient Index and low-abundance of *W. barnesiae* are indicated by gray horizontal shading.

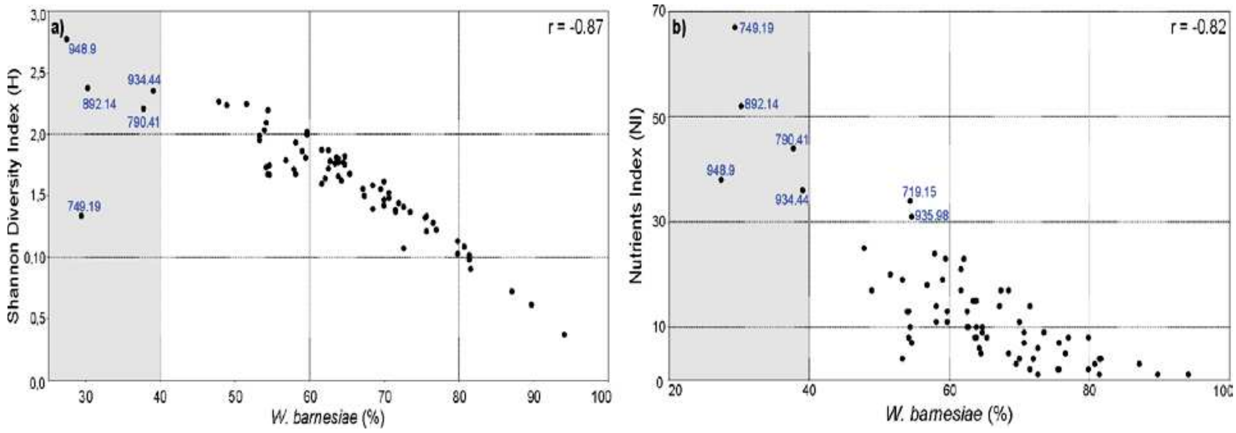

Figure 5. Array of *Watznaueria barnesiae* abundance compared to Shannon Diversity Index (H) and Nutrients Index (NI). a) For the relationship between *W. barnesiae* (%) and H the person correlation coefficients (r) is negative and significant, suggesting that the assemblage suffered from dissolution. b) For the relationship between *W. barnesiae* (%) and NI the r is negative and significant, showing high NI values when the percentage of *W. barnesiae* is below 40%.

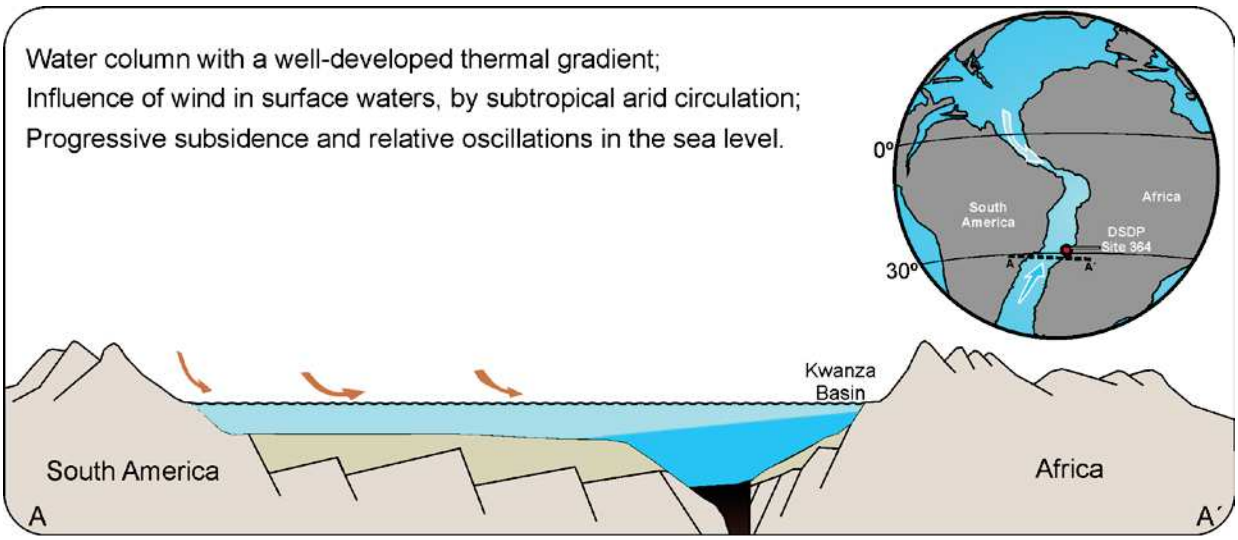

Figure 6. Paleoceanographic inferences for the South Atlantic. The thermal gradient of the water column is evidenced by the paleobiogeographic contrast between planktonic and benthonic microfossil assemblages. The arrows illustrate different causes for these variations, such as wind in surface waters (brown) and fluctuations in the inflow of surface (light blue) and deep-water (dark blue) masses (Poulsen et al., 2001; Azevedo, 2004; Hay, 2008; Hasegawa et al., 2012; Haq, 2014; Kochhann et al., 2014; Pérez-Díaz & Eagles, 2017).

Table 1. Calcareous nannofossil paleoecological indices considered in this study.

	Paleoecologic preferences						
Calcareous nannofossil	Dissolution resistant	Neritic environment	Restricted sea (and/or Epicontinental Basin, Upwelling assemblage, Oceanic Plateau)	Continental Margins (Near-shore)	Offshore (Deep basin and Open ocean)	High carbonate productivity/surface water fertility	Low carbonate productivity/surface water fertility
Biscutum spp. (include *Biscutum ubiquem*, *Biscutum* sp. 1 and *Biscutum sp. 2)*			2, 3, 10, 12, 23	2, 3, 24, 35		2, 3, 8, 9, 11, 12, 14, 16, 20, 21, 22, 24, 26, 27, 29, 31, 32, 33, 36	
Discorhabdus ignotus			12			12, 14, 15, 27	
Zeugrhabdotus erectus			3, 10	2, 3, 24		2, 8, 9, 11, 14, 22, 26, 27, 29, 31, 32, 33	
Watznaueria barnesiae	2, 5, 7, 8, 9, 14, 16, 18, 19, 23, 25, 30, 31				3, 8, 29, 35		9, 16, 19, 22, 24, 27, 28, 31, 32
Nannoconus spp. (include *Nannoconus* sp.1, *N. fragilis, N. truittii subsp. frequens, N. truittii subsp. rectangularis, N. truittii subsp. truittii and N. troelsenii*)	17, 29	2, 4, 8, 9, 24	1, 3, 8, 9, 13, 29	3, 6, 9, 13		12, 14, 34	
Braarudosphaera spp. (include *B. africana, B. batiliformis, B. hockwoldensis, B. primula, B. pseudobatilliformis* and *B. regularis*)		2, 6, 24	3	3, 6		3	

1. Thierstein (1976); 2. Roth (1981); 3. Roth & Bowdler (1981); 4. Doeven (1983); 5. Roth (1984); 6. Stradner et al., (1984); 7. Perch-Nielsen (1985); 8. Roth (1986); 9. Roth & Krumbach (1986); 10. Roth (1989); 11. Watkins (1989); 12. Premoli-Silva et al., (1989); 13. Busson & Noel (1991); 14. Erba (1992a); 15. Erba (1992b); 16. Erba et al., (1992); 17. Erba (1994); 18. Erba et al., (1995); 19. Willians & Bralower (1995); 20. Eshet & Almogi-Labin (1996); 21. Gardin & Monechi (1998); 22. Fisher & Hay (1999); 23. Mutterlose & Kessels (2000); 24. Street & Bown (2000); 25. Luciani et al., (2001); 26. Gardin (2002); 27. Herrle et al., (2003); 28. Friedrich et al., (2005); 29. Less et al., (2005); 30. Watkins & Self Trail (2005); 31. Kulhanek & Wise (2006); 32. Thibault & Gardin (2006); 33. Hardas & Mutterlose (2007); 34. Browning & Watkins (2008); 35. Linnert et al., (2011); 36. Thibault & Husson (2016).

Table 2. Data from the five samples with increased Nutrient Index and low-abundance of *Watznaueria barnesiae*. Planktonic and benthonic foraminifera data, according to Kochhann et al., (2013, 2014).

Samples (mbsf)	Richness (S)	Shannon Diversity (H)	Equitability (E)	*W. barnesiae* (%)	*D. ignotus* (%)	*Biscutum* spp. (%)	*Z. erectus* (%)	*Nannoconus* spp. (%)	*Braarudosphaera* spp. (%)	Nutrient Index	Susceptibility F1 (m^3/kg)	Susceptibility F3 (m^3/kg)	TOC (%)	$CaCO_3$ (%)	% Planktonic foraminiferal (Kochhann et al., 2013)	% Benthic foraminiferal (Kochhann et al., 2014)	Preservation Index (Kochhann et al., 2013)
749.19	28,00	1,337	0,4013	29	2	58	0	0	0	67	2,44E-07	2,30E-07	0,11	30,90	97.1	2.9	Good
790.41	33,00	2,209	0,6317	38	15	14	0	8	1	44	2,53E-08	2,36E-08	0,14	90,03	100,00	0,00	Moderate
892.14	30,00	2,375	0,6984	30	20	13	0	2	2	52	2,60E-08	2,54E-08	0,15	78,16	100,00	0,00	Poor
934.44	31,00	2,352	0,6849	39	18	4	0	0	2	36					100,00	0,00	Moderate
948.9	37,00	2,772	0,7676	27	12	5	0	2	6	38	2,08E-08	1,80E-08	0,19	81,59	100,00	0,00	Poor

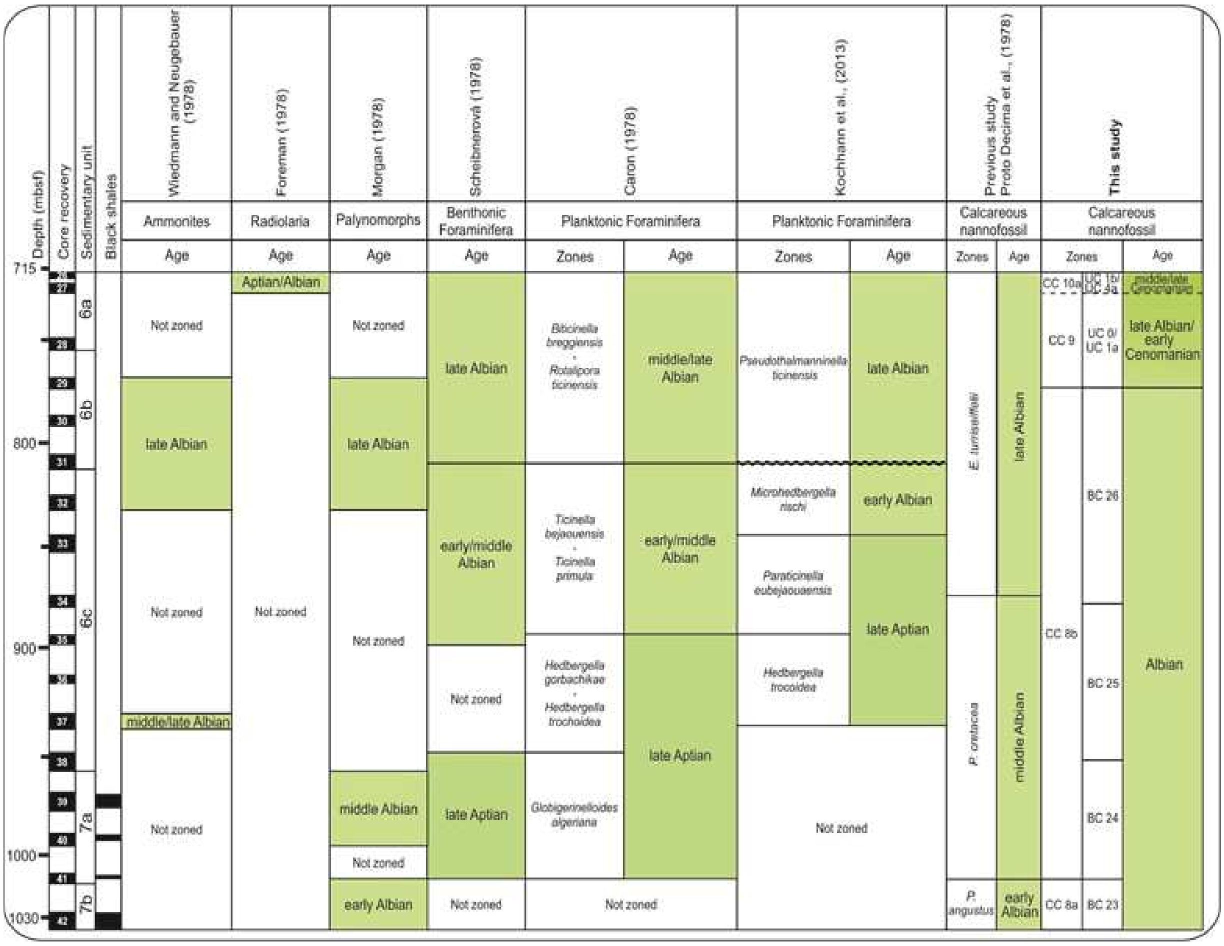

Figure S1. Correlation between the biostratigraphic zonations of calcareous nannofossils, planktonic and benthonic foraminifera, ammonites, palynomorphs and radiolarians for Site 364.

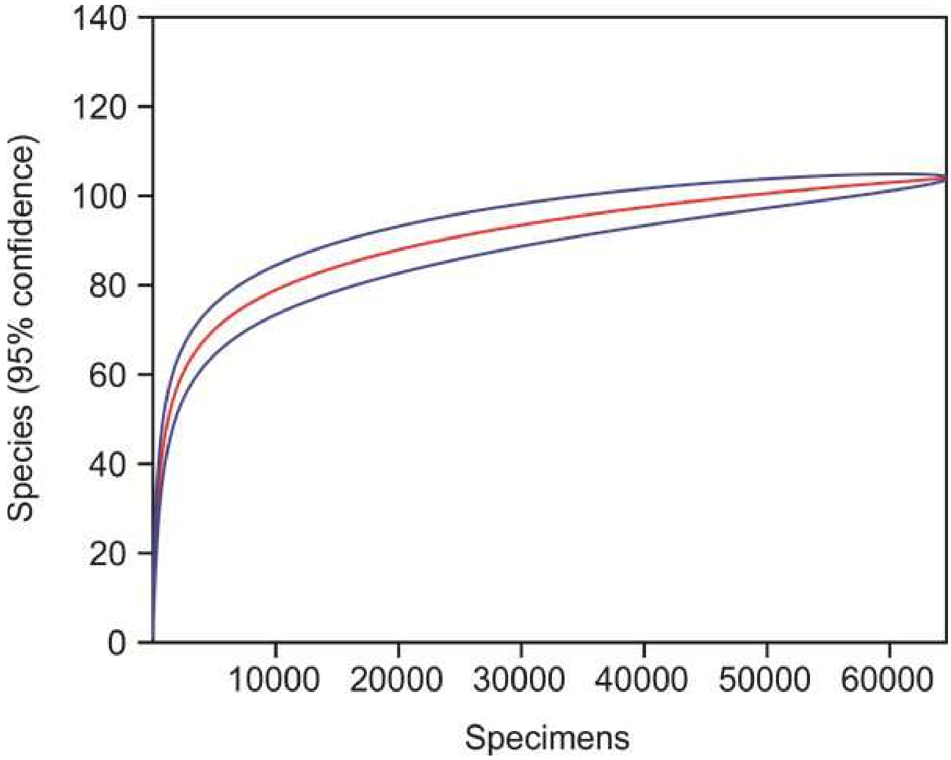

Figure S2. Rarefaction curve, based on 72 samples, show number of specimens against number of species richness recorded in different samples from Site 364. This curve strongly suggests that the majority of the calcareous nannofossil species have been found. Future collecting efforts may occasionally yield new species, but the total number of species is not expected not change substantially.

Table S1. Calcareous nannofossil data and biostratigraphic summary, Site 364, Kwanza Basin.

Core	Section	Interval (cm)	Depth (mbsf)	Preservation	Nº Field of View	Species Richness	Total	Coccospheres	*Watznaueria barnesiae*	*Discorhabdus ignotus*	Biological events	Previous study Proto Decima (1978)		CC ZONES/SUBZONES	BC and UC ZONES/SUBZONES	AGE/STAGE
26	5	73-77	717.23	O1-E1	19	36	456	x	271	38	Presence of *C. striatus*, *E. perch-nielseniae*, *R. asper* and *A. biramiculatus*.	*E. turriseiffelii*	late Albian	CC 10a	UC 1b/ UC 4a	middle/late Cenomanian
26	6	115-117	719.15	O1-E1	34	27	456	x	248	44						
Coring gap - 1.50 m																
27	2	125-128	722.75	O1-E1	38	32	456	x	291	21						
27	3	67-71	723.67	O1-E1	20	30	456	x	368	7						
27	4	74-77	725.24	O1-E1	25	37	456	x	269	11						
27	5	66-70	726.66	O2-E2	28	38	456	x	283	14	LAD *W. britannica*					
Coring gap - 19 m																
28	1	69-73	749.19	O1-E1	21	27	456		134	7				CC 9	UC 0/ UC 1a	late Albian/ early Cenomanian
28	2	70-74	750.7	O1-E1	12	26	456		364	3						
28	3	87-91	752.37	O1-E1	18	43	456		281	40						
28	4	64-68	753.64	O1-E1	27	31	456	x	306	44						
Coring gap - 12.50 m																
29	1	69-71	768.19	O1-E1	33	42	456		235	44						
29	2	33-37	769.33	O1-E1	28	43	456		289	48						
29	3	67-71	771.17	O1-E1	17	41	456	x	291	40						
29	4	34-37	772.34	O1-E1	39	42	456		218	64	FAD *E. turriseiffelii*					
Coring gap - 12.50 m																
30	1	66-70	787.16	O2-E2	44	35	456		319	39				CC 8b	BC 26	Albian
30	2	94-98	788.94	O1-E1	15	39	456	x	223	19						
30	3	91-94	790.41	O1-E1	79	33	456		172	68						
Coring gap - 14 m																
31	1	79-82	806.29	O1-E1	24	27	456	x	247	8						
31	2	40-42	807.4	O1-E1	42	31	456	x	259	34						
31	3	41-44	808.91	O1-E1	58	28	456		265	14						
31	4	94-98	810.94	O1-E1	54	33	456		286	28						
Coring gap - 12.50 m																
32	1	123-127	825.73	O1-E1	41	40	456		295	31						
32	2	40-44	826.4	O2-E2	56	32	456		351	27						
32	3	90-92	828.4	O1-E1	110	43	456	x	295	23						
32	4	46-50	829.46	O1-E1	142	37	456		265	22						
Coring gap - 12.50 m																
33	1	107-111	844.57	O1-E2	197	26	456		306	37						
33	2	92-95	845.92	O1-E1	13	32	456	x	322	29						
33	3	93-95	847.43	O1-E1	22	25	456	x	312	49						
33	4	63-67	848.63	O2-E1	18	24	456		281	37						
33	5	65-69	850.15	O2-E1	21	31	456	x	364	7						
Coring gap - 20 m																
34	1	133-136	873.33	O1-E1	45	27	456		298	7		*P. cretacea*	middle Albian			
34	2	93-96	874.43	O1-E1	63	27	456		331	11						
34	3	96-99	875.96	O1-E1	31	30	456	x	322	14						
34	4	92-96	877.42	O1-E1	23	42	456		272	18	FAD *E. monechiae*					
Coring gap - 12.50 m																
35	1	114-117	892.14	O1-E1	41	30	456		138	93					BC 25	
35	2	46-49	892.96	O2-E1	43	33	456	x	264	63						
35	3	99-101	894.99	O1-E1	44	34	456	x	247							
Coring gap - 14 m																
36	1	125-128	911.25	O1-E1	73	25	456	x	371	5						
36	2	52-54	912.02	O2-E2	456	21	297	x	231	1						
36	3	75-77	913.75	O1-E2	210	33	456		335	14						
Coring gap - 14 m																
37	1	66-68	929.66	O2-E2	100	25	456		409	1						
37	2	120-122	931.7	O2-E2	70	27	456		326	20						
37	3	45-47	932.45	O1-E2	46	40	456	x	243	4						
37	4	94-97	934.44	O1-E1	61	31	456		178	84						
37	5	98-101	935.98	O1-E1	413	20	456		249	81						
Coring gap - 11 m																
38	1	90-93	948.9	O2-E1	77	37	456		125	55						
38	2	103-105	950.53	O1-E1	62	41	456		272	26						
38	3	47-49	951.47	O1-E1	51	36	456		285	9	FAD *A. biramiculatus*					
38	4	27-30	952.77	O1-E1	27	29	456		312	13					BC 24	
38	5	53-55	954.53	O1-E1	15	31	456	x	293	8						
38	6	25-28	955.75	O1-E1	46	27	456	x	249	20						
Coring gap - 9.5 m																
39	1	145-148	968.45	O1-E1	34	38	456		248	12						
39	2	114-119	969.64	O1-E1	43	33	456	x	345	6						
39	3	118-122	971.18	O1-E1	39	33	456	x	349	14						
39	4	66-69	972.16	O1-E1	31	29	456	x	328	7						
39	5	89-92	973.89	O1-E1	36	39	456	x	294	11						
39	6	99-101	975.49	O2-E2	49	39	456	x	285	31						
Coring gap - 10.70 m																
40	1	142-147	987.42	O2-E2	198	17	456		372	3						
40	2	92-96	988.42	O2-E2	41	23	456	x	319	12						
40	3	71-75	989.71	O1-E1	33	31	456	x	326	7						
40	4	66-68	991.16	O1-E2	76	31	456		291	20						
40	5	63-66	992.63	O1-E1	21	44	456	x	319	10						
Coring gap - 12.50 m																
41	1	141-145	1006.41	O1-E2	56	38	456	x	290	12						
41	2	46-50	1006.96	O1-E1	46	31	456	x	344	7						
41	3	41-44	1008.41	O1-E1	73	40	456	x	246	19						
41	4	29-32	1009.79	O1-E1	44	15	456	x	429	2	FAD *T. orionatus*					
Coring gap - 13 m																
42	1	137-139	1025.37	O1-E1	342	20	456		397	11	Presence of *P. columnata*	*P. angustus*	early Albian	CC 8a	BC 23	
42	2	81-84	1026.31	O1-E1	41	21	456	x	331	2						
42	3	24-28	1027.24	O1-E2	37	26	456	x	371	2						
42	4	100-125	1029.50	O1-E2	29	35	456	x	317	7						
42	5	121-125	1031.21	O1-E2	41	27	456		345	25						
42	6	87-90	1032.37	O1-E2	45	32	456	x	243	6						

Core	Section	*Zeugrhabdotus embergeri*
26	5	4
26	6	2
27	2	4
27	3	1
27	4	7
27	5	2
28	1	1
28	2	
28	3	5
28	4	4
29	1	8
29	2	2
29	3	3
29	4	20
30	1	5
30	2	8
30	3	2
31	1	43
31	2	1
31	3	7
31	4	4
32	1	3
32	2	3
32	3	7
32	4	23
33	1	1
33	2	5
33	3	5
33	4	6
33	5	3
34	1	4
34	2	2
34	3	11
34	4	11
35	1	2
35	2	6
35	3	10
36	1	
36	2	2
36	3	
37	1	1
37	2	1
37	3	19
37	4	9
37	5	9
38	1	6
38	2	3
38	3	1
38	4	
38	5	1
38	6	3
39	1	12
39	2	11
39	3	6
39	4	
39	5	5
39	6	2
40	1	4
40	2	1
40	3	1
40	4	18
40	5	11
41	1	4
41	2	14
41	3	2
41	4	5
42	1	8
42	2	70
42	3	20
42	4	1
42	5	2
42	6	1

Table S2. Calcareous nannofossil and geochemical data, Site 364, Kwanza Basin.

Core	Section	Interval (cm)	Depth (mbsf)	Sedimentary Units	Total	Samples (mbsf)	Richness (S)	Shannon Diversity (H)	Equitability (E)	*W. barnesiae* (%)	*D. ignotus* (%)	*Biscutum* spp. (%)	*Z. erectus* (%)	Nutrient Index	Samples (mbsf)	$\delta^{13}C_{V\text{-}PDB}$ (‰)	$\delta^{18}O_{V\text{-}PDB}$ (‰)	Susceptibility F1 (m^3/kg)	Susceptibility F3 (m^3/kg)	TOC (%)	$CaCO_3$ (%)
26	5	73-77	717.23		456	717.23	36,00	1,809	0,5048	59	8	10	0	23	717,23	1,140000000000	-4,170000000000	0,000000063850	0,000000059560	0,13	46,65
26	6	115-117	719.15		456	719.15	27,00	1,674	0,508	54	10	18	0	34	719,15	1,060000000000	-3,290000000000	0,000000149900	0,000000141200	0,11	38,10
27	2	125-128	722.75		456	722.75	31,00	1,769	0,5152	64	5	1	0	8	722,75			0,000000136600	0,000000129900	0,13	41,09
27	3	67-71	723.67		456	723.67	30,00	1,085	0,3189	81	2	1	0	3	723,67	1,530000000000	-3,280000000000	0,000000063400	0,000000060670	0,08	50,68
27	4	74-77	725.24	6a	456	725.24	36,00	1,862	0,5197	59	2	11	0	19	725,24	1,710000000000	-2,890000000000	0,000000128800	0,000000121700	0,09	17,45
27	5	66-70	726.66		456	726.66	38,00	1,64	0,4509	62	3	16	0	23	726,66			0,000000137600	0,000000131400	0,12	58,91
28	1	69-73	749.19		456	749.19	28,00	1,337	0,4013	29	2	58	0	67	749,19			0,000000243600	0,000000230300	0,11	30,90
28	2	70-74	750.7		456	750.7	26,00	1,029	0,3158	80	1	6	0	8	750,7			0,000000260000	0,000000248600	0,12	42,81
28	3	87-91	752.37		456	752.37	43,00	1,873	0,4981	62	9	4	0	17	752,37	2,570000000000	-2,900000000000	0,000000048820	0,000000045030	0,05	73,07
28	4	64-68	753.64		456	753.64	31,00	1,556	0,4531	67	10	2	0	14	753,64	2,170000000000	-3,700000000000	0,000000053820	0,000000049510	0,10	68,35
29	1	69-71	768.19		456	768.19	42,00	2,245	0,6008	52	10	3	0	20	768,19	1,840000000000	-4,490000000000	0,000000034550	0,000000033640	0,09	85,58
29	2	33-37	769.33		456	769.33	43,00	1,763	0,4686	63	11	1	0	15	769,33	2,140000000000	-3,370000000000	0,000000094490	0,000000089870	0,13	68,41
29	3	67-71	771.17		456	771.17	41,00	1,798	0,4842	64	9	2	0	15	771,17			0,000000046630	0,000000044490	0,12	83,27
29	4	34-37	772.34		456	772.34	42,00	2,266	0,6063	48	14	2	0	25	772,34			0,000000100500	0,000000092140	0,10	81,74
30	1	66-70	787.16		456	787.16	35,00	1,468	0,413	70	9	0	0	11	787,16			0,000000034020	0,000000033390	0,07	85,40
30	2	94-98	788.94	6b	456	788.94	38,00	2,235	0,6146	49	4	6	0	17	788,94			0,000000179000	0,000000169700	0,49	42,62
30	3	91-94	790.41		456	790.41	33,00	2,209	0,6317	38	15	14	0	44	790,41			0,000000025320	0,000000023610	0,14	90,03
31	1	79-82	806.29		456	806.29	27,00	1,73	0,5248	54	2	3	0	8	806,29			0,000000279300	0,000000266100	0,19	32,54
31	2	40-42	807.4		456	807.4	31,00	1,787	0,5203	57	7	5	0	18	807,4	1,960000000000	-3,250000000000	0,000000243400	0,000000232300	0,19	31,52
31	3	41-44	808.91		456	808.91	28,00	1,675	0,5028	58	3	6	0	14	808,91					0,11	35,15
31	4	94-98	810.94		456	810.94	33,00	1,78	0,5091	63	6	1	0	10	810,94	2,070000000000	-3,580000000000	0,000000133500	0,000000124100	0,18	66,51
32	1	123-127	825.73		456	825.73	40,00	1,754	0,4753	65	7	1	0	10	825,73	2,110000000000	-4,080000000000	0,000000039930	0,000000038220	0,08	83,03
32	2	40-44	826.4		456	826.4	32,00	1,223	0,3529	77	6	1	0	8	826,4	2,330000000000	-3,600000000000	0,000000040660	0,000000038310	0,17	83,09
32	3	90-92	828.4		456	828.4	43,00	1,82	0,484	65	5	1	0	9	828,4			0,000000026850	0,000000025450	0,10	87,89
32	4	46-50	829.46		456	829.46	37,00	1,933	0,5353	58	5	2	0	11	829,46	2,570000000000	-3,620000000000	0,000000022420	0,000000020380	0,07	78,76
33	1	107-111	844.57		456	844.57	26,00	1,5	0,4603	67	8	5	0	17	844,57	2,210000000000	-4,130000000000	0,000000084940	0,000000078300	0,06	90,57
33	2	92-95	845.92		456	845.92	32,00	1,483	0,4279	71	6	1	0	9	845,92	2,420000000000	-3,690000000000	0,000000279400	0,000000264500	0,34	66,37
33	3	93-95	847.43		456	847.43	25,00	1,394	0,4331	68	11	4	0	17	847,43	2,720000000000	-2,780000000000	0,000000712000	0,000000691000	0,15	51,72
33	4	63-67	848.63		456	848.63	24,00	1,598	0,5029	62	8	8	0	21	848,63			0,000000696900	0,000000673200	0,15	57,65
33	5	65-69	850.15		456	850.15	31,00	1,132	0,3297	80	2	0	0	2	850,15	2,250000000000	-3,920000000000	0,000000508600	0,000000484900	0,07	68,57
34	1	133-136	873.33		456	873.33	27,00	1,678	0,5091	65	2	4	0	8	873,33			0,000000048780	0,000000046960	0,22	81,54
34	2	93-96	874.43		456	874.43	27,00	1,409	0,4274	73	2	2	0	6	874,43			0,000000088620	0,000000085020	0,90	50,38
34	3	96-99	875.96		456	875.96	30,00	1,524	0,4482	71	3	2	0	7	875,96	2,500000000000	-3,840000000000				
34	4	92-96	877.42		456	877.42	42,00	1,998	0,5345	60	4	4	1	11	877,42			0,000000103700	0,000000102300	0,21	55,53
35	1	114-117	892.14		456	892.14	30,00	2,375	0,6984	30	20	13	0	52	892,14			0,000000026010	0,000000025380	0,15	78,16
35	2	46-49	892.96	6c	456	892.96	33,00	1,715	0,4905	58	14	4	0	24	892,96			0,000000050540	0,000000048470	0,19	72,38
35	3	99-101	894.99		456	894.99	34,00	2,092	0,5934	54	0	8	1	13	894,99			0,000000057610	0,000000055350	2,89	50,21
36	1	125-128	911.25		456	911.25	25,00	1,019	0,3165	81	1	3	0	4	911,25	2,940000000000	-2,690000000000				
36	3	75-77	913.75		456	913.75	33,00	1,369	0,3915	73	3	4	0	9	913,75			0,000000011400	0,000000010380	0,13	88,99
37	1	66-68	929.66		456	929.66	25,00	0,6154	0,1912	90	0	0	0	1	929,66			0,000000034400	0,000000033450	0,10	83,34
37	2	120-122	931.7		456	931.7	27,00	1,387	0,4209	71	4	7	0	14	931,7	1,990000000000	-3,760000000000				
37	3	45-47	932.45		456	932.45	40,00	1,987	0,5386	53	1	12	1	19	932,45	2,050000000000	-3,360000000000				
37	4	94-97	934.44		456	934.44	31,00	2,352	0,6849	39	18	4	0	36	934,44	1,940000000000	-3,770000000000				
37	5	98-101	935.98		456	935.98	20,00	1,67	0,5575	55	18	7	0	31	935,98					0,09	90,64
38	1	90-93	948.9		456	948.9	37,00	2,772	0,7676	27	12	5	0	38	948,9			0,000000020800	0,000000018040	0,19	81,59
38	2	103-105	950.53		456	950.53	41,00	2,019	0,5438	60	6	3	0	13	950,53	1,370000000000	-2,680000000000				
38	3	47-49	951.47		456	951.47	36,00	1,87	0,5219	63	2	5	0	10	951,47			0,000000032120	0,000000029580	1,13	62,89
38	4	27-30	952.77		456	952.77	29,00	1,584	0,4703	68	3	1	0	5	952,77	1,570000000000	-3,860000000000				
38	5	53-55	954.53		456	954.53	31,00	1,623	0,4726	64	2	2	0	6	954,53	1,560000000000	-3,980000000000				
38	6	25-28	955.75		456	955.75	27,00	1,747	0,5301	55	4	0	0	7	955,75			0,000000027750	0,000000025860	1,27	63,06
39	1	145-148	968.45		456	968.45	38,00	2,195	0,6033	54	3	4	0	10	968,45			0,000000030990	0,000000028880	3,02	46,85
39	2	114-119	969.64		456	969.64	33,00	1,333	0,3812	76	1	0	0	2	969,64			0,000000036620	0,000000031290	4,60	42,48
39	3	118-122	971.18		456	971.18	33,00	1,28	0,3661	77	3	1	0	5	971,18			0,000000036740	0,000000033830	1,58	56,16
39	4	66-69	972.16		456	972.16	29,00	1,441	0,428	72	2	1	0	4	972,16			0,000000034820	0,000000035940	1,81	47,20
39	5	89-92	973.89		456	973.89	39,00	1,769	0,4828	64	2	1	0	5	973,89			0,000000011470	0,000000010150	1,44	75,26
39	6	99-101	975.49		456	975.49	39,00	1,72	0,4696	63	7	2	0	13	975,49	-0,420000000000	-4,580000000000				
40	1	142-147	987.42		456	987.42	17,00	0,906	0,3198	82	1	3	0	4	987,42	0,150000000000	-3,050000000000				
40	2	92-96	988.42	7a	456	988.42	23,00	1,42	0,453	70	3	0	0	4	988,42	1,360000000000	-4,110000000000				
40	3	71-75	989.71		456	989.71	31,00	1,37	0,399	71	2	0	0	2	989,71						
40	4	66-68	991.16		456	991.16	31,00	1,658	0,4827	64	4	2	0	10	991,16						
40	5	63-66	992.63		456	992.63	44,00	1,615	0,4269	70	2	1	0	4	992,63	0,120000000000	-5,070000000000				
41	1	141-145	1006.41		456	1006.41	38,00	1,812	0,498	64	3	3	0	8	1006,41			0,000000031830	0,000000029550	3,03	47,68
41	2	46-50	1006.96		456	1006.96	31,00	1,321	0,3846	75	2	0	0	2	1006,96			0,000000030920	0,000000027450	2,26	42,12
41	3	41-44	1008.41		456	1008.41	40,00	2,034	0,5515	54	4	4	0	13	1008,41	-0,210000000000	-5,470000000000				
41	4	29-32	1009.79		456	1009.79	15,00	0,3715	0,1372	94	0	0	0	1	1009,79						
42	1	137-139	1025.37		456	1025.37	20,00	0,7225	0,2412	87	2	0	0	3	1025,37	-2,590000000000	-4,850000000000				
42	2	81-84	1026.31		456	1026.31	21,00	1,073	0,3525	73	0	1	0	1	1026,31			0,000000040070	0,000000037540	8,91	11,08
42	3	24-28	1027.24	7b	456	1027.24	26,00	0,9838	0,302	81	0	0	0	1	1027,24						
42	4	100-125	1029.50		456	1029.50	35,00	1,554	0,437	70	2	1	0	3	1029,5						
42	5	121-125	1031.21		456	1031.21	27,00	1,211	0,3673	76	5	0	0	7	1031,21						
42	6	87-90	1032.37		456	1032.37	32,00	1,953	0,5635	53	1	1	0	4	1032,37			0,000000023150	0,000000021740	0,40	39,77

Table S3. Minimum, maximum and average of calcareous nannofossil and geochemical data, in the basal and top sections studied from Site 364, Kwanza Basin.

Data		Basal Section (1032.37-968.45 mbsf)	Top Section (955.75-717.23 mbsf)
Sedimentary Unit		7	6
Richness (S)	Minimum	15	20
	Average	31	33
	Maximum	44	43
Shannon Diversity (H)	Minimum	0.37	0.62
	Average	1.42	1.71
	Maximum	2.2	2.77
Equitability (E)	Minimum	0.14	0.19
	Average	0.41	0.49
	Maximum	0.60	0.77
W. barnesiae (%)	Minimum	53	27
	Average	71	61
	Maximum	94	90
D. ignotus (%)	Minimum	0.4	0
	Average	2	6
	Maximum	7	20
Biscutum spp. (%)	Minimum	0	0
	Average	1	6
	Maximum	4	58
Nutrient Index	Minimum	1	1
	Average	5	17
	Maximum	13	67
$\delta^{13}C_{V\text{-}PDB}$ (‰)	Minimum	-2.59	1.06
	Average	1.36	2.03
	Maximum	-0.27	2.94
$\delta^{18}O_{V\text{-}PDB}$ (‰)	Minimum	-5.47	-4.49
	Average	-4.52	-3.55
	Maximum	-3.05	-2.68
Susceptibility F1 (m^3/kg)	Minimum	1,15E-08	1.14E-08
	Average	2,87E-08	1.34E-07
	Maximum	4,01E-08	7.12E-07
Susceptibility F3 (m^3/kg)	Minimum	1,02E-08	1.04E-08
	Average	2,71E-08	1.28E-07
	Maximum	3,75E-08	6.91E-07
χ_{fd} (%)	Minimum	-3.22	1.35
	Average	7.6	5.4
	Maximum	14.56	13.27
TOC (%)	Minimum	0.40	0.055
	Average	3	0.3
	Maximum	8.91	2.89
CaCO3 (%)	Minimum	11.08	17.45
	Average	45.40	64.22
	Maximum	75.26	90.64

CONSIDERAÇÕES FINAIS

O estudo dos nanofósseis calcários do Albiano no Site 364 apresenta uma assembleia contendo 103 táxons que são típicos do intervalo Albiano–Cenomaniano. Foi possível observar uma ocorrência contínua de bioeventos descritos para este intervalo de tempo. Portanto, a partir do estudo bioestratigráfico não foram observados indícios de retrabalhamento e hiatos na seção estudada.

A assembleia recuperada também fornece uma importante contribuição ao entendimento da influência das correntes marinhas superficiais, considerando que a assembleia é constituída em sua totalidade por espécies com afinidade subtropical-tropical. Este dado paleobiogeográficos corroboram os estudos de Kochhann et al., (2013, 2014) sobre as influências das águas superficiais da região central do Oceano Atlântico na Bacia de Kwanza, Angola.

A dissolução do carbonato de cálcio é um processo com significativos efeitos na preservação e abundância dos nanofósseis calcários no *Site* 364, os dados sedimentológicos, micropaleontológicos e geoquímicos permitem observar registros dos efeitos da dissolução de modo qualitativo ao longo da seção estudada. O material carbonático sofreu dissolução e forte recristalização na seção basal do testemunho, onde é possível observar graus baixos a médios destes processos nos táxons observados. Os sinais isotópicos sofreram alterações, possivelmente devido a dissolução, assim como o conteúdo de carbonato de cálcio inorgânico oscila entre valores médios e altos (principalmente nos intervalos com dolomita). Os valores de carbono orgânico total (COT) obtidos correspondem de modo satisfatório ao intervalo (unidade sedimentar 7) descrito por Bolli et al., (1978), nesta unidade a dissolução afetou a abundância dos nanofósseis calcários, resultando na baixa preservação de espécies susceptíveis a dissolução. Devido a esta alteração, não foi possível realizar inferências acerca da relação entre os depósitos de folhelhos negros e a alta fertilidade de nanofósseis calcários.

Apesar da dissolução, a assembleia recuperada é relativamente bem diversificada e os táxons suscetíveis à dissolução foram observados, mas não de modo abundante. Em cinco amostras (na unidade sedimentar 6) foi possível realizar inferências paleoceanográficas para a Bacia de Kwanza, nesta unidade a dissolução não foi tão severa como na unidade 7. Nestas cinco amostras foi possível inferir dados de fertilidade e produtividade de carbonatos nas águas superficiais, durante o intervalo Albiano–Cenomaniano do *Site* 364.

Os 103 táxons descritos e identificados neste trabalho, são apresentados nas páginas que seguem.

SYSTEMATIC PALEONTOLOGY: PLATE 1 – HETEROCOCCOLITHS

Order EIFFELLITHALES Rood *et al.,* 1971

Family **CHIASTOZYGACEAE** Rood *et al.,* 1971

Genus *Tranolithus* Stover, 1966

Tranolithus gabalus Stover, 1966

Description: Medium to large coccoliths; specie have an elliptical outline; the rim is simple and unicyclic; the central opening is spanned transversely by two large blocks.

Tranolithus orionatus (Reinhardt, 1966a) Reinhardt, 1966b

Description: Medium to large coccoliths; specie have an elliptical outline; the rim is simple and unicyclic; the central area have four massive blocks.

Tranolithus minimus (Bukry, 1969) Perch-Nielsen, 1984

Description: Small to medium coccoliths; elliptical outline; the rim is simple and unicyclic; the central area feature a bridge and two large blocks with high birefringence.

Genus *Vekshinella* Loeblich & Tappan, 1963

Vagalapilla angusta (Stover 1966) Roth, 1981

Description: Large to very large coccoliths; elliptical outline; the rim is narrow and bicyclic with the same width, the inner cycle is brighter; the central area have a cross with angles of less than 20º between cross arms and principle axes.

Genus *Staurolithites* Caratini, 1963

Staurolithites laffittei Caratini, 1963

Description: Small to medium coccoliths; elliptical outline; the rim is bicyclic; the central area have a central cross aligned with the axes.

Staurolithites crux (Deflandre & Fert, 1954) Caratini, 1963

Description: Small coccoliths; elliptical outline; the rim is narrow; and the wide central area have a central cross, with high birefringence, aligned with the axes.

***Staurolithites* sp. 1**

Description: Medium coccoliths; elliptical outline; the rim is unicyclic and large; the central area is closed and have a cross.

Genus *Glaukolithus* Reinhardt (1964)

Glaukolithus diplogrammus (Deflandre) Reinhardt, 1964

Description: Medium to large coccoliths; elliptical outline; the rim is simple; the central area is broad and have two bars narrow and parallels.

Glaukolithus bicrescenticus (Stover 1966)

Description: Medium to large coccoliths; elliptical outline; the rim is simple; the central area is narrow and have two bars broad and parallels.

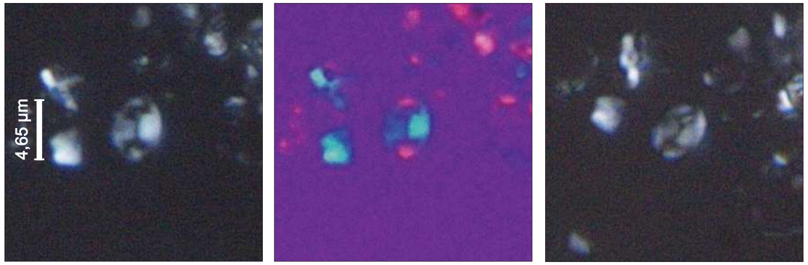

Tranolithus gabalus (DSDP Site 364 / Depth 1.032,37 mbsf)

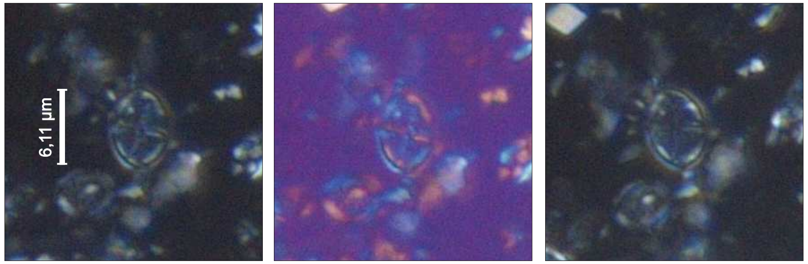

Vagalapilla angusta (DSDP Site 364 / Depth 877,42 mbsf)

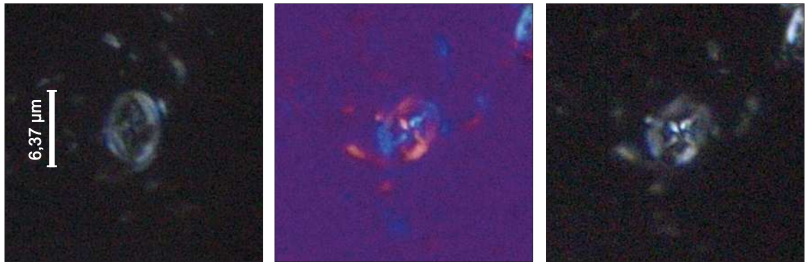

Staurolithites laffittei (DSDP Site 364 / Depth 894,99 mbsf)

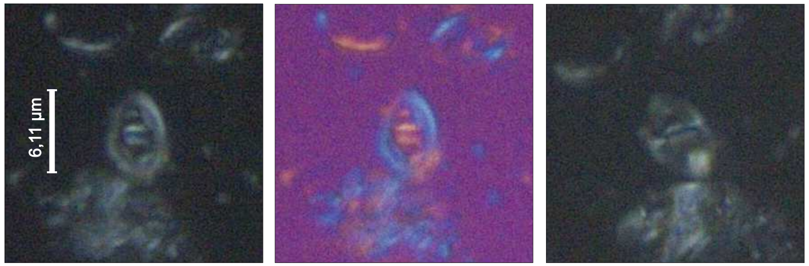

Glaukolithus bicrescenticus (DSDP Site 364 / Depth 719,15 mbsf)

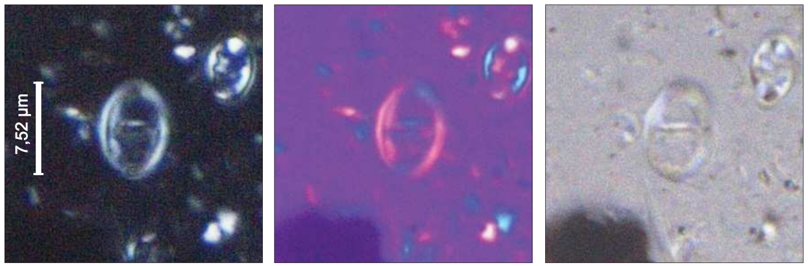

Glaukolithus diplogrammus (DSDP Site 364 / Depth 807,40 mbsf)

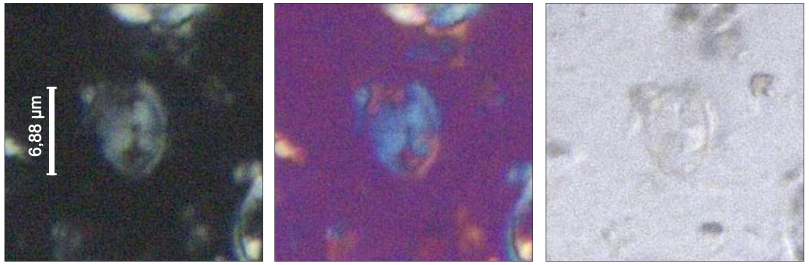

Tranolithus orionatus (DSDP Site 364 / Depth 723,67 mbsf)

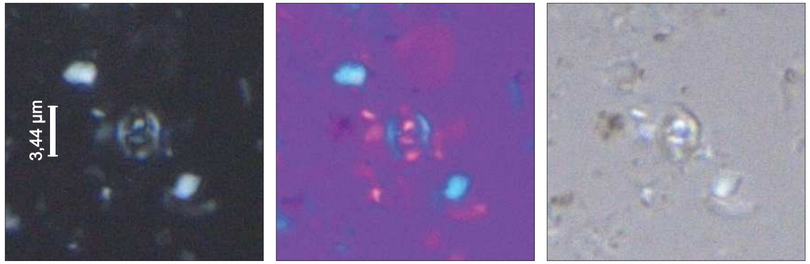

Tranolithus minimus (DSDP Site 364 / Depth 1032,37 mbsf)

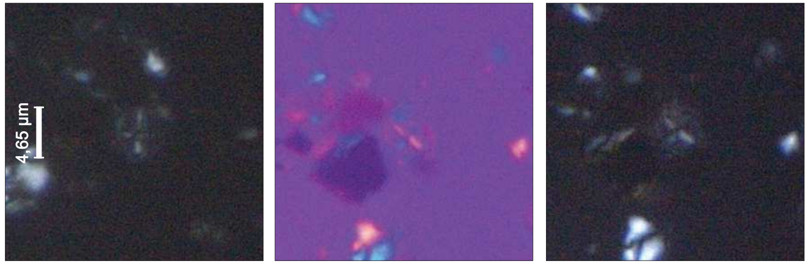

Staurolithites crux (DSDP Site 364 / Depth 1027,24 mbsf)

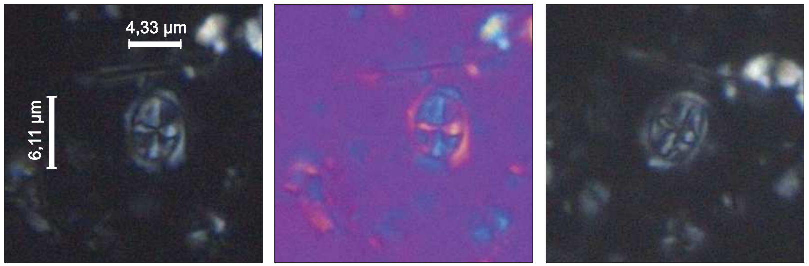

Staurolithites sp. 1 (DSDP Site 364 / Depth 1.008,41 mbsf)

10 µm

SYSTEMATIC PALEONTOLOGY: PLATE 2 – HETEROCOCCOLITHS

Genus *Zeugrhabdotus* Reinhardt, 1965

Zeugrhabdotus angelozziae Pérez Panera 2012

Description: Medium to large; specie have an elliptical outline; the rim is bicyclic; the central-area spanned by two parallel bars disposed oblique to the main axes of the ellipse.

Zeugrhabdotus howei Bown in Kennedy *et al.,* 2000

Description: Medium coccoliths; elliptical outline; the rim is unicyclic; the central-area have a bar granular.

Zeugrhabdotus embergeri (Noël, 1959) Perch-Nielsen, 1984

Description: Large coccoliths; elliptical outline; the rim is bicyclic; the central-area have a bar granular with diamond ornamentation.

Zeugrhabdotus clarus Bown, 2005

Description: Small to medium coccoliths; elliptical outline; the rim is bicyclic, strongly curved extinction lines cross the bright inner cycle; the central-area have a bar granular.

Zeugrhabdotus erectus (Deflandre in Deflandre & Fert, 1954) Reinhardt, 1965

Description: Small coccoliths; elliptical outline; the rim is unicyclic, the central-area have a bar granular birefringent.

Genus *Chiastozygus* Gartner, 1968

Chiastozygus litterarius (Górka, 1957) Manivit, 1971

Description: Medium to large coccoliths; elliptical outline; the rim is usually unicyclic, the central-area have a crossbars arranged as an x.

Chiastozygus platyrhethus Hill, 1976

Description: Medium to large coccoliths; elliptical outline; the rim is usually unicyclic, the central-area wide have a large central cross.

Genus *Loxolithus* Noël, 1965

Loxolithus armilla (Black in Black & Barnes, 1959) Noël, 1965

Description: Medium to large coccoliths; elliptical outline; the rim is usually unicyclic, strongly curved extinction lines cross the cycle; central-area is broad and void.

Family **EIFFELLITHACEAE** Reinhardt, 1965

Genus *Helicolithus* Noël, 1970

Helicolithus trabeculatus (Górka, 1957) Verbeek, 1977

Description: Small to medium coccoliths; elliptical outline; the rim is usually bicyclic; the central-area have a symmetrical diagonal cross bars.

Genus *Tegumentum stradneri* Thierstein in Roth & Thierstein, 1972

Tegumentum stradneri Thierstein in Roth & Thierstein, 1972

Description: Medium to large coccoliths; specie with a broadly to normally elliptical; the rim is bicyclic, inner cycle is brighter (high birefringence); the central area is large with a diagonal cross bar that appear sigmoidal curved in pointed terminations.

Zeugrhabdotus angelozziae (DSDP Site 364 / Depth 1.006,41 mbsf)

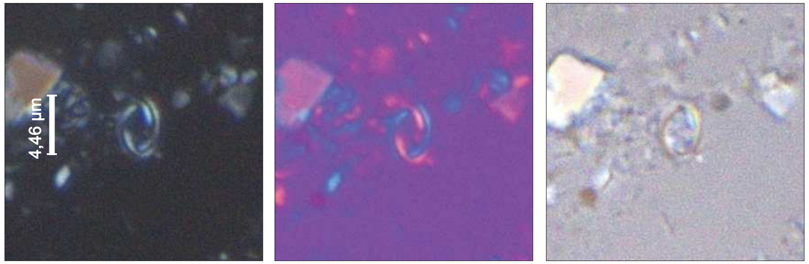

Zeugrhabdotus clarus (DSDP Site 364 / Depth 975,49 mbsf)

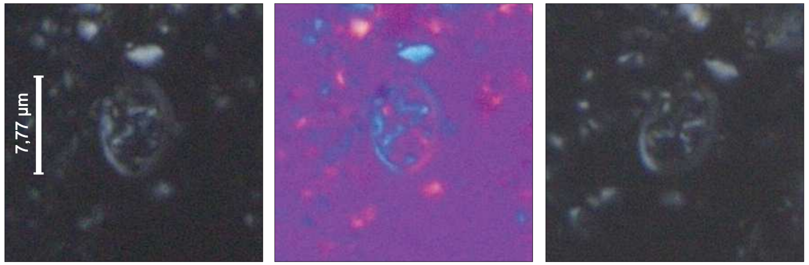

Chiastozygus litterarius (DSDP Site 364 / Depth 1.009,79 mbsf)

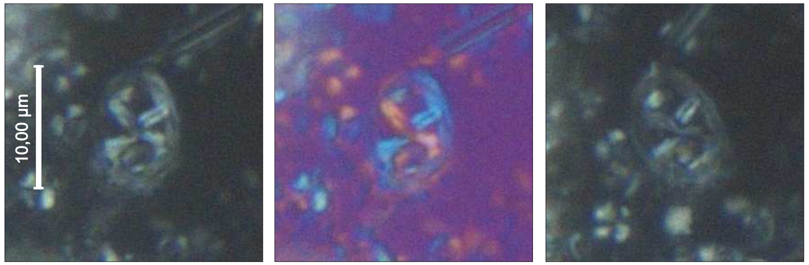

Chiastozygus platyrhethus (DSDP Site 364 / Depth 753,64 mbsf)

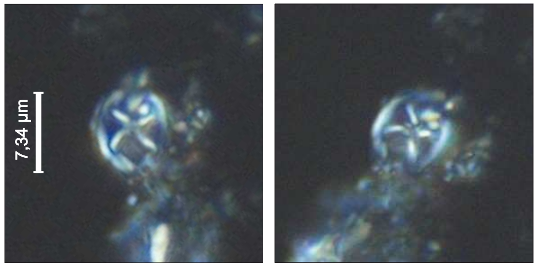

Tegumentum stradneri (DSDP Site 364 / Depth 768,19 mbsf)

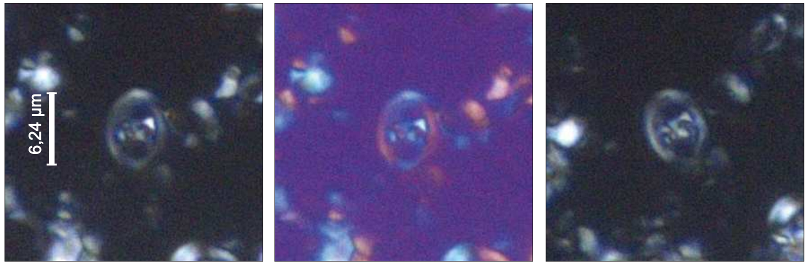

Zeugrhabdotus howei (DSDP Site 364 / Depth 911,25 mbsf)

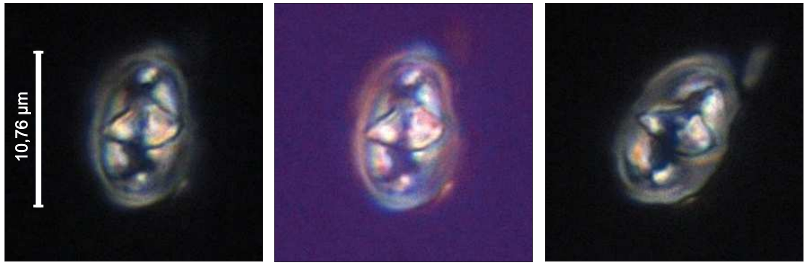

Zeugrhabdotus embergeri (DSDP Site 364 / Depth 877,42 mbsf)

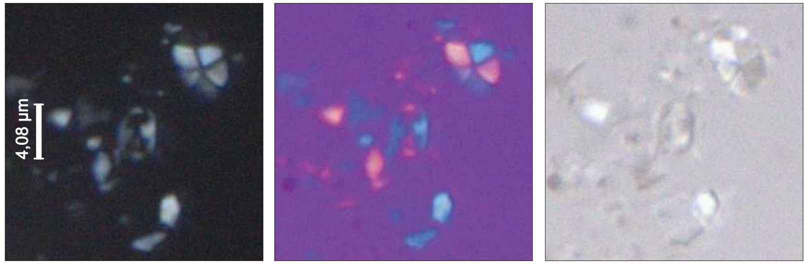

Zeugrhabdotus erectus (DSDP Site 364 / Depth 1032,37 mbsf)

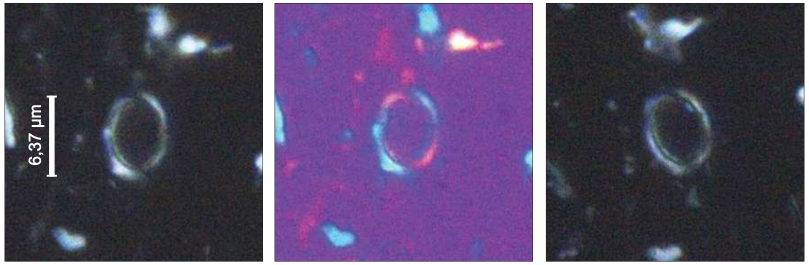

Loxolithus armilla (DSDP Site 364 / Depth 932,45 mbsf)

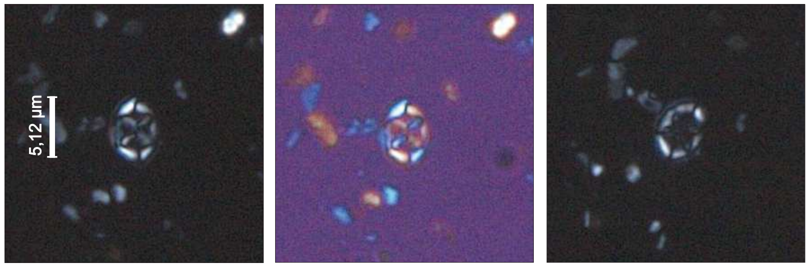

Helicolithus trabeculatus (DSDP Site 364 / Depth 768,19 mbsf)

10 µm

SYSTEMATIC PALEONTOLOGY: PLATE 3 – HETEROCOCCOLITHS

Genus *Eiffellithus* Reinhardt, 1965

Eiffellithus hancockii Burnett, 1997

Description: Small coccoliths; elliptical outline; angular orientation is axial; the central-area is very narrow with an axial cross bar.

Eiffellithus turriseiffelii (Deflandre & Fert, 1954) Reinhardt, 1965

Description: Large to very large coccoliths; elliptical outline; angular orientation is diagonal; the central-area have a diagonal cross bar with arms terminations pointed to blunt and/or forked.

Eiffellithus monechiae Crux, 1991

Description: Medium coccoliths; elliptical outline; angular orientation is axial; the central-area have an axial cross bar with arms terminations pointed to blunt and/or bifurcate. In the diagonal angular orientation the cross bar is subparallel when the ellipse.

Eiffellithus equibramus Watkins & Bergen, 2003

Description: Medium coccoliths; elliptical outline; angular orientation is diagonal; the central-area have a diagonal cross bar with arms terminations pointed to blunt and/or forked. In the diagonal angular orientation the cross bar is subparallel when the ellipse.

Eiffellithus vonsalisiae Watkins & Bergen, 2003

Description: Medium to large coccoliths; elliptical outline; angular orientation is intermediate; the central-area have a diagonal cross bar with arms terminations pointed to blunt and/or forked.

Eiffellithus parvus Watkins & Bergen, 2003

Description: Medium coccoliths; elliptical outline; angular orientation is diagonal; the central-area have a diagonal cross bar with arms terminations pointed to blunt and/or forked.

Eiffellithus praestigium Watkins & Bergen, 2003

Description: Medium coccoliths; elliptical outline; angular orientation is axial; the central-area have an axial cross bar with arms terminations pointed to blunt, forked and/or bifurcate. In the diagonal angular orientation the cross bar is diagonal.

Eiffellithus casulus Shamrock & Watkins, 2009

Description: Small to medium coccoliths; elliptical outline; angular orientation is diagonal; the central-area have a diagonal cross bar with arms terminations pointed to blunt and/or forked. The cross bar suture is weak.

Eiffellithus perch-nielseniae Shamrock & Watkins, 2009

Description: Medium to large coccoliths; elliptical outline; angular orientation is intermediate; the central-area have a diagonal cross bar with arms terminations pointed to blunt, bifurcate and/or forked. The cross bar suture is weak.

Eiffellithus collis Hoffmann, 1970

Description: Specimen have 7.45µm length, is a medium coccoliths; elliptical outline; angular orientation is diagonal, with 52.55º; the central-area have a diagonal cross bar with arms terminations pointed to blunt. In the diagonal angular orientation the cross bar is axial. Axial ratio is normal (specimen example: 1.4).

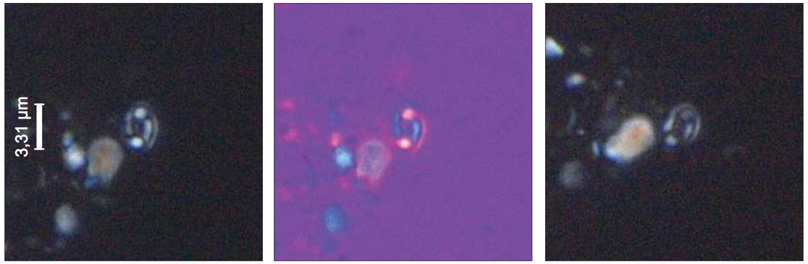

Eiffellithus hancockii (DSDP Site 364 / Depth 1.032,37 mbsf)

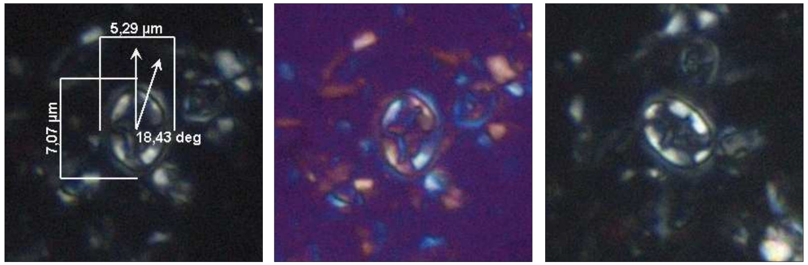

Eiffellithus monechiae (DSDP Site 364 / Depth 875,96 mbsf)

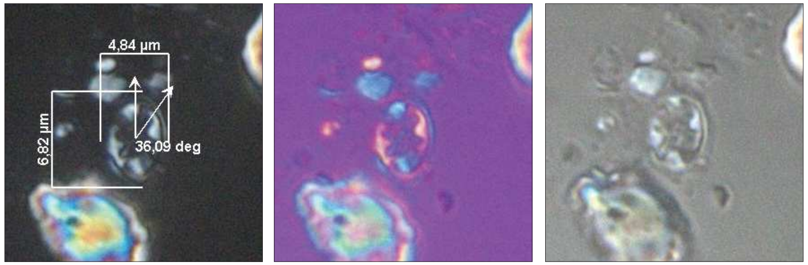

Eiffellithus vonsalisiae (DSDP Site 364 / Depth 826,40 mbsf)

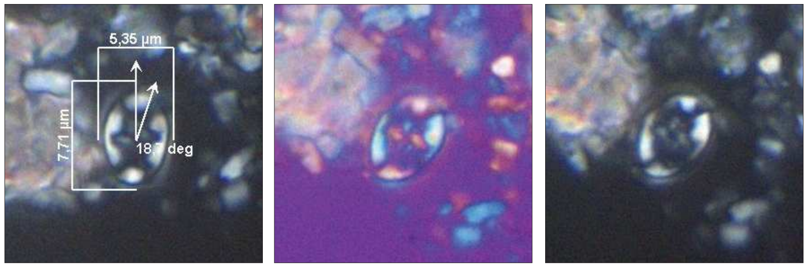

Eiffellithus praestigium (DSDP Site 364 / Depth 829,46 mbsf)

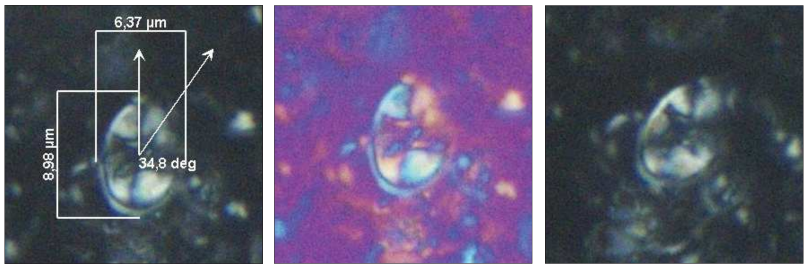

Eiffellithus perch-nielseniae (DSDP Site 364 / Depth 719,15 mbsf)

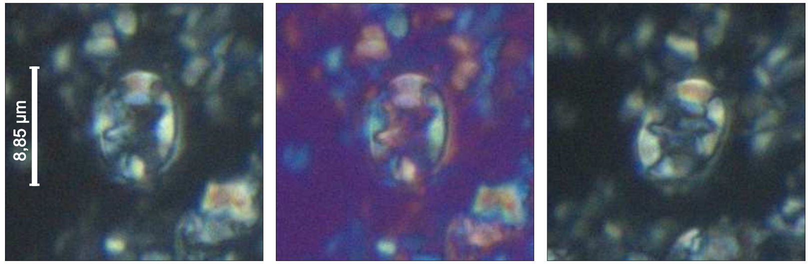

Eiffellithus turriseiffelii (DSDP Site 364 / Depth 772,34 mbsf)

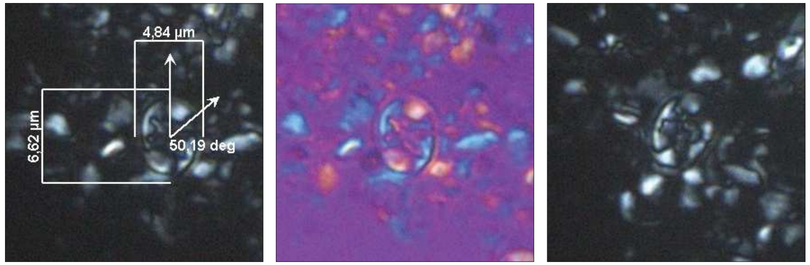

Eiffellithus equibiramus (DSDP Site 364 / Depth 826,40 mbsf)

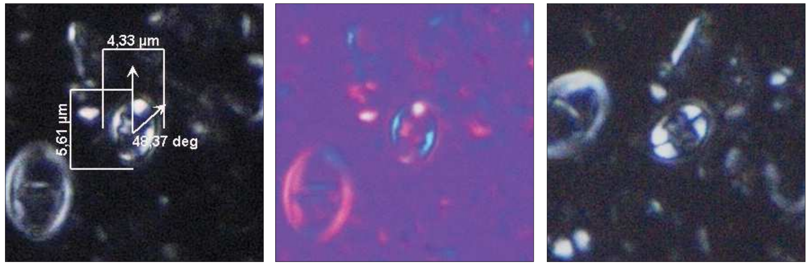

Eiffellithus parvus (DSDP Site 364 / Depth 807,40 mbsf)

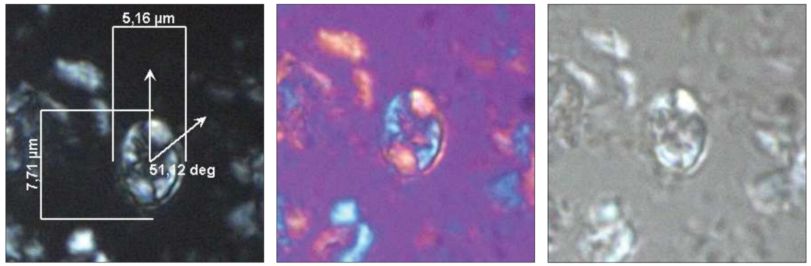

Eiffellithus casulus (DSDP Site 364 / Depth 772,34 mbsf)

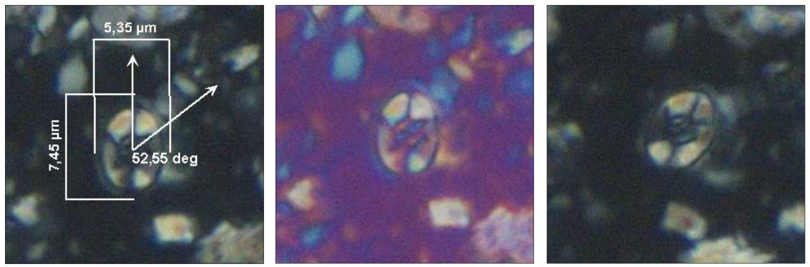

Eiffellithus collis (DSDP Site 364 / Depth 752,37 mbsf)

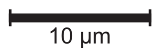

SYSTEMATIC PALEONTOLOGY: PLATE 4 – HETEROCOCCOLITHS

Family **RHAGODISCACEAE** Hay, 1977

Genus *Rhagodiscus* Reinhardt, 1967

Rhagodiscus asper (Stradner, 1963) Reinhardt, 1967

Description: Medium coccoliths; elliptical outline; the rim is unicyclic; the central-area is wide covered by a plate that contains a granulated area and a large hole in the center.

Rhagodiscus angustus (Stradner, 1963) Reinhardt, 1971

Description: Small to medium coccoliths; long-elliptical outline; the rim is unicyclic; the central-area is wide covered by a plate that contains a large hole in the center.

Rhagodiscus achlyostaurion (Hill, 1976) Doeven, 1983

Description: Small to medium coccoliths; elliptical outline; the rim is bicyclic, and the external cycle is greater and with high birefringence; the central-area is wide covered by a plate that contains a large hole in the center with high birefringence.

Order ARKHANGELSKIALES Bown & Hampton, 1997 in Bown & Young, 1997

Family **ARKHANGELSKIELLACEAE** Bukry, 1969 emend Bown & Hampton, 1997 in Bown & Young, 1997

Genus *Broinsonia* Bukry, 1969

Broinsonia signata (Noël, 1969) Noël, 1970

Description: Medium coccoliths; elliptical outline; the rim is usually bicyclic; the central-area is broad and have a central cross with open quadrants, the central cross have arms with a line of extinction that is formed by a suture.

Broinsonia enormis (Shumenko, 1968) Manivit, 1971

Description: Small to medium coccoliths; elliptical outline; the rim is usually unicyclic; the central-area have a central cross with open quadrants.

Family **KAMPTNERIACEAE** Bown & Hampton, 1997 in Bown & Young, 1997

Genus *Gartnerago* Bukry, 1969

Gartnerago stenostaurion (Hill, 1976) Perch-Nielsen, 1984

Description: Small to large coccoliths; elliptical outline; the rim is unicyclic and narrow; the central-area is broad and have a plate usually crossed by four radial extinction lines.

***Gartnerago* sp. 1**

Description: Small to large coccoliths; elliptical outline; the rim is unicyclic and narrow; the central-area is broad and have a plate usually crossed by four radial extinction lines.

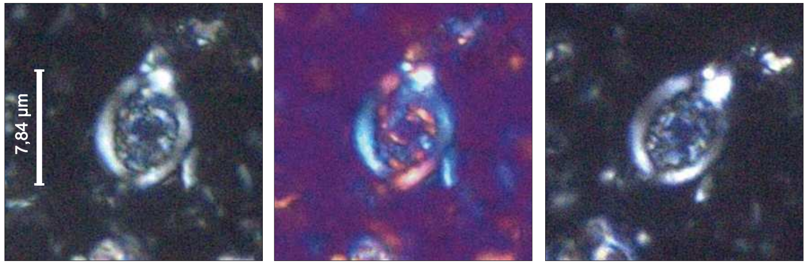

Rhagodiscus asper (DSDP Site 364 / Depth 894,99 mbsf)

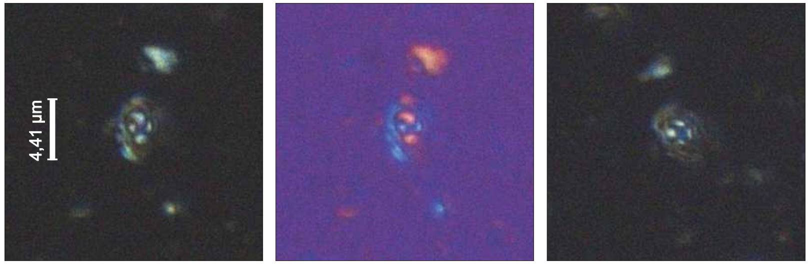

Rhagodiscus achlyostaurion (DSDP Site 364 / Depth 932,45 mbsf)

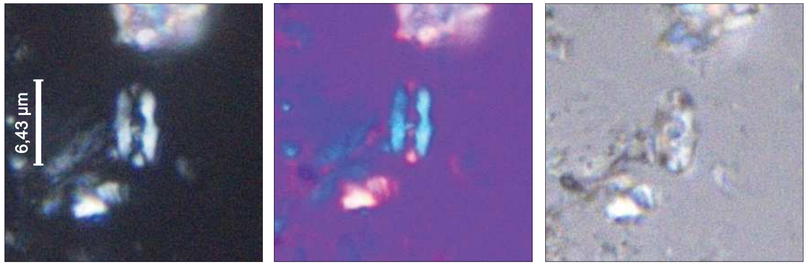

Rhagodiscus angustus (DSDP Site 364 / Depth 1.032,37 mbsf)

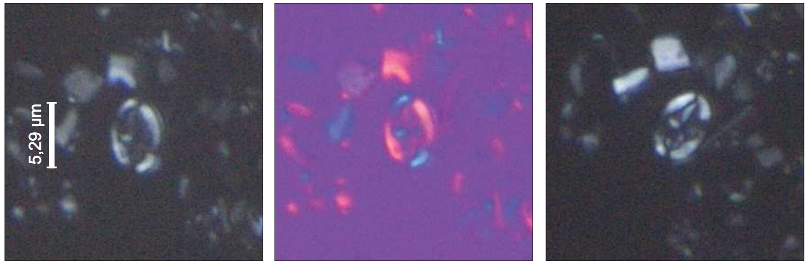

Broinsonia enormis (DSDP Site 364 / Depth 771,17 mbsf)

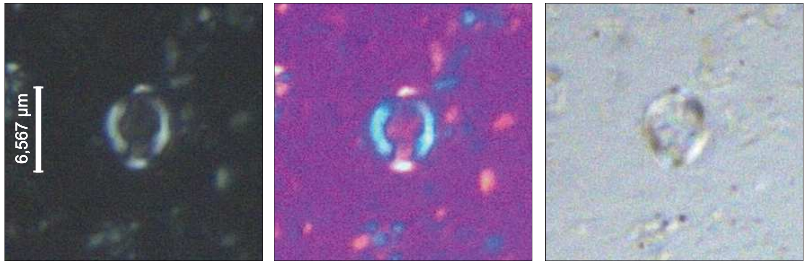

Broinsonia signata (DSDP Site 364 / Depth 722,75 mbsf)

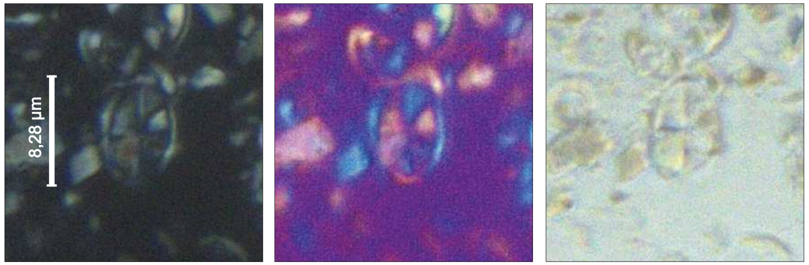

Gartnerago stenostaurion (DSDP Site 364 / Depth 769,33 mbsf)

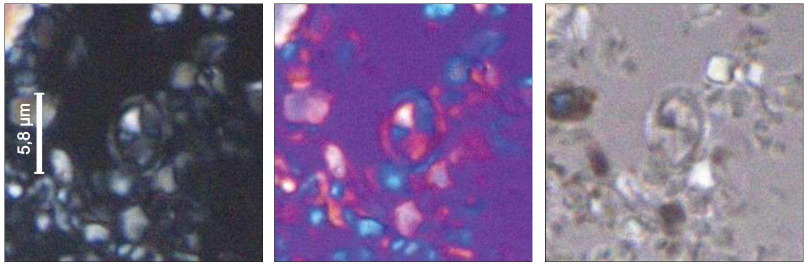

Gartnerago sp. 1 (DSDP Site 364 / Depth 934,44 mbsf)

10 µm

SYSTEMATIC PALEONTOLOGY: PLATE 5 – HETEROCOCCOLITHS

Order STEPHANOLITHIALES Bown & Young, 1997

Family **STEPHANOLITHIACEAE** Black 1968

Genus *Stoverius* Perch-Nielsen, 1986

Stoverius achylosus (Stover, 1966) Perch-Nielsen, 1986

Description: Small to large; elliptical to circular outline; rim is bicyclic; central-area is spanned by cross bars that meet at a high angle.

Genus *Cylindralithus* Bramlette & Martini, 1964

Corollithion signum Stradner, 1963

Description: Small; hexagonal outline; rim bicyclic with inner cycle with high birefringence; central-area has an axial cross; bar is composed of two elements.

Cylindralithus nudus Bukry, 1969

Description: Small to medium; elliptical; rim is bicyclic; central-area is narrow and open.

Cylindralithus serratus Bramlette & Martini, 1964

Description: Medium; circular; rim bicyclic and serrated; central-area is narrow and open.

Genus *Corollithion* Stradner, 1961

Order PODORHABDALES Rood *et al.,* 1971 emend. Bown, 1987

Family **AXOPODORHABDACEAE** Wind & Wise in Wise & Wind, 1977

Genus *Axopodorhabdus* Wind & Wise in Wise & Wind, 1977

Axopodorhabdus biramiculatus (Stover 1966) Corbett & Watkins, 2014

Description: medium to large; elliptical; rim is bicyclic with inner cycle with high birefringence; central-area have an axial cross, with 4 almost circular openings to its sides.

Tetrapodorhabdus coptensis Black, 1971

Description: medium to large; elliptical outline; rim is bicyclic; central-area is broad and have a diagonal cross bar, with four almost circular openings to its sides.

Family **BISCUTACEAE** Black, 1971

Genus *Biscutum* Black in Black & Barnes, 1959

Biscutum ubiquem Brace & Watkins, 2014

Description: small to medium; elliptical; rim is bicyclic, inner cycle is thick; central-area is small and void.

***Biscutum* sp. 1**

Description: Medium; elliptical outline; the rim is unicyclic; the central-area is broad, closed and have two bars transverse.

***Biscutum* sp. 2**

Description: Medium; elliptical; rim unicyclic; have 2 bars transverse in the center.

Genus *Discorhabdus* Noël, 1965

Discorhabdus ignotus (Górka, 1957) Perch-Nielsen, 1968

Description: Very small to medium; circular; rim is bicyclic; central-area is closed.

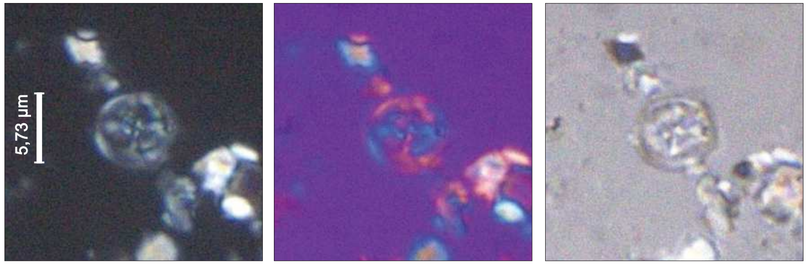

Stoverius achylosus (DSDP Site 364 / Depth 1.029,50 mbsf)

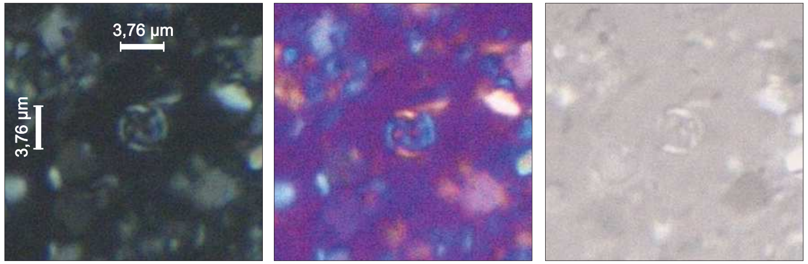

Corollithion signum (DSDP Site 364 / Depth 752,37 mbsf)

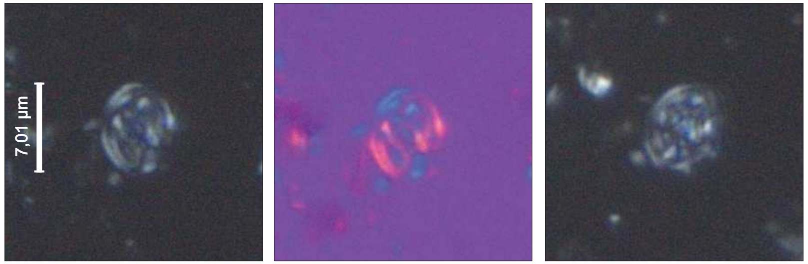

Axopodorhabdus biramiculatus (DSDP Site 364 / Depth 951,47 mbsf)

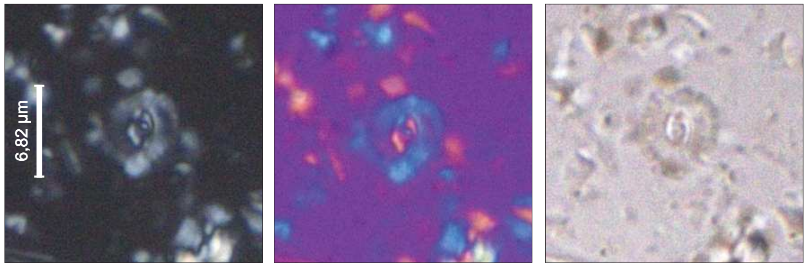

Biscutum ubiquem (DSDP Site 364 / Depth 911,25 mbsf)

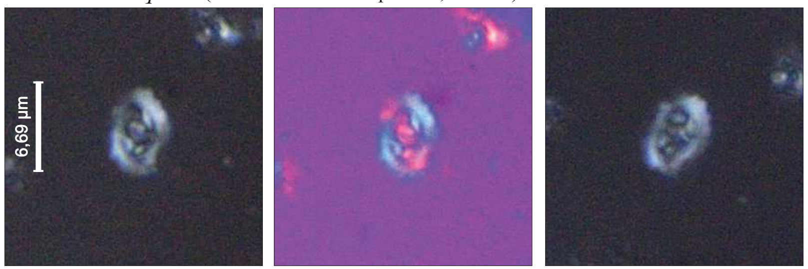

Biscutum sp. 2 (DSDP Site 364 / Depth 810,94 mbsf)

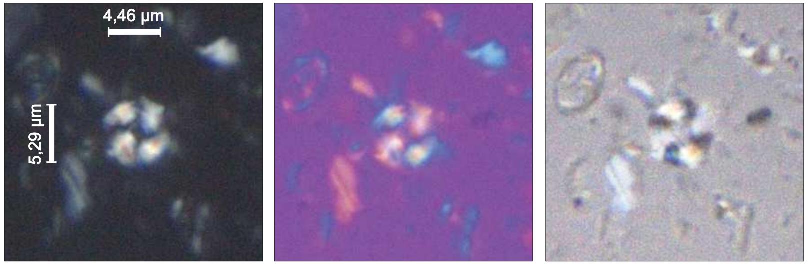

Cylindralithus nudus (DSDP Site 364 / Depth 935,98 mbsf)

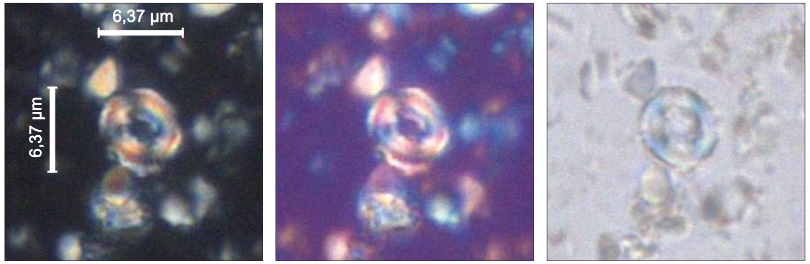

Cylindralithus serratus (DSDP Site 364 / Depth 911,25 mbsf)

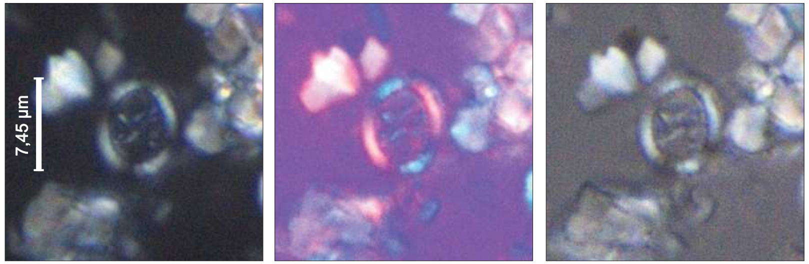

Tetrapodorhabdus coptensis (DSDP Site 364 / Depth 790,41 mbsf)

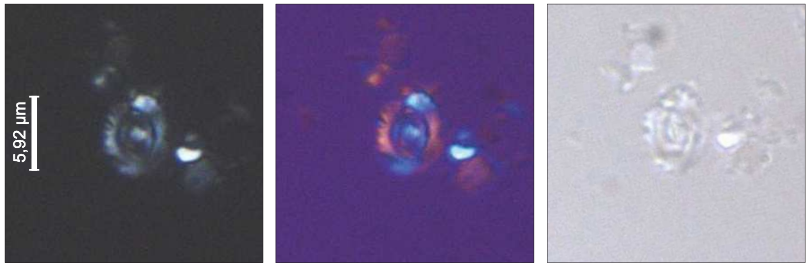

Biscutum sp. 1 (DSDP Site 364 / Depth 935,98 mbsf)

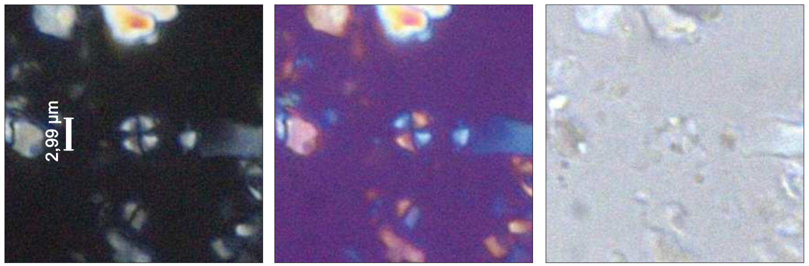

Discorhabdus ignotus (DSDP Site 364 / Depth 892,14 mbsf)

10 µm

SYSTEMATIC PALEONTOLOGY: PLATE 6 – HETEROCOCCOLITHS

Genus *Sollasites* Black, 1967

***Sollasites* sp. 1**

Description: Medium to large; elliptical; rim is unicyclic; central-area is closed with axial plates.

Family **CRETARHABDACEAE** Thierstein, 1973

Genus *Cretarhabdus* Bramlette & Martini, 1964

Cretarhabdus crenulatus Bramlette & Martini (1964)

Description: medium to large coccoliths; elliptical outline; the rim is unicyclic with high birefringence; the central-area is broad with a two lateral bars in each quadrant.

Cretarhabdus surirellus (Deflandre and Fert 1954) Reinhardt, 1970

Description: medium to large coccoliths; elliptical outline; the rim is unicyclic with high birefringence; the central-area is broad with a three lateral bars in each quadrant.

Cretarhabdus conicus Bramlette & Martini, 1964

Description: medium to large coccoliths; elliptical outline; the rim is bicyclic; the central-area is perforated by many pores, and have a cross bar with pointed tips.

Cretarhabdus striatus (Stradner, 1963) Black, 1973

Description: medium to large coccoliths; elliptical outline; the rim is bicyclic; the central-area is wide and have a central cross, and a double marginal plates with numerous pores are arranged in lines which meet at oblique angles at the straight central cross.

Cretarhabdus inaequalis Crux, 1987

Description: Large coccoliths; elliptical outline; the rim is bicyclic; the central-area have an irregular grill.

Genus *Retecapsa* Black, 1971

Retecapsa angustiforata Black, 1971

Description: medium to large coccoliths; elliptical outline; the rim is bicyclic; the central-area is wide and have an axial cross with one broad lateral bar in each quadrant, the 8 central area holes are of relatively equal size.

Genus *Helenea* Worsley, 1971

Helenea chiastia Worsley, 1971

Description: medium to large coccoliths; elliptical to subcircular outline; the rim is bicyclic, with inner cycle high birefringence; the central-area is narrow and have an axial cross.

Genus *Flabellites* Thierstein, 1973

Flabellites oblongus (Bukry, 1969) Crux in Crux *et al.,* 1982

Description: medium to large coccoliths; elliptical outline; the rim is bicyclic; the central-area is granular with a bridge formed by four small calcite crystals arranged in a diagonal cross.

Genus *Grantarhabdus* Black, 1971

Grantarhabdus coronadventis (Reinhardt, 1966) Grün and Allemann, 1975

Description: medium to large coccoliths; subcircular outline; the rim is bicyclic; the central-area is have a diagonal cross bars that meet at a high angle.

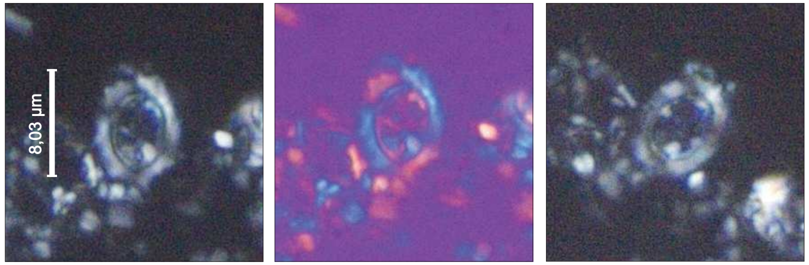

Sollasites sp. 1 (DSDP Site 364 / Depth 934,44 mbsf)

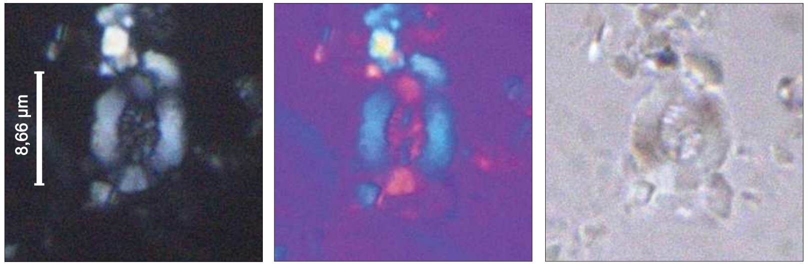

Cretarhabdus surirellus (DSDP Site 364 / Depth 1.031,21 mbsf)

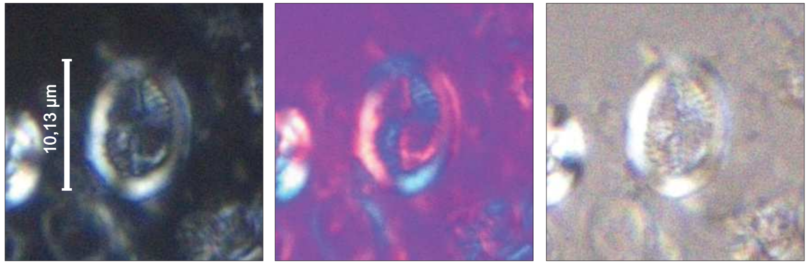

Cretarhabdus striatus (DSDP Site 364 / Depth 788,94 mbsf)

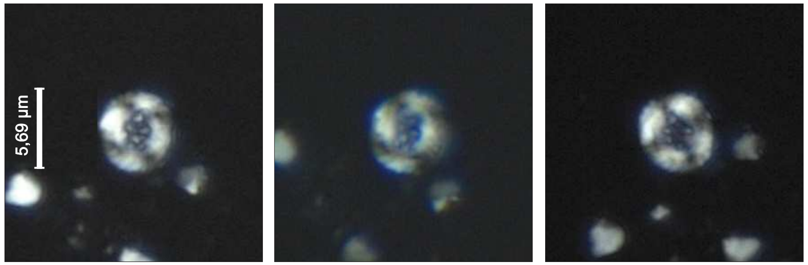

Helenea chiastia (DSDP Site 364 / Depth 726,66 mbsf)

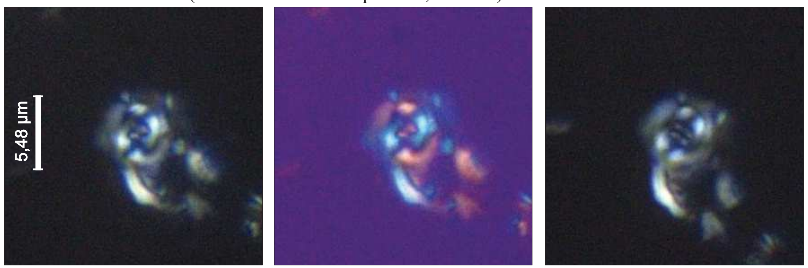

Flabellites oblongus (DSDP Site 364 / Depth 892,96 mbsf)

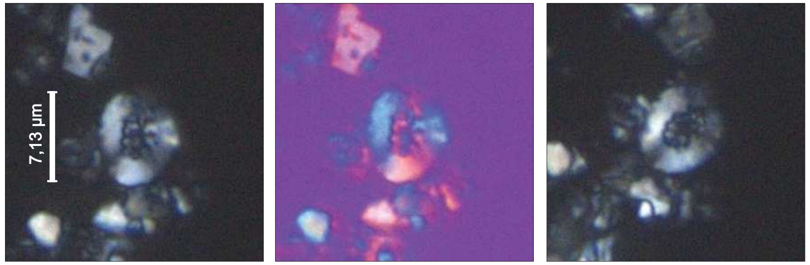

Cretarhabdus crenulatus (DSDP Site 364 / Depth 973,89 mbsf)

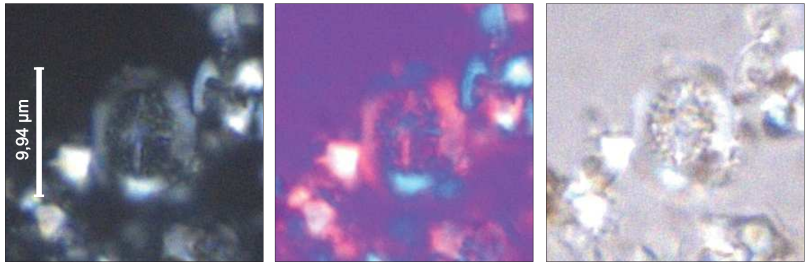

Cretarhabdus conicus (DSDP Site 364 / Depth 951,47 mbsf)

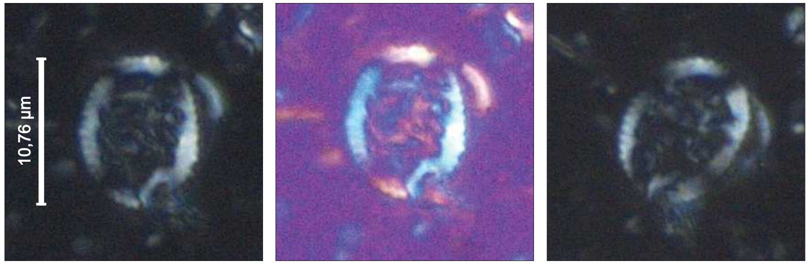

Cretarhabdus inaequalis (DSDP Site 364 / Depth 932,45 mbsf)

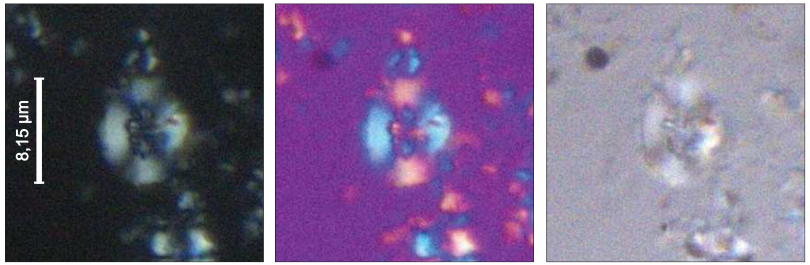

Retecapsa angustiforata (DSDP Site 364 / Depth 726,66 mbsf)

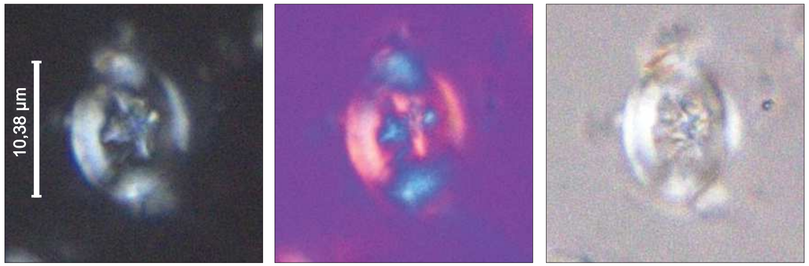

Grantarhabdus coronadventis (DSDP Site 364 / Depth 790,41 mbsf)

10 µm

SYSTEMATIC PALEONTOLOGY: PLATE 7 – HETEROCOCCOLITHS

Family **PREDISCOSPHAERACEAE** Rood *et al.,* 1971

Genus *Prediscosphaera* Vekshina, 1959

Prediscosphaera columnata (Stover, 1966) Perch-Nielsen, 1984

Description: Medium to large coccoliths; circular to subcircular outline; the rim is bicyclic, distal cycle is broad and the inner cycle very narrow; the central-area have a cross bar.

Prediscosphaera spinosa (Bramlette & Martini, 1964) Gartner, 1968

Description: Medium to large coccoliths; elliptic outline; the rim is bicyclic, distal cycle is broad and the inner cycle very narrow; the central-area have an axial cross bar.

Prediscosphaera cretacea (Arkhangelsky, 1912) Gartner, 1968

Description: Medium to large coccoliths; elliptic outline; the rim is bicyclic, distal cycle is broad and the inner cycle very narrow; the central-area have a diagonal cross bar.

Family **TUBODISCACEAE** Bown & Rutledge, 1997 in Bown & Young, 1997

Genus *Manivitella* Thierstein, 1971

Manivitella pemmatoidea (Deflandre in Manivit, 1965) Thierstein, 1971

Description: Medium to large coccoliths; Ellipse outline; the rim is bicyclic, the inner cycle brighter; the central-area is broad and void.

Order WATZNAUERIALES Bown, 1987

Family **WATZNAUERIACEAE** Rood *et al.,* 1971

Genus *Watznaueria* Reinhardt, 1964

Watznaueria barnesiae (Black in Black & Barnes, 1959) Perch-Nielsen, 1968

Description: medium coccoliths; elliptical outline; the rim is unicyclic; the central-area is closed or very narrow, with no central area structures.

Watznaueria britannica (Stradner, 1963) Reinhardt, 1964

Description: medium coccoliths; elliptical outline; the rim is unicyclic; the central-area is narrow with spanned by a transverse bar.

Watznaueria biporta Bukry, 1969

Description: medium to large coccoliths; elliptical outline; the rim is unicyclic; the central-area have two well-defined pores aligned in the long axis.

Watznaueria manivitiae Bukry, 1973

Description: large coccoliths; elliptical outline; the rim is unicyclic; the central-area is closed.

Watznaueria supracretacea (Reinhardt, 1964) Wind & Wise, 1977

Description: Small to medium coccoliths; elliptical outline; the rim is unicyclic serrate; the central-area is closed with spanned by a transverse bar connecting the sides of the ellipse.

Watznaueria ovata Bukry, 1969

Description: medium; elliptical; the rim is bicyclic; the central-area is broad and void.

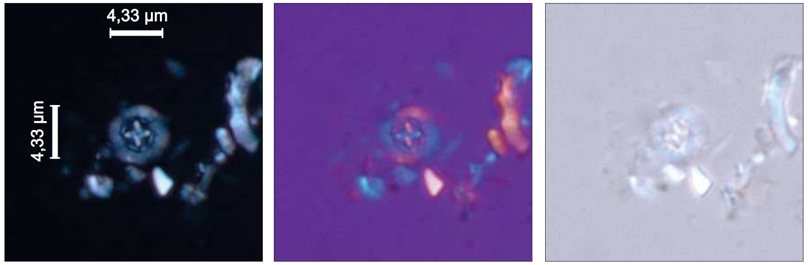

Prediscosphaera columnata (DSDP Site 364 / Depth 892,96 mbsf)

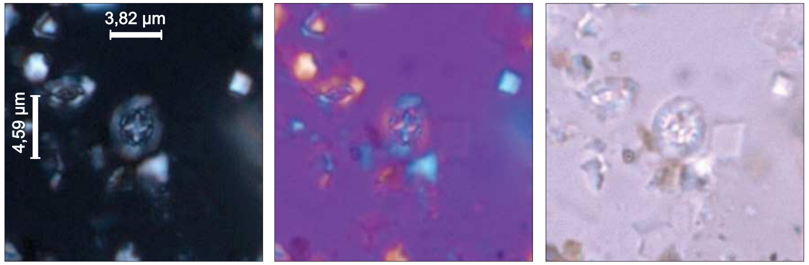

Prediscosphaera spinosa (DSDP Site 364 / Depth 1006,96 mbsf)

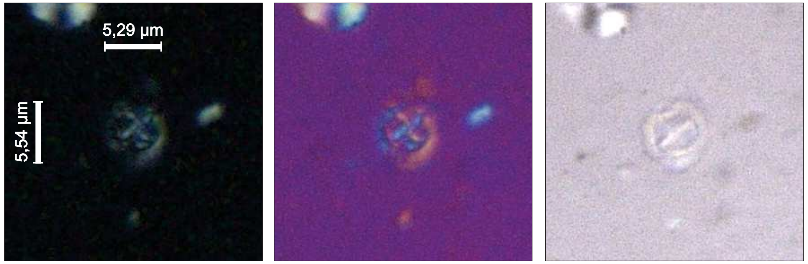

Prediscosphaera cretacea (DSDP Site 364 / Depth 725,24 mbsf)

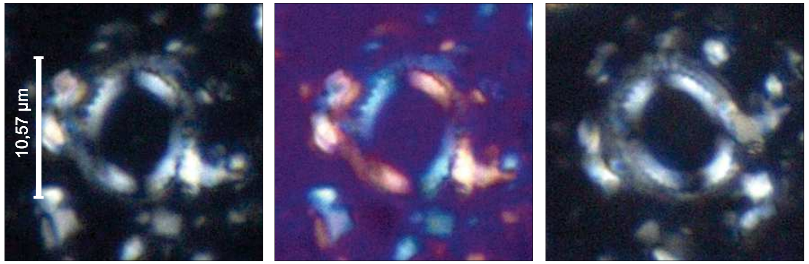

Manivitella pemmatoidea (DSDP Site 364 / Depth 911,25 mbsf)

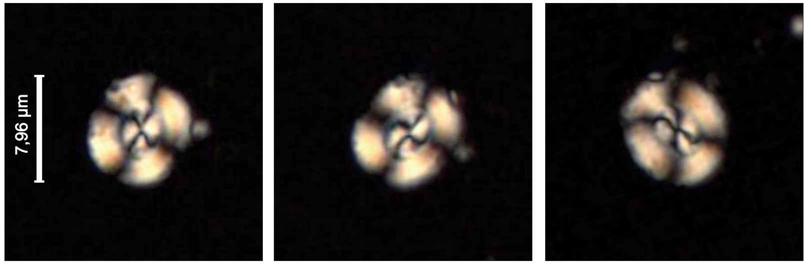

Watznaueria barnesiae (DSDP Site 364 / Depth 829.46 mbsf)

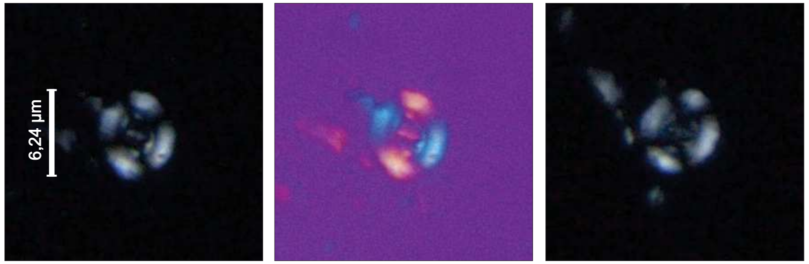

Watznaueria britannica (DSDP Site 364 / Depth 1006,96 mbsf)

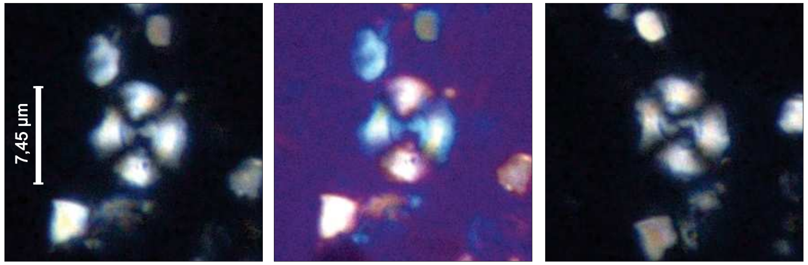

Watznaueria biporta (DSDP Site 364 / Depth 911,25 mbsf)

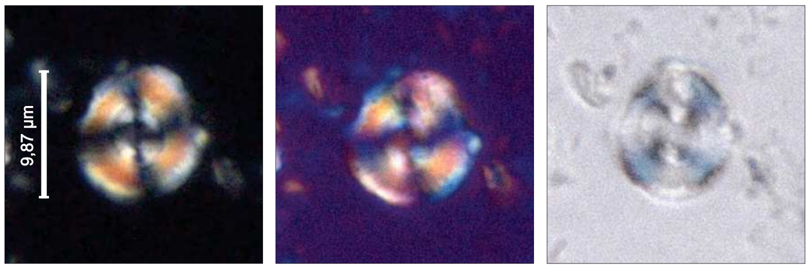

Watznaueria manivitiae (DSDP Site 364 / Depth 877,42 mbsf)

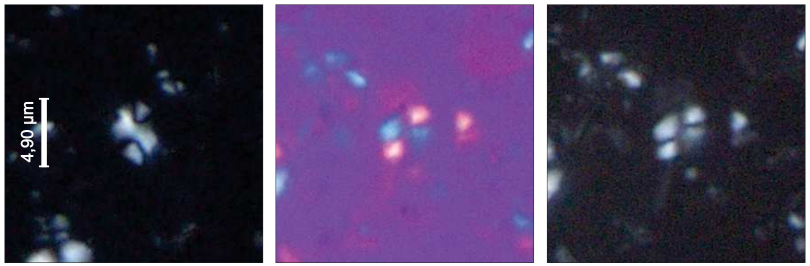

Watznaueria supracretacea (DSDP Site 364 / Depth 1027,24 mbsf)

Watznaueria ovata (DSDP Site 364 / Depth 719,15 mbsf)

10 µm

SYSTEMATIC PALEONTOLOGY: PLATE 8 – HETEROCOCCOLITHS

Genus *Cyclagelosphaera* Noël, 1965

Cyclagelosphaera rotaclypeata Bukry, 1969

Description: small to medium coccoliths; elliptical outline; the rim is bicyclic; the central-area is filled with radial elements.

Cyclagelosphaera margerelii Noël, 1965

Description: small to medium coccoliths; elliptical outline; the rim is bicyclic; the central-area is closed.

HETEROCOCCOLITHS PLACOLITHS INC SEDIS

Genus *Haqius* Roth, 1978

Haqius circumradiatus (Stover, 1966) Roth, 1978

Description: Medium to large; circular outline; the rim is bicyclic; the central-area is narrow or closed.

NANNOLITHS INC SED - RADIATE MULTIELEMENT

Genus *Hayesites* Manivit, 1971

Hayesites albiensis Manivit, 1971

Description: Small; stellate outline with 6-8 rays, the central-area is narrow containing a circle.

Hayesites irregularis (Thierstein in Roth & Thierstein, 1972) Covington & Wise, 1987

Description: Small; stellate outline with 9-11 rays, the central-area is narrow containing a circle.

Genus *Assipetra* Roth, 1973

Assipetra terebrodentarius (Applegate et al. in Covington & Wise, 1987) Bergen, 1994

Description: Medium to large; globular formed by complexly blocks in radial sutures.

Family **MICRORHABDULACEAE** Deflandre, 1963

Genus *Lithraphidites* Deflandre, 1963

Lithraphidites alatus Roth & Thierstein, 1972

Description: Medium to large; the overall shape is like a closed umbrella.

Lithraphidites carniolensis Deflandre, 1963

Description: Medium to large; rod-shaped nannoliths, that tapers towards both ends.

Genus *Microrhabdulus* Deflandre, 1959

Microrhabdus primitivus Troelsen & Quadros, 1971

Description: Medium to large; cylindrical shape with nearly parallel sided, shows chequerboard extinction.

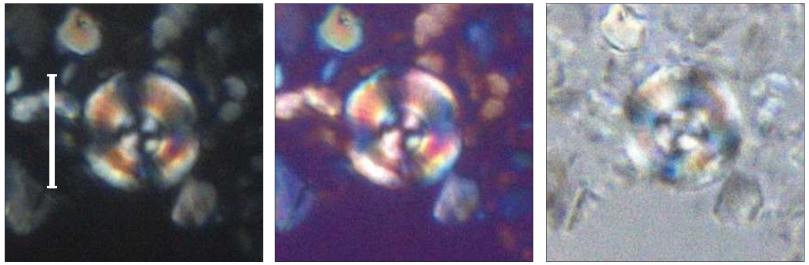
Cyclagelosphaera margerelii (DSDP Site 364 / Depth 912,02 mbsf)

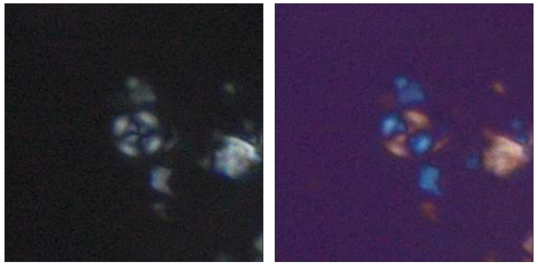
Cyclagelosphaera rotaclypeata (DSDP Site 364 / Depth 912,02 mbsf)

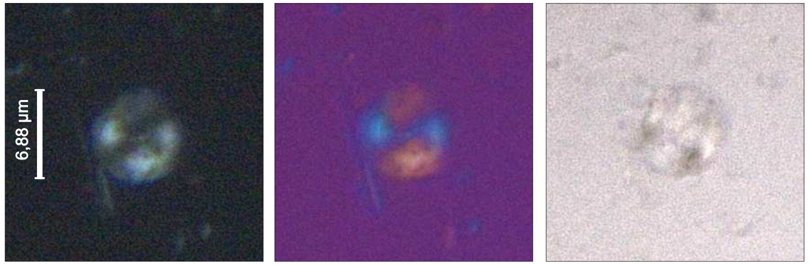

Haqius circumradiatus (DSDP Site 364 / Depth 722,75 mbsf)

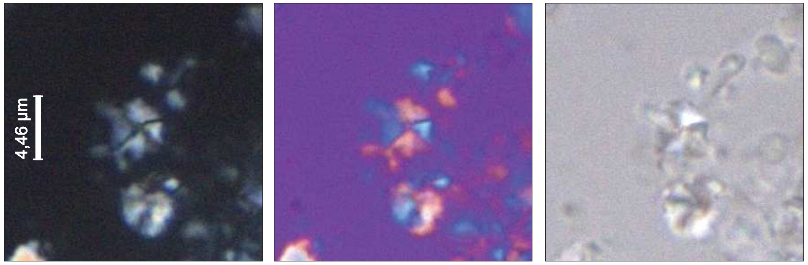

Hayesites albiensis (DSDP Site 364 / Depth 1.031,21 mbsf)

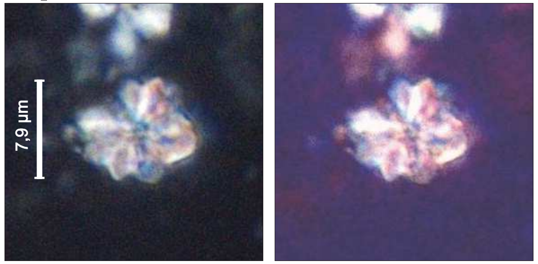

Assipetra terebrodentarius (DSDP Site 364 / Depth 931,70 mbsf)

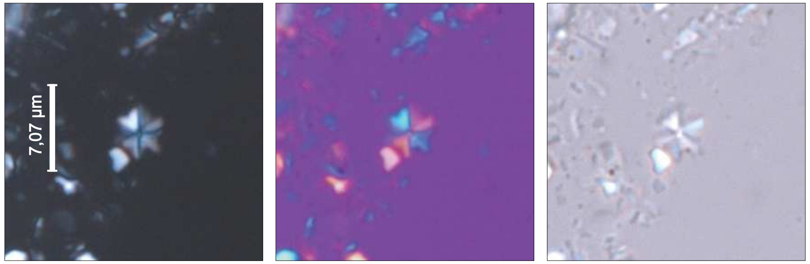

Hayesites irregularis (DSDP Site 364 / Depth 850,15 mbsf)

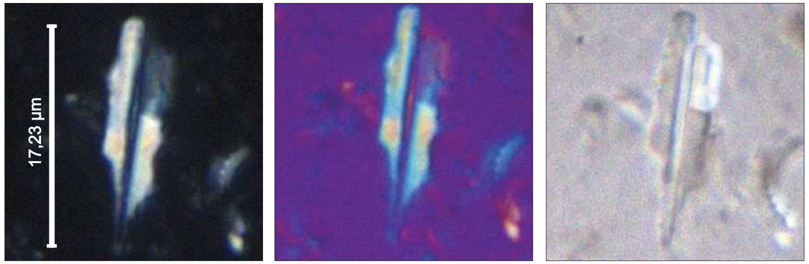

Lithraphidites alatus (DSDP Site 364 / Depth 932,45 mbsf)

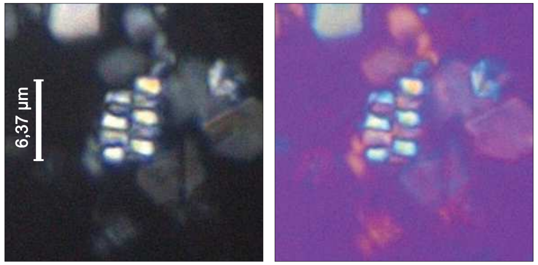

Microrhabdus primitivus (DSDP Site 364 / Depth 828,40 mbsf)

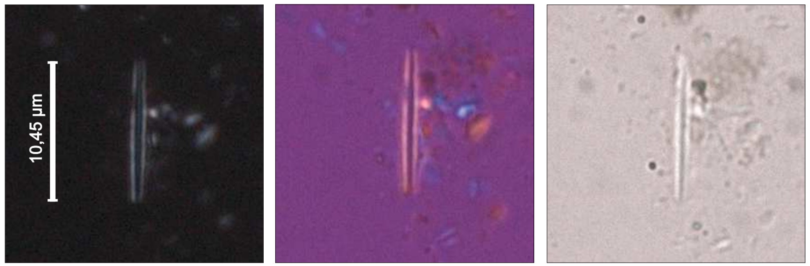

Lithraphidites carniolensis (DSDP Site 364 / Depth 717,23 mbsf)

10 µm

SYSTEMATIC PALEONTOLOGY: PLATE 9 – NANNOLITHS INC SED

Family **LAPIDEACASSACEAE** Black, 1971

Genus *Lapideacassis* Black, 1971

***Lapideacassis* sp. 1**

Description: Large; cylindrical with tapering outline; curved upper part; central area is diffuse; without apical spine.

***Lapideacassis* sp. 2**

Description: Large; cylindrical with tapering outline; curved upper part; central area is diffuse; without apical spine and protruding ledge just above the base on one side.

***Lapideacassis* sp. 3**

Description: Large; cylindrical with tapering outline, form of bell; curved upper part; central area is diffuse; without apical spine.

***Lapideacassis* sp. 4**

Description: Medium; circular outline, apical view of *Lapideacassis*.

***Lapideacassis* sp. 5**

Description: Large to very large; cylindrical with tapering outline; curved upper part; central area is diffuse; on one side have two apical spines oriented at about 45 degrees.

Lapideacassis glans Black, 1971

Description: Small species; cylindrical with tapering outline, form of bell; curved upper part; central area is diffuse; with protruding ledge just above the base.

Lapideacassis* cf. *bispinosa (Perch-Nielsen & Franz, 1977) Burnett, 1997

Description: Large to very large; cylindrical with tapering outline; curved upper part; central area is diffuse; have two apical spines at about 45 degrees.

Lapideacassis mariae Black, 1971

Description: Large species; cylindrical with tapering outline, form of bell; curved upper part; central area is diffuse; without apical spine and protruding ledge just above the base.

Lapideacassis cornuta (Forchheimer & Stradner, 1973) Wise & Wind, 1977

Description: Large to very large; cylindrical with tapering outline; curved upper part; central area is diffuse; have two apical spines at about 45 degrees.

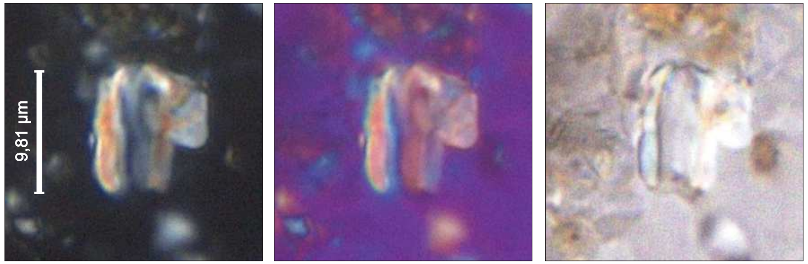

Lapideacassis sp. 1 (DSDP Site 364 / Depth 1.006,96 mbsf)

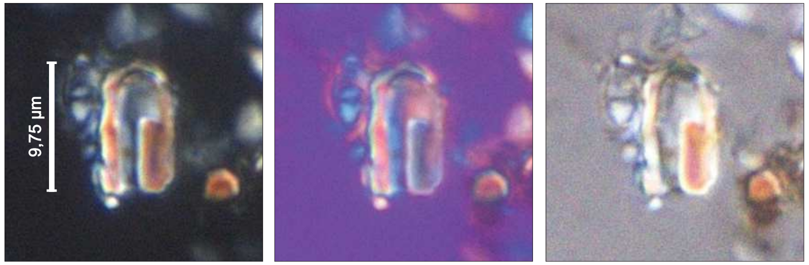

Lapideacassis sp. 2 (DSDP Site 364 / Depth 1006,41 mbsf)

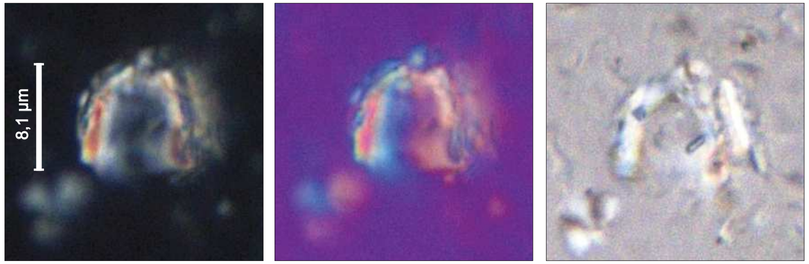

Lapideacassis sp. 3 (DSDP Site 364 / Depth 932,45 mbsf)

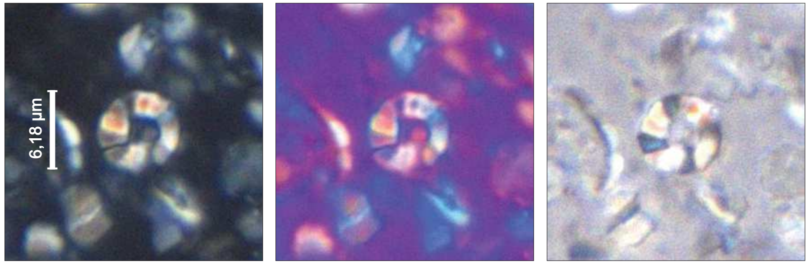

Lapideacassis sp. 4 (DSDP Site 364 / Depth 929,66 mbsf)

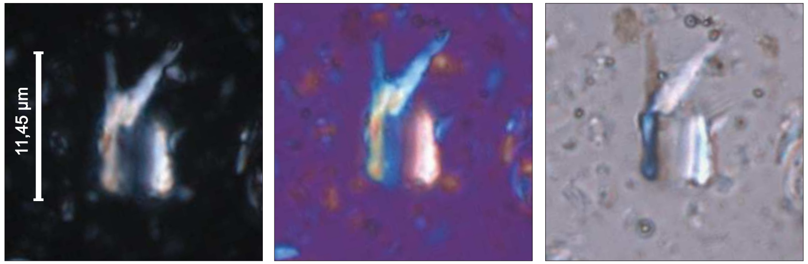

Lapideacassis cf. *bispinosa* (DSDP Site 364 / Depth 932,45 mbsf)

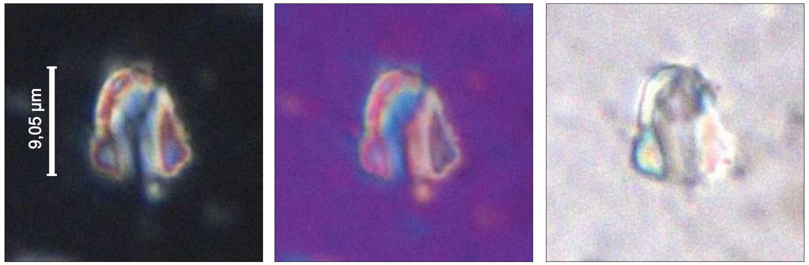

Lapideacassis glans (DSDP Site 364 / Depth 932,45 mbsf)

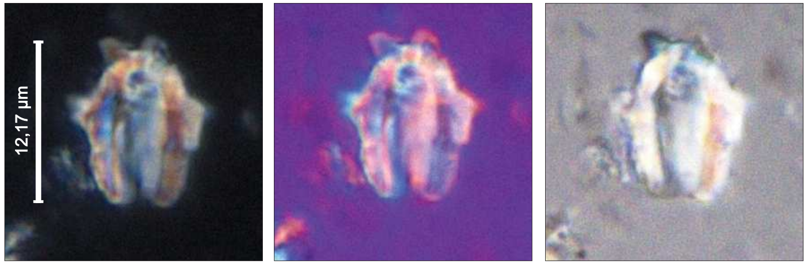

Lapideacassis cornuta (DSDP Site 364 / Depth 932,45 mbsf)

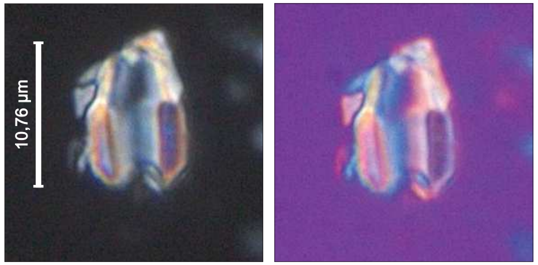

Lapideacassis mariae (DSDP Site 364 / Depth 971,18 mbsf)

10 µm

SYSTEMATIC PALEONTOLOGY: PLATE 10 – NANNOLITHS AND BRAARUDOSPHAERALES

Family **POLYCYCLOLITHACEAE** Forchheimer, 1972 emend. Varol, 1992

Genus *Radiolithus* Stover, 1966

Radiolithus undosus (Black, 1973) Varol, 1992

Description: Medium; stellate outline, nannolith constructed from nine segments and have a large diaphragm and small wall.

Radiolithus planus Stover, 1966

Description: Medium; nannolith constructed from nine segments and have a large diaphragm and small wall.

Genus *Eprolithus* Stover, 1966

Eprolithus floralis (Stradner, 1962) Stover, 1966

Description: Medium; nannolith constructed from nine segments and have a medium diaphragm and medium wall.

Genus *Micula* Vekshina, 1959

Order BRAARUDOSPHAERALES Aubry 2013 emend Lees & Bown 2016

Family **BRAARUDOSPHAERACEAE** Deflandre, 1947

Genus *Braarudosphaera* Deflandre, 1947

Braarudosphaera africana Stradner, 1961

Description: Medium; stellate outline, nannolith constructed from five segments which form a pentalit with long and relatively narrow rays.

Braarudosphaera primula Black, 1973

Description: Medium; stellate outline, nannolith constructed from five segments which form a pentalit with rounded tips to the segments.

Braarudosphaera hockwoldensis Black, 1973

Description: Medium; stellate outline, nannolith constructed from five segments which form a pentalit with shallow and narrow rays.

Braarudosphaera pseudobatilliformis Alves *et al.* 2017

Description: Medium; stellate outline, nannolith constructed from five segments which form a pentalit with one segment asymmetrically enlarged.

Braarudosphaera regularis Black, 1973

Description: Medium; stellate outline, nannolith constructed from five segments which form a pentalit with pentagonal outline and bilateral symmetry, i.e. the sutures bisect the edges.

Braarudosphaera batilliformis Troelsen & Quadros, 1971

Description: Medium; stellate outline, nannolith constructed from five segments which form a pentalith with one segment bearing a ridge which extends into a protruding spine.

***Braarudosphaeraceae* sp. 1**

Description: Medium; pentagon outline, nannolith constructed from five triangular segments.

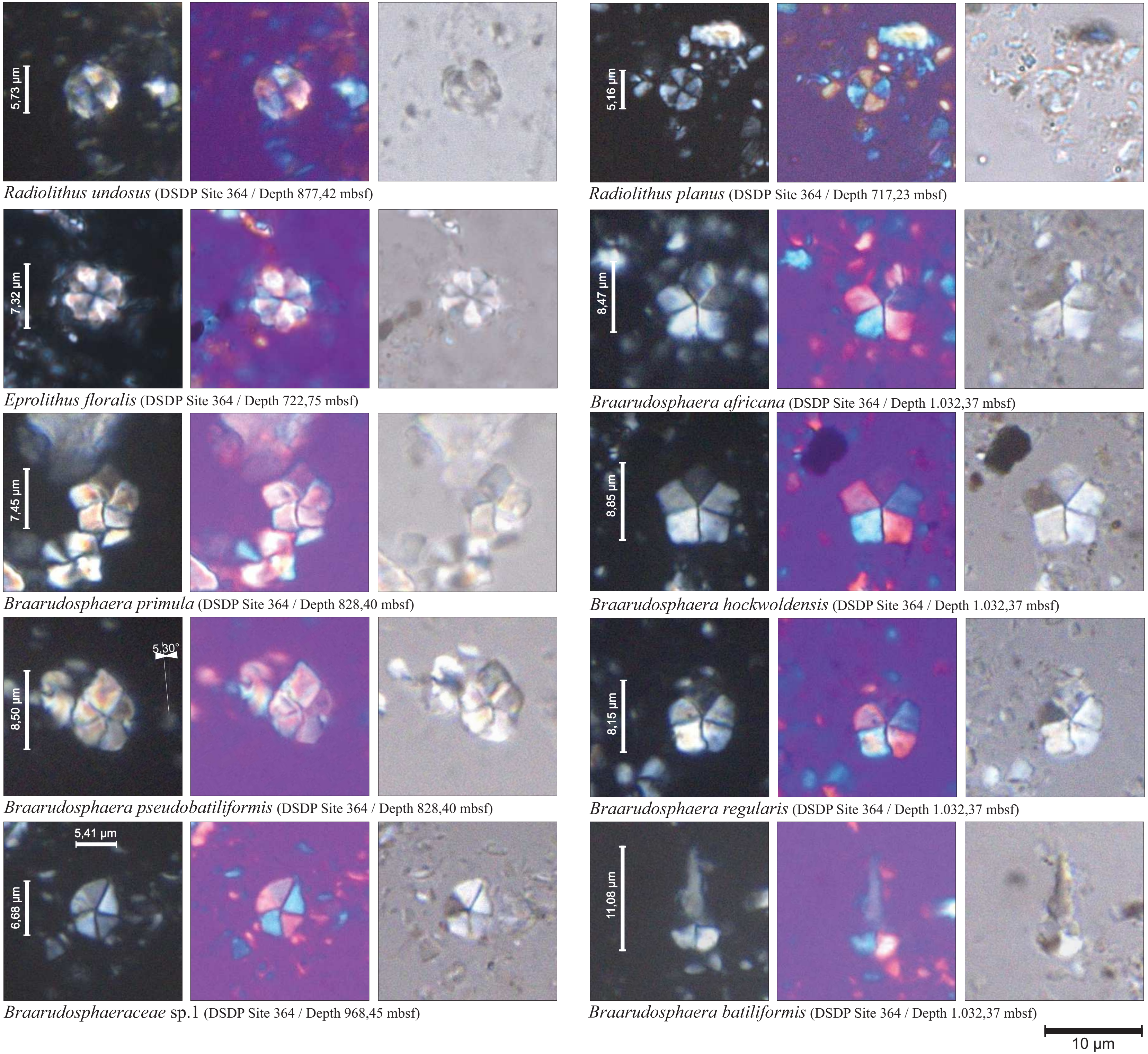

Radiolithus undosus (DSDP Site 364 / Depth 877,42 mbsf)

Radiolithus planus (DSDP Site 364 / Depth 717,23 mbsf)

Eprolithus floralis (DSDP Site 364 / Depth 722,75 mbsf)

Braarudosphaera africana (DSDP Site 364 / Depth 1.032,37 mbsf)

Braarudosphaera primula (DSDP Site 364 / Depth 828,40 mbsf)

Braarudosphaera hockwoldensis (DSDP Site 364 / Depth 1.032,37 mbsf)

Braarudosphaera pseudobatiliformis (DSDP Site 364 / Depth 828,40 mbsf)

Braarudosphaera regularis (DSDP Site 364 / Depth 1.032,37 mbsf)

Braarudosphaeraceae sp.1 (DSDP Site 364 / Depth 968,45 mbsf)

Braarudosphaera batiliformis (DSDP Site 364 / Depth 1.032,37 mbsf)

SYSTEMATIC PALEONTOLOGY: PLATE 11 – BRAARUDOSPHAERALES AND CALCAREOUS DINOFLAGELLATES

Order BRAARUDOSPHAERALES Aubry 2013 emend Lees & Bown 2016

Family **NANNOCONACEAE** Deflandre, 1959

Genus *Nannoconus* Kamptner, 1931

***Nannoconus* sp. 1**

Description: Medium to large; circular outline, apical view of *Nannoconus*.

***Nannoconus* sp. 2**

Description: Medium to large; elliptical outline, oblique angle of *Nannoconus*.

Nannoconus truittii truittii Brönnimann, 1955

Description: Lengths 6-12 μm, medium to very large; width 6-12 μm; axial channel>thickness of the walls; length>width or length = width; pole termination is only one rounded edges.

Nannoconus fragilis Deres and Achéritéguy, 1980

Description: Lengths 6-8 μm, medium to large; width 7-9 μm; axial channel>thickness of the walls; length<width; pole termination is only one rounded edges.

Nannoconus truittii frequens Deres and Achéritéguy, 1980

Description: Lengths 11-13 μm, very large; width 8-10 μm; axial channel>thickness of the walls; length>width or length = width; pole termination is only one rounded edges.

Nannoconus truittii rectangularis Deres and Achéritéguy, 1980

Description: Lengths 6-8 μm, medium to large; width 9-11 μm; axial channel>thickness of the walls; length<width; pole termination is only one rounded edges or truncated.

Nannoconus troelsenii Alves *et al.,* 2017

Description: medium to large; circular form, central area is closed.

Nannoconus planus Stradner, 1963

Description: Medium to large; axial channel = thickness of the walls; length>width.

Order **CALCAREOUS DINOFLAGELLATES**

Thoracosphaera Kamptner 1927

***Thoracosphaera* sp.1**

Description: Granular forms, usually circular.

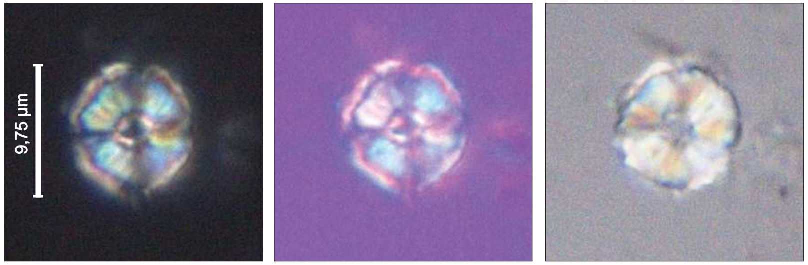

Nannoconus sp. 1 - Apical angle (DSDP Site 364 / Depth 790,41 mbsf)

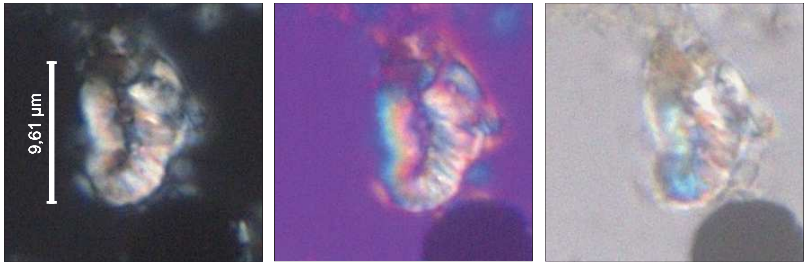

Nannoconus sp. 2 - Oblique angle (DSDP Site 364 / Depth 992,63 mbsf)

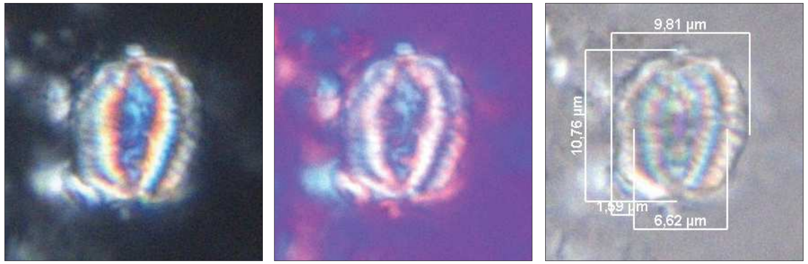

Nannoconus t. truittii (DSDP Site 364 / Depth 1.032,37 mbsf)

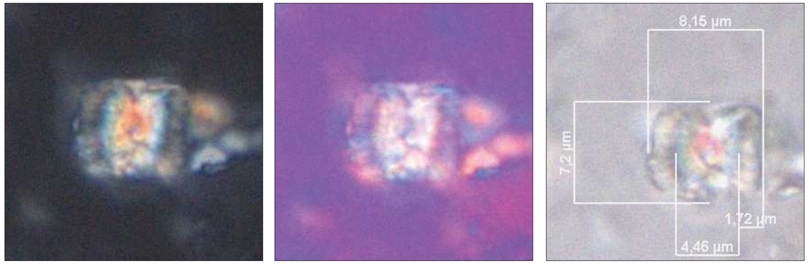

Nannoconus fragilis (DSDP Site 364 / Depth 973,89 mbsf)

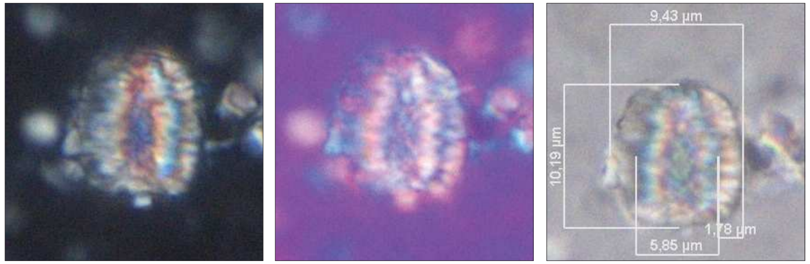

Nannoconus t. frequens (DSDP Site 364 / Depth 1.032,37 mbsf)

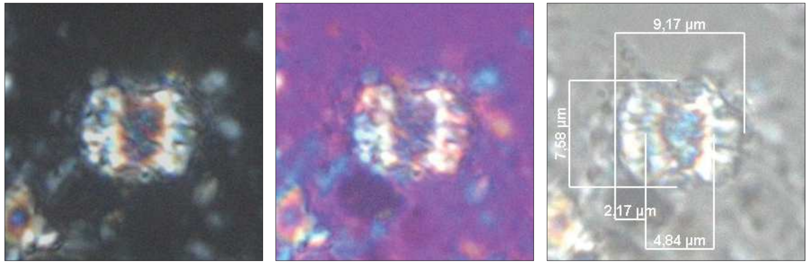

Nannoconus t. rectangularis (DSDP Site 364 / Depth 790,41 mbsf)

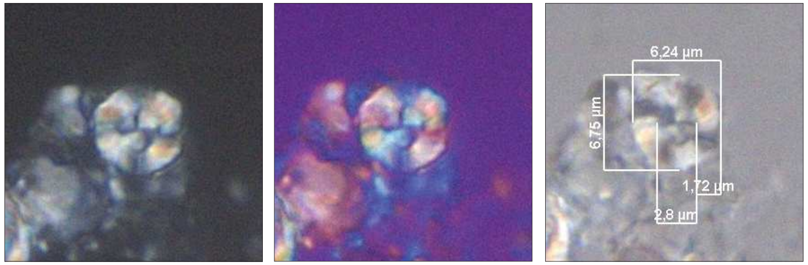

Nannoconus troelsenii (DSDP Site 364 / Depth 826,40 mbsf)

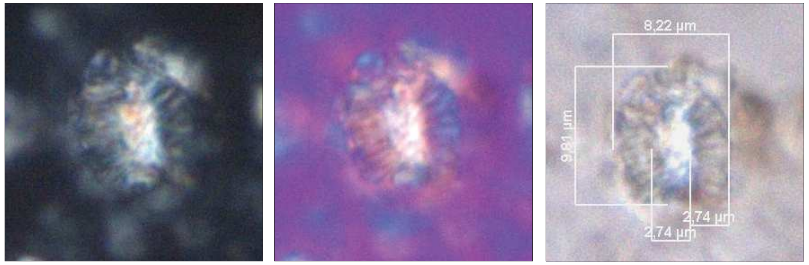

Nannoconus planus (DSDP Site 364 / Depth 973,89 mbsf)

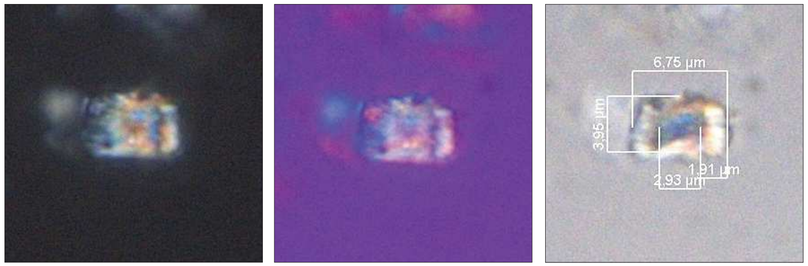

Nannoconus troelsenii (DSDP Site 364 / Depth 968,45 mbsf)

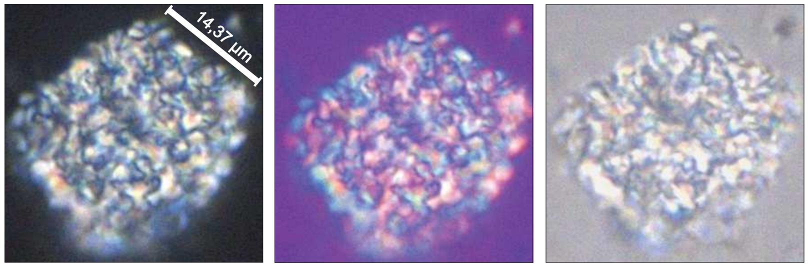

Thoracosphaera sp.1 (DSDP Site 364 / Depth 1.032,37 mbsf)

10 µm